Biochemical, biophysical and electrophysiological characterisation of the recombinant voltage-gated sodium channel from the marine bacterium Maricaulis Maris MCS10

Magdalena Teresa Wianecka

Publication date

01-01-2011

Licence

Document Version
1

Citation for this work (HarvardUL)

BIOCHEMICAL, BIOPHYSICAL AND ELECTROPHYSIOLOGICAL CHARACTERISATION OF THE RECOMBINANT VOLTAGE-GATED SODIUM CHANNEL FROM THE MARINE BACTERIUM *MARICAULIS MARIS* MCS10

PhD Thesis

Magdalena Teresa Wianecka

Supervisor: Dr Tewfik Soulimane

Submitted to the University of Limerick,

April 2011

Abstract

The eukaryotic voltage-gated sodium channel Na_v is an integral membrane protein that transports sodium across the cell membrane. While the Na_v has a four-domain structure with six α-helical transmembrane segments in each domain, the first bacterial homologue, which was identified in 2001 in *Bacillus halodurans* (NaChBac), consists of only one domain. Its simple constitution makes NaChBac and prokaryotic homologues interesting targets for structural analysis.

The present study is focused on the production, biochemical and biophysical characterisation as well as crystallisation of the voltage-gated sodium channel from *Maricaulis maris* MCS10 (NaChMM). Thus, an optimised protocol for the production of milligram quantities (6 mg/L) of highly pure recombinant NaChMM was established. The integrity of the protein was demonstrated by SDS-PAGE/Western-blot and further evaluated by N-terminal sequencing and mass spectrometry. While the gel-filtration trials suggest the presence of a homogenous population in several tested detergents, cross-linking and Blue-Native gel experiments provide insight into the inhomogeneity of the sample represented by the detection of monomeric, dimeric and tetrameric states. Furthermore, extensive crystallisation trials (~ 8,000) were performed using robotics and potential preliminary crystallisation conditions were discussed.

In comparison, an attempt was made to produce and further characterise the recently described sodium channels from *Bacillus halodurans* C-125 and *Silicibacter pomeroyi* DSS-3, which led to the conclusion that both sodium channels can only be produced at a low scale and are less stable in a solution.

The *in vivo* activity of NaChMM was investigated using the whole-cell patch clamp method. In contrast to NaChBac, NaChMM demonstrates a fast activation and inactivation kinetics. Surprisingly, NaChMM presents a double mechanism of inactivation, which has been to date observed only in the mammalian Na_v. Due to the differences in the constitution of Na_v *vs.* NaChMM, the NaChMM inactivation mechanisms cannot be classified as the so-called C-type or N-type mechanisms which are only present in Na_v. A further investigation by site-directed mutagenesis is therefore required.

Declaration

I hereby declare that this work is the result of my own investigations and that this thesis has not been submitted previously in this form or any other form to this or any other university in candidature for a higher degree.

_____

Magdalena Wianecka

Acknowledgements

Niniejszą pracę doktorancką dedykuję mojej kochanej Mamie, najważniejszej

osobie w moim życiu, na którą mogę liczyć w każdej sytuacji

///

I would like to dedicate this work to my Loving Mom the most important

person in my life that I can count on in every situation

Table of Contents

List of Tables

List of Figures

1. Introduction

1.1. Membrane proteins

Membrane proteins constitute approximately a quarter of all proteins present in eukaryotic and prokaryotic organisms (Wallin and von Heijne, 1998). They play a key role in transport and signal transduction across the cell membranes. About 60 % of all produced drugs target membrane proteins (Terstappen and Reggiani, 2001; Davey, 2004). In general, membrane proteins can be divided into three categories: integral membrane proteins (IMPs), lipid-anchored proteins and peripheral membrane proteins. The IMPs are integrated into either side of the cellular membrane. They are specifically called transmembrane proteins since they are exposed to the exterior and interior of the cell at the same time and include the voltage-gated sodium channel (Sato *et al.*, 2001). They provide hydrophilic channels that take part in the transport of ions or molecules across biological membranes (Campbell, 2002). The second group, the lipid-anchored proteins, such as the glycosylphosphatidylinositol-anchored proteins (GPI-APs), are usually covalently-bound to glycolipids or phospholipids and are incorporated in this way into the phospholipid bilayer (Overath *et al.*, 1994). Finally, the peripheral proteins are non-permanently attached to the surface by interacting with the integral membrane proteins or with the hydrophilic head of the membrane-associated phospholipids. They can also be located on either side of the cell membrane surface, an example of which is the actin binding protein hisactophilin (Hanakam *et al.*, 1995; Scheel *et al.*, 1989). Cholesterol-bound proteins stabilize the cell membrane to maintain its fluidity (Samuel *et al.*, 2001). Moreover, due to different membrane protein orientations in the lipid bilayer, cell membrane has a "sidedness" that reflects its functional asymmetry. The individual lipid and protein units in a membrane form a fluid mosaic with a constantly changing pattern (Engelman, 2005). The maintenance of cell shape is provided by the membrane proteins that are attached to the cytoskeleton and extracellular matrix (ECM). In addition, the enzymatic activity and cell-cell recognition also form the common functions of membrane proteins. The transport of ions and molecules across the lipid bilayer occurs either passively or actively.

The passive transport directly across the lipid bilayer does not require any energy from the outside since it follows along the concentration gradient as the driving force, although the cell may use protein channels in the case of facilitated diffusion. By contrast, active transport uses proteins to transport hydrophilic particles such as ions against the concentration gradient using energy that is usually supplied by ATP or by the electrochemical gradient; the ATP-binding cassette (ABC) transporters constitute well-known examples of the ATP-utilising active transporters (Colabufo *et al.*, 2009). The transport of ions and molecules is not necessarily required to occur in isolation; flux coupling through the antiporters and symporters allows transports of two or more ions or molecules simultaneously.

1.2. Challenges in membrane protein structural biology

The IMPs constitute approximately 20-30 % of the reported open reading frames (ORFs) in both prokaryotes and eukaryotes (Wallin and von Heijne, 1998).

Despite major advances in structural biology over the past decade, structural information on the IMPs is still very limited. Although electron microscopy (Kuhlbrandt and Williams, 1999) and NMR (Wuthrich, 2003) were used for the elucidation of membrane protein structures, it is X-ray diffraction that remains the method of choice for the high-resolution structure determination of membrane proteins, which is required for the understanding of the mode of action of any given protein target. To date, there are 1373 known transmembrane structures (2 % of all known protein structures), reported by Protein Data Bank of Transmembrane proteins (PDBTM) (Tusnady *et al.*, 2004; Tusnady *et al.*, 2005). They are also well documented and regularly updated on Stephen White's website (http://blanco.biomol.uci.edu/Membrane_Proteins_xtal.html; UC Irvine, USA). The considerably low number of known membrane proteins' structures is due to their unstable nature and difficulties with the expression, purification and crystallisation of recombinant membrane proteins, as most of the structures solved to date belong to proteins abundant in nature, such as the respiratory complexes.

Figure 1 presents the trend in the evolution of membrane protein structures compared to soluble proteins. The growth of membrane protein

structure determination is exponential and comparable to the trend line for soluble proteins, however with a delay of approximately 25 years. The first structure of a soluble protein (myoglobin) was in fact solved by Perutz and Kendrew in 1960 (Kendrew *et al.*, 1960) and the first structure of a membrane protein (photosynthetic reaction centre from *Rhodopseudomonas viridis*) was solved by the Deisenhofer's group in 1985 (Deisenhofer *et al.*, 1985).
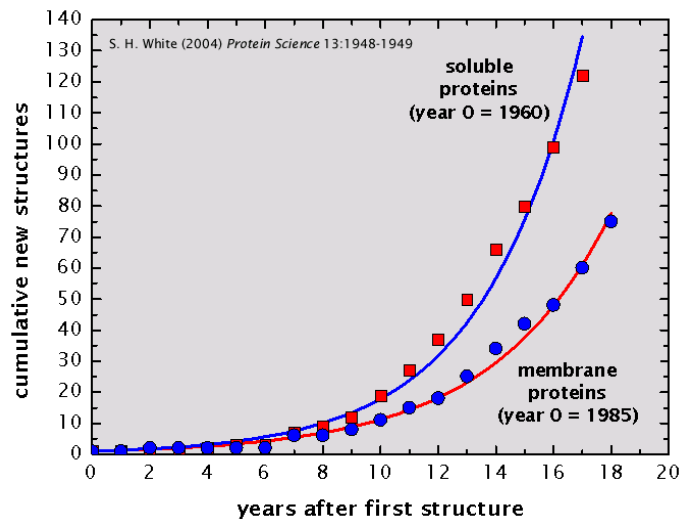
Figure 1: Time scale and comparison of the number of solved structures of soluble proteins and the number of known structures of membrane proteins (adapted from White, 2004).
Red squares – data for soluble proteins; blue circles – data for membrane proteins. The solid curves represent fits of the data to the equation m *= exp(*b*y), where* m *is the cumulative total of new structures and* y *is the number of years since the publication of the first structure. The parameter* b *= 0.289 and 0.242 for soluble and MPs, respectively.*

The α-helical and β-barrel proteins are the two topological structures of membrane proteins (von Heijne, 1999). While the β-barrel proteins can be easily refolded from inclusion bodies and used for further studies (Bannwarth and Schulz, 2003), the α-helical membrane proteins are very difficult to refold (Kiefer, 2003). Therefore, the correct insertion of expressed proteins into the cell membrane is important. Membrane proteins require additional endogenously-expressed factors assisting in the proper targeting and insertion into the cell membrane (van Geest and Lolkema, 2000). Nevertheless, some of the heterologously expressed membrane proteins can be efficiently targeted and inserted via pathways that they do not use natively (Kunji *et al.*, 2005).

Membrane protein production and stability can be improved by genetic engineering manipulations. Tucker and Grisshammer (1996) investigated the influence of introduction of a variety of C-terminal synthetic tags, including a polyhistidine tag, a strepavidin tag and a c-*myc* epitope, on recombinant membrane protein stability. The addition of soluble proteins as fusions to either end (C-terminus or N-terminus) was reported to improve the production yield of poorly expressed membrane proteins. Weiss and Grisshammer (2002) were investigating the influence of introduction of the following fusions to recombinant membrane proteins: glutathione S-transferase (GST), green fluorescent protein (GFP), maltose-binding protein (MBP) (Weiss and Grisshammer, 2002; Tucker and Grisshammer, 1996) and Mistic, a small protein unique to *Bacillus subtilis* (Roosild *et al.*, 2005). The co-expression of target proteins with molecular chaperones, such as DnaK-DnaJ, was shown to improve the folding of the over-expressed proteins (Chen *et al.*, 2003). Moreover, the membrane protein co-expression with signal recognition particle (SRP)-targeting pathway proteins (Economou, 1999; Lee and Bernstein, 2001), Sec translocon and YidC in *E. coli* increases the possibility of a proper insertion of recombinant protein into the membrane (Raine *et al.*, 2003). Furthermore, the expression with an addition of ligands may help to stabilise proteins, which results in increased production (Andre *et al.*, 2006; Weiss *et al.*, 1998). A number of parameters were analysed for the stabilisation of membrane protein production (expression media, expression length and inducer concentration) and more than fifteen years of studies indicate that it is the culture growth temperature that has the key impact on the protein quality (Schein, 1989; Vasina and Baneyx, 1996; Sorensen and Mortensen, 2005). In order to increase the expression yield of membrane proteins, specialized expression hosts were developed (Francis and Page, 2010). Due to the degeneracy of the genetic code table, most amino acids are encoded by more than one codon but only a limited set of codons for any particular amino acid is in fact represented in an organism (Ikemura, 1981; Dong *et al.*, 1996). Consequently, the tRNA population within the cell reflects the proportion of the codons (codon bias). *E. coli* constitutes an interesting example, since it rarely uses four codons encoding for Arg, one codon each encoding for following amino acids Gly, Ile, Leu and Pro. Rare codons present in proteins which are foreign to *E. coli* may influence the heterologous expression simply by affecting

the number of tRNAs of the aforementioned amino acids (Kane, 1995; Goldman *et al.*, 1995). Accordingly, when a heterologous protein is expressed in *E. coli*, the insufficiently charged tRNAs can lead to serious difficulties in protein translation, which results in the translational stalling, premature translation termination, translation frame shifting and amino acid misincorporation (Kurland and Gallant, 1996). The presence of small number of rare codons may result in a limited production of recombinant protein. This problem was solved by creating *E. coli* strains BL21 CodonPlus (DE3)-RIL and Rossetta, both of which contain extra copies of tRNA genes that are rare in *E. coli* but used more frequently in other organisms (Gustafsson *et al.*, 2004). Due to this the heterologous protein production in *E. coli* was greatly improved. What is more, the genetic modifications of *E. coli* BL21(DE3) led to the creation of the Walker strains C41(DE3) and C43(DE3) (Miroux and Walker, 1996) that gained higher plasmid stability and were able to endure toxicity effects of membrane protein over-expression (Dumon-Seignovert *et al.*, 2004).

Membrane proteins can be purified by applying almost any of the existing protein purification techniques available for soluble proteins. Nonetheless, due to the hydrophobic nature of membrane proteins, they require solubilising agents in the buffer solutions during the purification process. The choice of a detergent is very important, as it may have a negative effect on protein activity and structural stability (Ostermeier and Michel, 1997). The properties of a detergent used, along with the shape and size of its micelle, depend on the mixture of buffering conditions, salt, membrane lipids and the present protein molecules (Le Maire *et al.*, 1983). Moreover**,** fluidity and packing efficiency of the detergent monomers around the protein molecule will affect protein stability (Musatov *et al.*, 2000). Unsuitable detergent choices may lead to protein aggregation and affect protein quaternary structure (Musatov *et al.*, 2000). Screening of a panel of detergents for purification is thus important. The stability of a membrane protein in various detergents can be assayed in various ways. First and the most common method is the analysis of a peak shape and a retention time in a gel filtration chromatography, which may give clear information about aggregation or oligomerisation (Wiener, 2004). Second, small-scale stability test can be performed by monitoring the absorbance at 280 and 320 nm throughout the time. If the concentrated protein sample diluted ten-fold into one or more new

detergent(s) will remain stable, the 320 nm value will remain constant (Wiener, 2004). In order to maintain the native-like activity of a protein, the choice of ideal conditions for its purification may be difficult, as the very subtle changes may not be detectable in routine assays (De Foresta *et al.*, 1994; Nurani *et al.*, 2008).

In contrast to soluble proteins, membrane protein crystallisation is more problematic, but not impossible. This paragraph focuses on the methodologies used for membrane protein crystallisation rather than membrane protein targets themselves. There are several basic methods established for membrane protein crystallisation: the classical *in surfo* (such as vapour diffusion and batch), the newly-developed *in meso* (cubic or sponge phase) and bicelle crystallisation methodologies (Hunte, 2003; Caffrey, 2003). *In surfo* methods use the protein-detergent complex directly in crystallisation trials (Hunte, 2003, Iwata, 2003). The detergent presence in the sample introduces an additional dimension to the matrix of crystallisation screening. Highly-automated systems are useful for an extensive crystallisation screening, as they require nanolitre amounts of material (McPherson, 2004; Caffrey, 2003). The crystallised protein sample needs to be highly-pure and homogenous (Ducruix, 1992). Certain proteins may however crystallize even from very heterogeneous mixtures, as was shown for the bovine heart cytochrome *c* oxidase (Yoshikawa *et al.*, 1996). The likelihood of success in crystal growth is greatly enhanced by increased purity and homogeneity of the sample (McPherson, 2004). The parallel concentration of a detergent may appear when the protein is concentrated. This phenomenon can negatively influence crystallisation, which results in the formation of poorly-ordered crystals, or no crystals at all (Wiener, 2004). Hence, the small cut-off membranes for sample concentration ought to be avoided and the ideal final detergent concentration of the concentrated protein sample should be approximately twice the critical micelle concentration (CMC) of the detergent (Barnard *et al.*, 2007). In comparison with the soluble proteins, incubation temperature has a greater influence on membrane protein crystallisation. This is due to the fact that membrane protein crystals have large amounts of a detergent in the crystal lattice. As the CMC of a detergent depends on temperature, small fluctuations of temperature that result in the change of effective detergent concentration can

easily disrupt crystal growth (Barnard *et al.*, 2007). The factors influencing protein crystallisation are listed in Table 1.

Table 1: Factors affecting crystallisation (McPherson, 2004).

Physical	Chemical	Biochemical
Temperature	pH/ Ionic strength/ Specific ions	Sample purity
Surfaces	Precipitant type	Ligands, inhibitors
Methodology/approach to equilibrium	Precipitant concentration	Sample aggregation state
Gravity/ pressure/ time	Degree of supersaturation	Post-translational modifications
Rate of equilibration	Reductive/oxidative environment	Proteolysis/hydrolysis
Medium viscosity	Non-macromolecular impurities	Chemical/genetic modifications
Vibrations/sound/mechanical perturbations	Detergents/surfactants/amphophiles	Inherent symmetry of the macromolecule
Electrostatic/magnetic fields	Concentration of sample	Stability of the macromolecule
Medium's dielectric properties	Cross-linkers/polyions	Isoelectric point

When every effort to crystallise a macromolecule fails, the most appropriate solution is to choose another homolog protein or to modify the chosen protein using genetic engineering techniques and introducing truncations, mutations, chimeric conjugates, an antibody or many other modifications that could significantly enhance the probability of crystallisation (McPherson, 2004). The other way to proceed is to try other methods of crystallisation, such as the *in meso* or bicelle methods.

In meso crystallisation method uses lipid, water, and protein in appropriate proportions to create a structured, transparent, lipidic matrix (Landau and Rosenbusch, 1996; Caffrey, 2003; Caffrey and Cherezov, 2009). The mixture of these three components at certain temperatures spontaneously forms the lipidic cubic phase (LCP) (Cherezov *et al.*, 2002). This method was successfully applied in the crystallisation of bacteriorhodopsin (Landau and Rosenbusch, 1996; Nollert *et al.*, 2001). The possible organisation of protein molecules into crystals growing from lipidic phases was hypothesised by Caffrey

(2000). Unfortunately, the LCP crystallisation is a time-consuming process as much as it is difficult to handle. It may also interfere with the hydrophilic regions of membrane proteins. Therefore, the sponge phase crystallisation method, which is a liquid version of cubic phase, was developed (Wadsten *et al.*, 2006). In bicelle crystallisation method, the membrane proteins environment containing detergent is replaced by lipid and the crystallogenesis occurs from the lipid bilayer (Faham and Bowie, 2002). As previously mentioned, crystallisation can be performed using protein-detergent-lipid complexes which are considered to be favourable crystallisation samples (Zhang *et al.*, 2003). Furthermore, the usage of proteoliposomes in crystallisation results in the formation of layered stacks or a direct assembly of proteoliposomes into a regular matrix. The described concepts of crystallisation are presented in Figure 2.
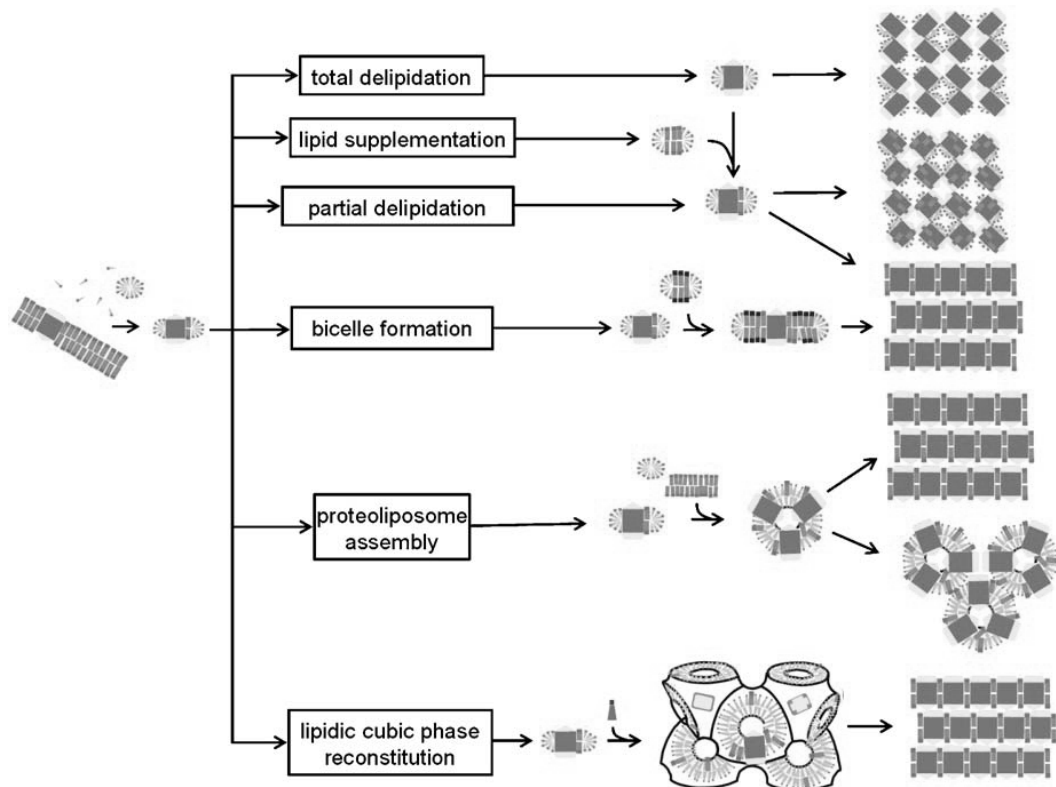
Figure 2: Representation of different concepts of membrane protein crystallisation and final packing arrangements (adapted from Nollert, 2005).

1.3. Voltage-gated ion channels family

The transport of ions across cell membrane maintains the desired ionic balance between the outside and the inside of the cell. While the lipid bilayer is semipermeable, it does not allow ions to travel through, with the exception of special cellular devices. One of the groups of transporters responsible for maintaining an inside-outside voltage gradient is a group of ion channels. The most common ions involved in a number of physiological processes are Na^+, K^+, Ca^{2+} and Cl^-. Their transport is performed in a down-gradient manner (concentration and electrochemical gradients). There are hundreds of genes encoding for different ion channels in the human genome (Gabashvili *et al.*, 2007) that are based on their gating criteria, ion selectivity and sequence similarity. These ion channels are divided into several subtypes. According to the channel gating mechanism, these proteins are classified as ligand-gated ion channels (Keramidas *et al.*, 2004) or voltage-gated channels (Bezanilla, 2000), where the opening and closing of channel's gate is respectively driven by chemical or electrical signals (Armstrong and Hille, 1998). Mechanically gated channels act upon a mechanical force, such as stretching or pressure that cause physical stress on a cell (Kamkin *et al.*, 2010). Moreover, certain channels respond to temperature changes (Cesare *et al.*, 1999).

Voltage-gated ion channels allow the movement of selected ions across the cell membrane and, therefore, stimulate fundamental human physiological processes (Marban *et al.*, 1998). The channels depend on electrical impulses that are in charge of their opening and closing (Armstrong and Hille, 1998). They are present in the membrane as cylindrical glycoproteins that consist of multiple α-helical regions. This pore-forming α-subunit can be created by aggregation of several copies of the same protein (i.e. prokaryotic voltage-gated sodium channel) or by the spontaneous folding of very large, single proteins (i.e. mammalian voltage-gated sodium channel). Additionally, the function of pore subunits can be supported by the so-called auxiliary subunits (denoted β, γ and so on) (Isom *et al.*, 1994). Depending on the channel selectivity, a specific residue is situated in different positions in the pore space (Corry, 2006). One of the most important and conserved parts of the voltage-gated ion channels are the positively charged α-helices that respond to changes in the membrane electrical

charge (Corry, 2006). Those parts of the protein are called the "voltage sensor" and contain regularly distributed, positively charged residues (mostly arginines) through the protein length (Bezanilla, 2000).

1.3.1. Mechanism of action of voltage-gated ion channels

The cell membrane is positively charged relative to the exterior, creating the electrical potential. The typical values of the resting membrane potential are between -40 mV and -95 mV (Hille, 2001). At resting potentials, voltage-gated ion channels stay closed and no ion movement is observed, in which instance the channel-inactivating segment is free in the cytosol (Figure 3B). When the cell membrane depolarisation occurs (i.e. the membrane potential changes), the positively charged α-helices are dragged towards the cell exterior, forcing the channel to open for an influx of ions (Figure 3C) (Yarov-Yarovoy *et al.*, 2006). Cell membrane depolarisation will appear as fast but short impulses that cause the channel to close. However, if depolarization persists, the overload of ions transported from the outside will trigger the inactivating segment (the "ball on a chain" mechanism), which will block the channel from the inside and disable ion transport (Figure 3D). The refractory period of the ion channel (the ion channel state after inactivation) is important in determining the unidirectionality of the action potential. A few milliseconds after the inside-negative resting potential is re-established, the positively charged α-helices return to their starting position and, as the channel closes, the inactivating segment is released (Figure 3B). The processes of membrane recovery from depolarisation back to its resting potential takes less than milliseconds (Hille, 2001). While the voltage-gated ion channel is inactivated (Figure 3D), it will not open upon a second depolarization impulse unless it recovers to its closed state (Figure 3B). The opening and closing of ion channels is strictly correlated with the conformational changes of the channel and depends on the incoming direction of signals, either from the inside or the outside of the cell.
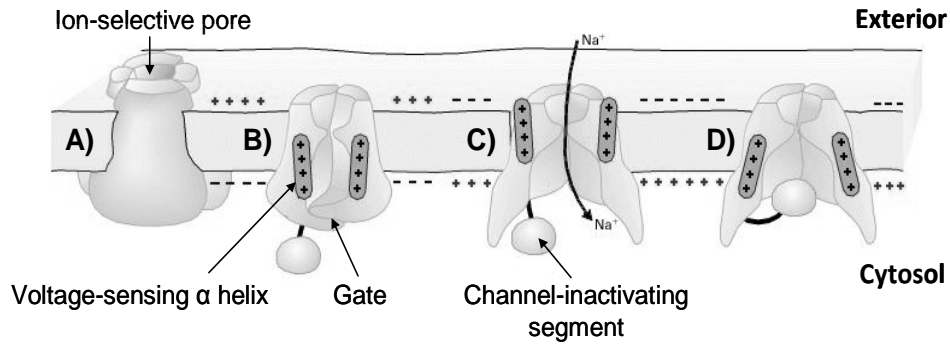
Figure 3: Three-dimensional representation and principle of action of voltage-gated sodium channel.
Adapted from Miller, 1991.

1.3.2. Classification of voltage-gated ion channels

There are four families of voltage-gated ion channels which are distinguishable by their selectivity for sodium, potassium, calcium and chloride ions. The widest group of voltage-gated ion channels transports potassium ions and consists of seven subfamilies (Figure 4). Evolutionarily, the Ca^{2+} channels are closely related to the Na+ channels, even though the former is a divalent cation.

In contrast to Ca^{2+} channels, K^+ and Cl^- are present in bacteria. The structure-function relationships of the latter two channels were thus extensively investigated. These three voltage-gated ion channels are briefly summarised in the next chapters.
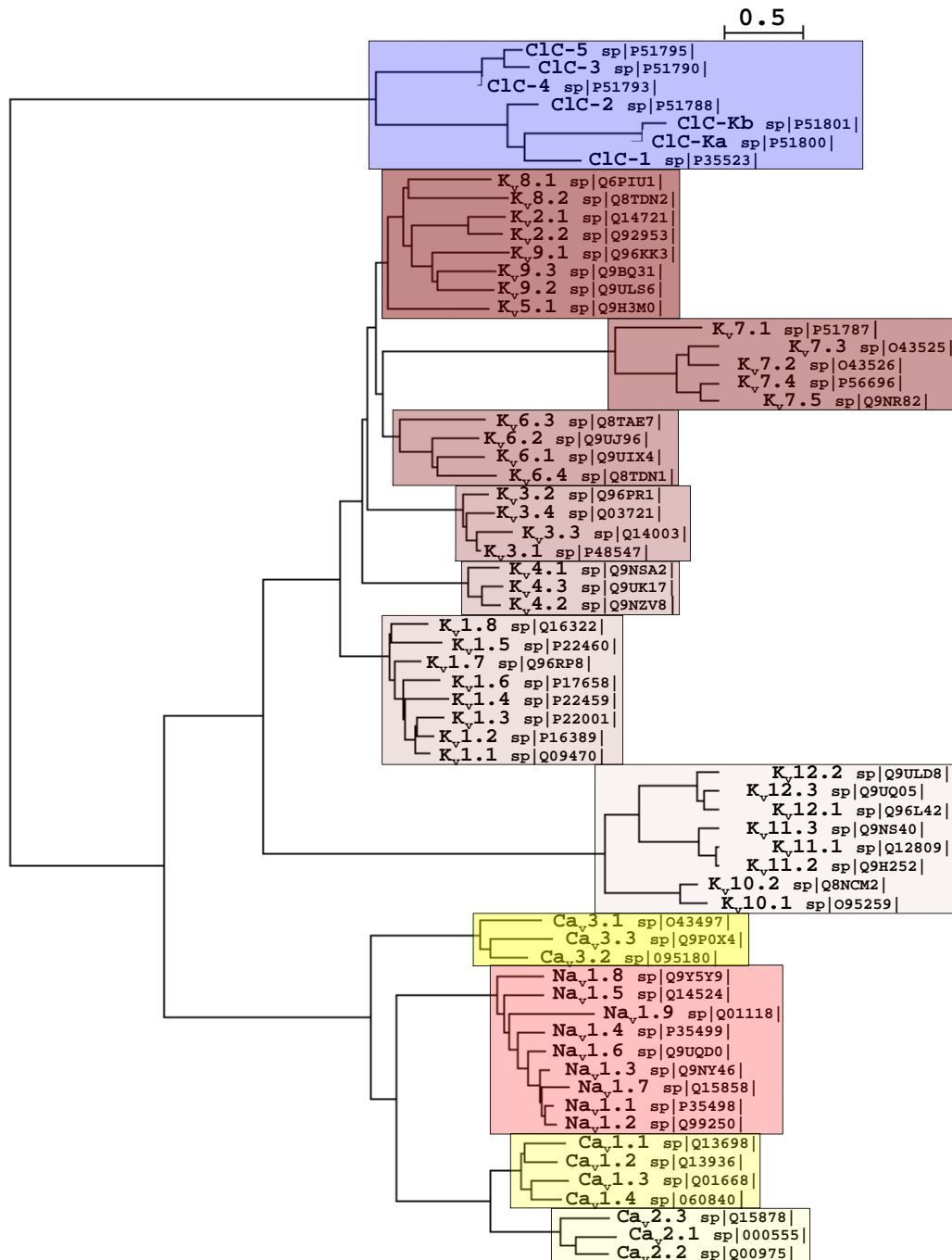
Figure 4: Phylogenetic tree of human voltage-gated ion channels.
Chloride channels family (blue), potassium channels family (brown shadowing), calcium channels family (yellow shadowing), and sodium channels family (red); full length amino acid sequence alignment was subjected to analysis by neighbourhood joining (PAUP).

1.3.2.1. Voltage-gated chloride channel family

The chloride channels are the most structurally distinct not only among all other voltage-gated channels, but also among themselves. One of the possible topologies is presented in Figure 5. This channel protein family is present in excitable epithelial cells (Lehmann-Horn and Jurkat-Rott, 1999). These channels are important for the setting of the resting membrane potential and the maintenance of cell volume (Jentsch *et al.*, 1995). The opening of chloride channels hyperpolarises the cell membrane and the ions flow from the extracellular medium, along their concentration gradient. This results in the excess of the positive charges on the outer surface of the membrane and the increase of the negative charges of the membrane on its cytosolic side. Chloride channels vary greatly in their structures, gating mechanisms and physiological functions they perform. They have low selectivity and may also conduct other ions, including iodide, thiocyanate or nitrate) (Fahlke, 2001). There are at least nine different C1C genes in mammals that are present in the muscle tissue, nervous system and kidney. Chloride channels are structurally unrelated to other channel proteins.

Chloride channel subunits contain between one and twelve transmembrane α-helical segments. Previously conducted studies strongly implicated a homodimeric form of functional chloride channels (Fahlke *et al.*, 1997; Ludewig *et al.*, 1996; Middleton *et al.*, 1996). Two different topological models were evaluated. The first configuration places the domain 4 (D4) extracellularly and the hydrophobic core of domains 9, 10, 11 and 12 (D9 - D12) crosses the membrane several times (Figure 5) (Schmidt-Rose and Jentsch, 1997). In the second configuration, domain 2 (D2) is situated extracellularly (Middleton *et al.*, 1994). In both models the N- and C-termini are located at the cell interior.
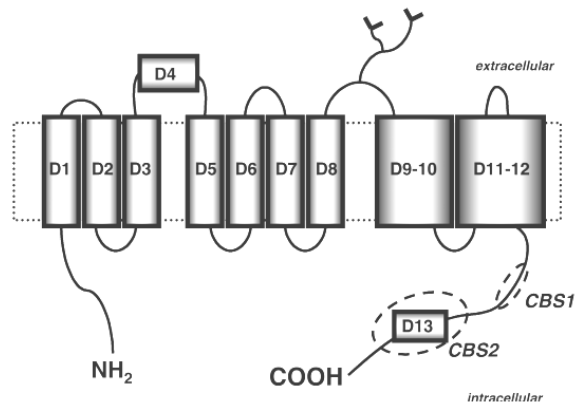
Figure 5: Membrane topology of a ClC protein.
CBS1 and CBS2 are cystathionine-β-synthase domains (taken from Wills and Fong, 2001).

The malfunctioning ClC1 (gene: *CLCN1*) chloride channel, which is widely found in muscles, is involved in myotonia congenital. Multiple mutations that can occur in the *CLCN1* gene may cause slow muscle relaxation after contraction. The mytonia congenital can have a recessive (Becker's disease) or a dominant (Thomsen's disease) character depending on the method of its inheritance. The mexiletine drug, which is also acting on sodium channels, has the highest therapeutic impact in the treatment of patients with myotonia congenital. (Kullmann and Hanna, 2002).

The role of prokaryotic chloride channels is not clear. It is however suspected that they might be responsible for extreme acid resistance (XAR) (Iyer *et al.*, 2002). Presented by Dutzler and co-workers (2002), the crystallographic structure of two prokaryotic ClC channels from *E. coli*, named "EriC," and from *Salmonella typhimurium*, named "StClC", in both cases revealed a formation of a functional homodimer (Figure 6). This fact implies that the ClC channels' family have dimeric structures that are characteristic for both prokaryotes and eukaryotes (Maduke *et al.*, 1999).
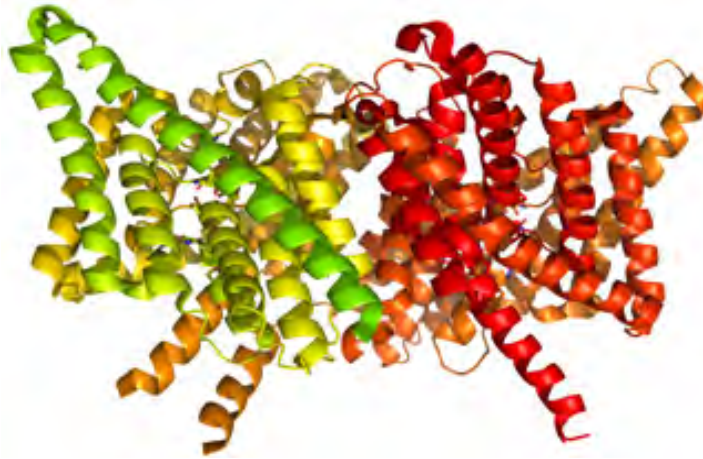
Figure 6: Crystal structure of ClC chloride channel (dimer) from *Salmonella typhimurium* at 3 Å.
PDB ID: 1KPL (Dutzler et al., 2002).

In contrast to the voltage-gated potassium channels, the ion-transport pore does not lay at the interface of the monomers in the functional ClC dimer. In turn, each of the subunits consists of its own ion-transport pore located in its centre (Jentsch et *al*., 2002). The Cl⁻ ion binding site, which lies approximately halfway through the cell membrane, comprises of three highly conserved residue regions: Gly-Ser-Gly-Ile-Pro (106-110), Gly-(Lys/Arg)-Glu-Gly-Pro (146-150), Gly-Xaa-Phe-Xaa-Pro (355-359) and an additional Tyr445 (Dutzler *et al.*, 2002).

1.3.2.2. Voltage-gated potassium channel family

Voltage-gated potassium channels are the simplest, yet the most diverse group among all voltage-gated channels. They were found in prokaryotes and in eukaryotes as homotetramers (Jan and Jan, 1997). The single subunit of sodium channel is composed of six transmembrane α-helices. Contrary to voltage-gated sodium channels, the potassium channels, which open upon hyperpolarization of the membrane, transport potassium ions along their concentration and electrochemical gradient from the inside to the outside of the cell. This results in an accumulation of an excess negative charge on the cytosolic surface of the membrane and an increase in a positive charge on the outer side of cell membrane. The voltage-gated potassium channels are commonly found in central nervous system and in the cardiovascular system. They repolarise the membrane potential and terminate an action potential in the brain and the heart. The $K_v4.2$ and $K_v1.4$ potassium channels are fast inactivating, which is important for the

initialisation of cardiac cells' membrane repolarisation. The potassium channels, such as $K_v1.5$, $K_v3.1$, $K_v2.1$ are slowly inactivating, which provides more prolonged repolarisation effects. The selectivity filter of potassium channels consists of Thr-Val-Gly-Tyr/Phe-Gly, the so-called signature sequences for this proteins' family.

The non-functional voltage-gated potassium channels result in muscle and neurological channelopaties. The periodic paralysis attacks can be a result of mutations in *KCNJ2* gene encoding for inwardly-rectifying potassium channel Kir2.1 (Plaster *et al.*, 2001). They can also be caused by mutations in *KCNE3* gene encoding for accessory subunit MiRP2 (Abbott *et al.*, 2001). The periodic paralysis caused by an improper functioning of Kir2.1 is one of the disorders Andersen's syndrome is comprised of, other including cardiac arrhythmia and craniofacial abnormalities. The mutations that alter the aforementioned genes, and are the reason for periodic paralysis attacks, decrease the potassium current flow through the channels. (Abbott *et al.*, 2001).

The neurological disorders, such as an episodic ataxia type 1, are caused by genetic mutations in the pore region of $K_v1.1$ potassium channel which is present in large numbers in the central nervous system (Browne *et al.*, 1994). The episodic ataxia type 1 can be trigged by stress or exertion and results in brief attacks of cerebellar incoordination, which may last for up to a few minutes. The native $K_v1.1$ belongs to potassium channels rapidly activating upon membrane depolarisation. The episodic ataxia type 1 can be a result of distinct mutations in *KCNA1* gene that can affect $K_v1.1$ activity in a variety of ways, i.e. they may increase the voltage threshold of channel's activation or even completely prevent the flux of potassium ions (Zuberi *et al.*, 1999; Eunson *et al.*, 2000; Zerr *et al.*, 1998).

The topologies of two closely related K^+ channels are presented in Figure 7, the first containing six α-helices and the second containing two α-helices. Both of them are nevertheless organised in homotetramers to create functional K^+ channels (MacKinnon, 1991). The inwardly-rectifying potassium channels represent a shorter version of voltage-gated potassium channel that consist only of the inner core (Doyle *et al.*, 1998).
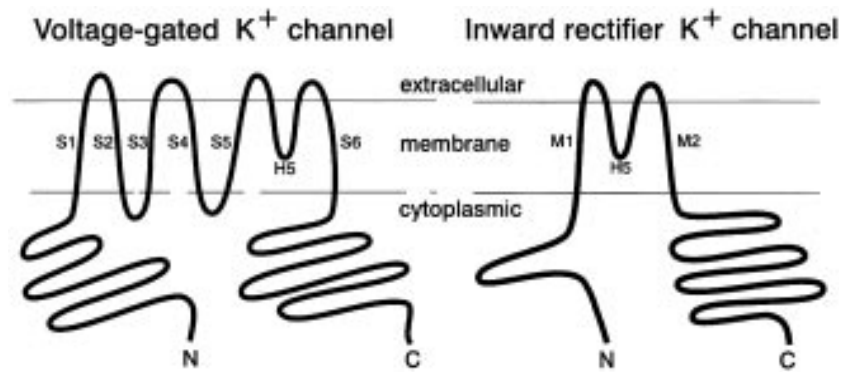
Figure 7: Topology comparison of voltage-gated potassium channel and inwardly rectifying potassium channel.
Taken from Kubo et al., 1993.

In 1998, the first structure of the KcsA potassium channel (proton-gated) from *Streptomyces lividans* (Figure 8) was elucidated by Roderick MacKinnon (Doyle *et al.*, 1998). An X-ray analysis revealed that four identical subunits create an inverted cone with the selectivity filter in its widest part facing cell exterior. The narrow selectivity filter is only 12 Å long, whereas the remainder of the pore is wider and lined out with hydrophobic residues.
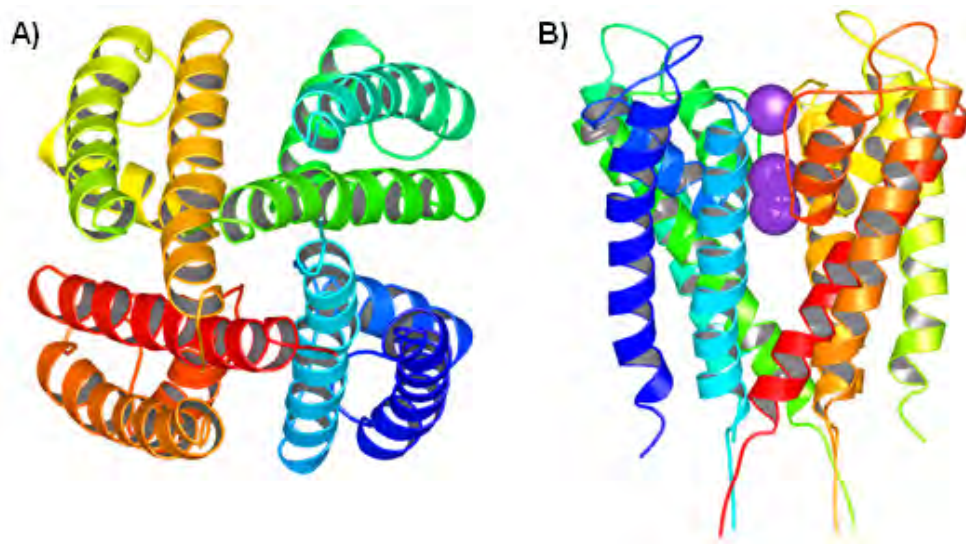
Figure 8: Tetrameric structure of KcsA potassium channel at 3.2 Å.
PDB ID: 1BL8; (Doyle et al., 1998) A) View from the bottom; B) View from the side including potassium ions inside the pore (purple spheres).

The selectivity filter of KcsA consists of Thr-Val-Gly-Tyr-Gly signature sequence, which is situated at the narrowest part of the transmembrane pore.

These residues thoroughly replace water molecules that solvate potassium ions in the solution, hence their strict selectivity (Figure 9) (Doyle *et al.*, 1998).
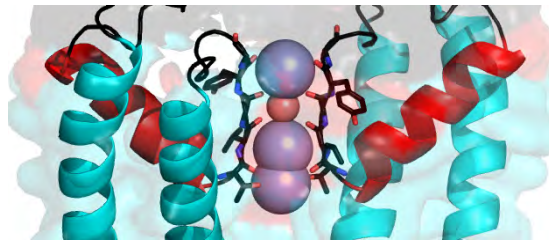
Figure 9: Selectivity filter of KscA potassium channel.
PDB ID: 1BL8; Red – pore helices; magenta – membrane helices; blue spheres – potassium ions; pink sphere – water molecule.

Crystal structures of KcsA suggest that in the conductive state of the channel, four ion binding sites are formed by the carbonyl oxygens in the pore. A potassium ion fits into each of these binding sites, thus satisfying its preference for an octahedral-chelating environment. The ion-oxygen distance in the octahedral cages of KcsA ranges from 2.7 Å to 3.1 Å, with an average of 2.85 Å (Doyle *et al.*, 1998; Bhate *et al.*, 2010).

1.3.2.3. Voltage-gated calcium channel family

In contrast to other voltage-gated ion channel families, the activity of α_1 subunit, which forms the ion conducting pore of calcium channels, is modulated by a large number of different auxiliary subunits (Figure 10) (Singer *et al.*, 1991). The main α_1 subunit comprises of four homologous domains, each of which contains six transmembrane helices. The β auxiliary subunit is intracellular and associates with the α_1 subunit. The γ auxiliary subunit is a glycoprotein that possesses four transmembrane segments. The α_2 auxiliary subunit is extracellular, highly glycosylated and associates with the membrane spanning δ subunit via disulfide bonds (Figure 10) (Gurnett and Campbell, 1996; Jay *et al.*, 1991; Lacinova, 2005).
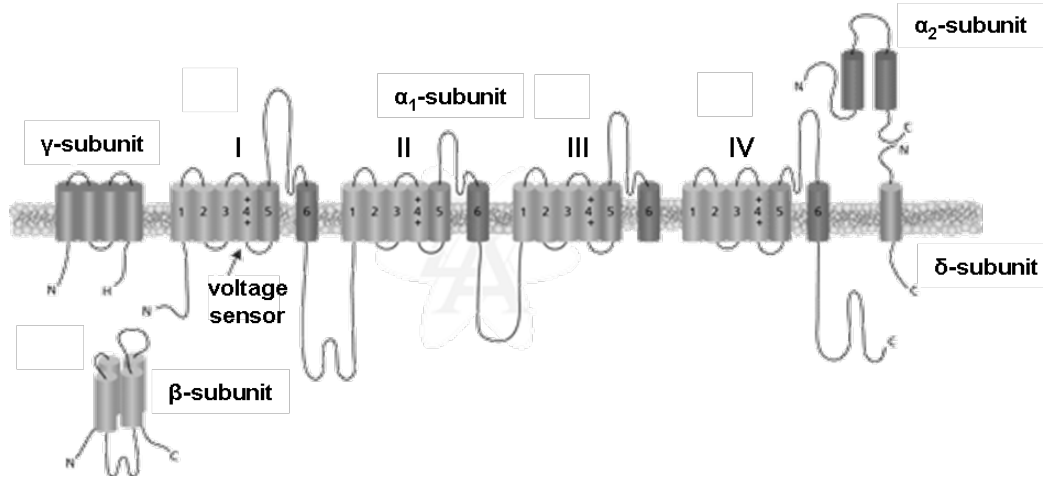
Figure 10: Topology of voltage-gated calcium channels.
Adapted from Sigma-Aldrich; http://www.sigmaaldrich.com/life-science/cell-biology/learning-center/pathway-slides-and/calcium-channel-structure.html.

The characteristic electrophysiological feature of voltage-gated calcium channel proteins is the extremely positive values of reversal potential, which implies that this family of proteins enable the influx of calcium ions. The transport of Ca^{2+} into the cell plays an important role in fibre contraction in heart and skeletal muscle tissues. The family of voltage-gated calcium channels can be divided into subtypes including long-lasting calcium channels (L-type: $Ca_v1.1$, $Ca_v1.2$, $Ca_v1.3$, $Ca_v1.4$), transient calcium channel (T-type: $Ca_v3.1$, $Ca_v3.2$, $Ca_v3.3$), neuronal calcium channel (N-type: $Ca_v2.2$), Purkinje cell calcium channel (P-type: $Ca_v2.1$) and toxin-resistant calcium channel (R-type: $Ca_v2.3$) (Lehmann-Horn and Jurkat-Rott, 1999).

Mutations of calcium channels may cause several muscle or neuronal channelopathies. Hypokalaemic periodic paralysis, which is classified as a dominant autosomal muscle channelopathy, is caused by mutations in *CACNC1* gene encoding for $Ca_v1.1$ calcium channel (Jurkat-Rott *et al.*, 1994; Ptacek *et al.*, 1994). In contrast to hyperkalemic periodic paralysis, the paralytic attacks last longer and can continue up to 24 hours. Moreover, hypokalaemic periodic paralysis is accompanied by paralysis caused by carbohydrate ingestion. The episodic ataxia type 2 (EA2), familial hemiplegic migraine (FHM) and spinocerebellar ataxia type 6 (SCA6) are hereditary channelopaties that alter proper functioning of the nervous system. The mutation of $Ca_v2.1$ α-subunit, which belongs to P/Q type calcium channels, results in dominantly inherited EA2

(Ophoff *et al.*, 1996). In comparison to the episodic ataxia type 1 (EA1), the fits are longer and vomiting is commonly present while the patient suffers from EA2. The FHM and SCA6 are caused by other dominantly inherited mutations of $Ca_v2.1$ (Zhuchenko *et al.*, 1997). Each disorder is caused by non-functional $Ca_v2.1$ calcium channel. Yet, the mechanism of action is affected by distinct mutations in gene encoding for $Ca_v2.1$. The presence of premature stop codons and splice-site mutations results in truncated $Ca_v2.1$ versions that are common for EA2 (Ophoff *et al.*, 1996). The mis-sense mutations lower the density of $Ca_v2.1$ channel in the cell membrane and also change the channel's kinetics. This kind of mutations and channel malfunctions are associated with FHM disease (Kraus *et al.*, 1998). Moreover, the $Ca_v2.1$ calcium cannels with extended polyglutamine sequence at the C-terminus are present in patients suffering from the SCA6 disease (Zhuchenko *et al.*, 1997). Although the aforementioned diseases are distinct, they still share some common symptoms (Denier *et al.*, 1999).

1.3.2.4. Voltage-gated sodium channel family

The voltage-gated sodium channel family is less diverse when compared to the families of potassium and calcium channel proteins. Furthermore, the functional properties of the known sodium channels are relatively similar. They are highly present in excitable tissues, for instance, in central and peripheral nervous systems, and in skeletal muscle.

Voltage-gated sodium channels initialize and propagate action potential. Those channels are characterised by fast kinetics, as they have the ability to open and close very rapidly. Similarly to the calcium channels, sodium channels reveal strongly positive reversal potential, which indicates that the sodium ions are transported down their concentration gradient from the outside of the cell to its interior, what is recorded as an inward current signal during patch clamp measurements. The α-subunit forms pores that transport ions across cell membrane, while the β subunits modulate activity of the α-subunit. Different parameters that describe voltage-gated sodium channels, such as voltage sensitivity, kinetics, localisation or the level of channel protein expression, are regulated by auxiliary subunits (Gurnett and Campbell, 1996). Several auxiliary subunits that support and modulate the activity of the main transport α-subunit

are known. The investigation of Isom and co-workers (1992) revealed the localisation of the β1-subunit and, what is more, the analysis of its amino acid sequence indicated a single transmembrane region with the glycosylated N-terminus localised at the outside of the cell.

1.3.2.4.1. Comparison between mammalian and prokaryotic voltage-gated sodium channels

Mammalian voltage-gated sodium channels consist of two subunits (α and β) (Catterall, 2000). The larger α-subunit with more than 2000 amino acid residues can conduct Na^+ ions across the membrane in a voltage-gated way, even in the absence of the β-subunit. The α-subunit consists of 24 transmembrane helices arranged as a pseudotetramer of four homologous, but not identical, domains with each domain consisting of six transmembrane helices (Catterall, 2000). Voltage-gated sodium channels transport sodium ions selectively across cellular membranes in response to changes in membrane potential. Their function is critical for a range of fundamental biological processes, such as neuronal signalling, muscle contraction and hormone secretion (Hille, 2001).

The eukaryotic voltage-gated sodium channel consists of a highly-processed α subunit, which is approximately 260 kDa, and is associated with auxiliary β subunits (Catterall, 2000). The pore-forming α subunit of Na_v is organized in four homologous domains (I–IV) (connected with loop-linkers), where each domain contains six transmembrane α helices (S1–S6) and an additional pore loop located between the S5 and S6 segments (Figure 11A). The S4 segments in each domain contain positively charged residues at every third position and it is a voltage sensor. The short intracellular loop connecting homologous domains III and IV serves as the inactivation gate that folds into the channel structure and blocks the pore from the inside during sustained depolarization of the membrane. The topology of the prokaryotic voltage-gated sodium channel is presented in Figure11C which clearly reveals the similar pattern of a single domain in Na_v channel.
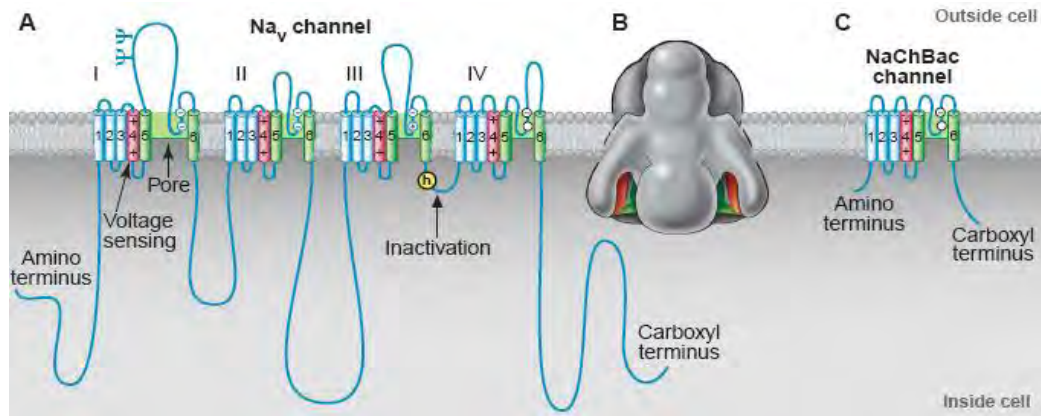
Figure 11: Comparison of mammalian Na$_v$ and prokaryotic NaChBac voltage-gated sodium channels (taken from Catterall, 2001).
(A) Topology of α subunit of the mammalian Na$_v$ voltage-gated sodium channel; the S5 and S6 segments and the pore loop region between them are highlighted in green; the positively charged S4 gating segments are highlighted in red; the inactivation gate and the Ile-Phe-Met (IFM) motive are highlighted in yellow; (B) The three-dimensional, bell shape structure of the Na$_v$ channel α subunit at 20 Å resolution, compiled from electron micrograph reconstructions (Sato et al., 2001); (C) NaChBac, the bacterial voltage-gated sodium channel).

In 2001, a group headed by David Clapham identified the first prokaryotic voltage-gated sodium channel from *Bacillus halodurans*, called NaChBac (Ren *et al.*, 2001). Subsequently, the group also identified eleven orthologs that form a voltage-gated sodium channel family (Koishi *et al.*, 2004). Bacterial voltage-gated sodium channels are postulated to be involved in processes such as motility, chemotaxis, and pH homeostasis (Ito *et al.*, 2004). In contrast to its eukaryotic counterpart, NaChBac from *B. halodurans* appears to consist of a single domain with six transmembrane helices (274 residues) and was also suggested to form a functional unit as a tetramer (Nurani *et al.*, 2008). Its kinetics of activation, inactivation and recovery from inactivation are 10-100 times slower than those of the mammalian voltage-gated sodium channels (Yue *et al.*, 2002). NaChBac reveals a high degree of homology to calcium channels. Although it is sodium-selective, it has recently been reported that by the introduction of point mutations of three aspartic acid residues in the pore domain, this sodium channel can be converted into a calcium selective channel (Yue *et al.*, 2002). What is more, NaChBac can be inhibited by calcium channel blockers (Ren *et al.*, 2001). Further functional studies of NaChBac combined with

mutagenesis identified important residues involved in the channel activation (Blanchet *et al.*, 2007; Zhao *et al.*, 2004a; Zhao *et al.*, 2004b) and inactivation (Pavlov *et al.*, 2005). The identification of Gly219 as a critical residue involved in the channel activation shed light on what may be a general mechanism for voltage-gated ion channel gating (Zhao *et al.*, 2004). The average size of functional prokaryotic channel protein is approximately 120 kDa and the requirements for auxiliary subunits have not yet been reported. The prokaryotic sodium channel requires four of these units for proper transfer of sodium ions (Ren *et al.*, 2001).

Two models of inactivation were reported for Na_v: fast (milliseconds) and slow (seconds) (Hille, 2001)**.** This indicated at least two gating modes which are probably mediated by different molecular mechanisms (Lehmann-Horn and Jurkat-Rott, 1999). Armstrong and co-workers (1973) established that the inactivation gate is accessible to cytoplasmic region. Moreover, the absence of charge movement during inactivation suggested positioning of the gate outside the membrane voltage field. Based on these studies, the ball-and-chain model was proposed (Armstrong and Bezanilla, 1977; Bezanilla and Armstrong, 1977). This type of inactivation mechanism was previously reported for potassium channels where the N-terminus serves as the docking ball, hence the so-called N-type inactivation (Hoshi *et al.*, 1990). Further studies implied that the III/IV loop of the sodium channel takes part in that fast inactivation process (Stuhmer *et al.*, 1989). The inactivation particle itself (the ball) seems to consist of three consecutive residues near the middle of the loop, namely, a Phe flanked by two other hydrophobic amino acids (IFM motive) (West *et al.*, 1992). However, a slight modification of this model was proposed, the so-called "hinged-lid", where one of the hinges consists of a pair of Gly situated in the vicinity of the Phe (Patton *et al.*, 1993; West *et al.*, 1992). The prokaryotic voltage-gated sodium channel does not contain an obvious cytoplasmic inactivation gate. It is thus more likely that the fast inactivation mechanism is not present in those channels. The second inactivation mechanism reported for Na_v and present in NaChBac is the slow inactivation, also known as a core-associated or C-type inactivation (Irie *et al.*, 2010). Not only it is kinetically distinct from the fast inactivation, but it also involves different structural elements – conformational changes inside the protein core (Lehmann-Horn and Jurkat-Rott, 1999). In contrast to Na_v, the

function of the prokaryotic voltage-gated sodium channel is relatively unknown. It was hypothesised that these channels may drive sodium-dependent flagellar motors in certain marine and alkaliphilic bacteria (Ito *et al.*, 2004).

1.4. Human diseases triggered by malfunction of voltage-gated sodium channels

The diseases caused by malfunction of ion channels are termed "channelopathies". The several neurological diseases, including neuromuscular disorders, movement disorders, migraine and epilepsy, are caused by inherited mutations of ion channels. The list of channelopaties is expanding rapidly and, depending on the system they interfere with inside the human body, they can be classified as muscle or neuronal channelopaties (Kullmann and Hanna, 2002). To date, nine genes encoding for sodium channel subtypes have been identified (*SCN1A-11A*, Sodium Channel isoform 1 Alpha). While *SCN1A* and *SCN2A* appear in the CNS, other types are found in the limbic system as well as in the heart and in the skeletal muscle (Alekov *et al.*, 2000). Since 2000, more than 150 unique mutations of the neuronal sodium channel *SCN1A* have been reported in patients with epilepsy (Meisler and Kearney, 2005). Many are sporadic mutations which cause a loss of function leading to an abnormal or diseased state. Coding variants of *SCN2A*, *SCN8A*, and *SCN9A* were also identified in patients with seizures, ataxia, and sensitivity to pain (Meisler and Kearney, 2005). The rapid pace of discoveries of these mutations in voltage-gated sodium channels suggests that the mutations are significant factors in the aetiology of neurological disease and contribute to cause many psychiatric disorders (Fujiwara *et al.*, 2003). The mutations of *SCN4A* gene encoding for $Na_v1.4$ sodium channel are responsible for the hyperkalaemic periodic paralysis which is an autosomal dominant disease (Fontaine *et al.*, 1990; Lehmann-Horn and Jurkat-Rott, 1999). The mutation is caused by single residue changes in the parts of the channel that are important for inactivation. In the presence of high K^+ levels, including those induced by diet, sodium channels fail to activate properly. This disease is characterized by muscle weakness, which is induced by different factors, including rest after exercise, potassium-rich foods, stress and certain pollutants (e.g. cigarette smoke), and can lead to uncontrolled shakes followed by paralysis. The thiazide diuretics and β-adrenoceptor agonists (Hanna *et al.*, 1998) as well as acetazolamide or

dichlorphenamide (Tawil *et al.*, 2000) all have positive effects in treatment of hyperkalaemia. With the exception of hyperkalaemic and normokalaemic periodic paralysis, the other phenotypic range of $Na_v1.4$ mutations can cause different disorders. The generalised epilepsy with febrile seizures plus (GEFS+) is caused by mutations in the genes encoding for $Na_v1.1$ and $Na_v1.2$ voltage-gated sodium channels (Escayg *et al.*, 2000; Sugawara *et al.*, 2001) and also by mutations present in the genes encoding for β1 auxiliary subunit (Wallace *et al.*, 1998). The $Na_v1.1$ and $Na_v1.2$ voltage-gated sodium channels, which are responsible for initiation and propagation of action potentials, are extensively present in the central nervous system. Furthermore, the inactivation of sodium channels is accelerated by the accessory subunit β1. The rates of sodium channels inactivation are lower than normal, which occurs due to the defect of $Na_v1.1$ and $Na_v1.2$ α subunits, or because the β1 subunit is non-functional (Wallace *et al.*, 1998). Various forms of epilepsy were reported, for example, drug-resistant epilepsy that is accompanied by intellectual impairment.

1.5. Patch clamp technique – *in vivo* activity assay

In this section the basics of the patch clamp method are outlined. The reason for the detailed description of the electrophysiological method is its non-standard usage in biochemistry. Internal and external composition of the cell leads to the differences in charge on each side of the membrane, creating a membrane potential. The concentration of ions like sodium, potassium, calcium, chloride on either side of the membrane is controlled by ion channels and pumps embedded in the membrane. Their opening or closing produce local changes in the membrane potential that causes electrical current to flow rapidly to other points in the membrane transmitting signals between different parts of electrically excitable cells (neurons). The number of different kind of ion channels in a particular cell is characteristic and can determine the type of cell that is being measured (axon of neurons has large density of sodium and potassium channels).

With minimum knowledge about the complexity of the lipid bilayer and the incorporated membrane molecules, Hodgkin and Huxley attempted in 1952 to characterize biophysical properties of cell membrane. Without the awareness of the existence of ion channels, they investigated electrical signals passing

through the giant squid axon cell membrane (Hodgkin and Huxley, 1952b), which revealed the presence of ion channels and gave an origin to the characterisation of sodium and potassium channels (Hodgkin and Huxley, 1952a). These groundbreaking discoveries became the base for further developments that led to both scientists being granted a Nobel Prize in 1963. The necessity of the application of Hodgkin and Huxley's method for smaller preparation as well as the ability of its usage in single cell recordings was implemented in further studies conducted by Erwin Neher and Bert Sakmann. In 1976, they reported that highly-accurate recordings of single channels can be obtained by introducing micropipettes to form high-resistance seals on tiny patches of the cell membrane (Neher and Sakmann, 1976). Their work had a great impact on medicine, as it improved the general understanding of essential biological processes that occur in the cell membrane, ion channel physiology and pathology. Neher and Sakmann's work was granted a Nobel Prize award in 1991.

Currently, the most popular electrophysiological technique is the "patch clamp" method which allows the measurement of electrical activity at a level of an individual ion channel. The method has multiple applications due to which the ionic currents can be monitored in a wide variety of tissue types and cells (Hamill *et al.*, 1981). The basics that underlie the patch clamp technique revolve around simple rules of physics, particularly laws of electricity. The most important is Ohm's Law that demonstrates the relationship between current, voltage and resistance (conductance):

$$V = I \times R \text{, or } I = \frac{V}{R},$$

where current (I) represents the net flow, voltage (V) represents driving force of current flow and resistance (R) represents the difficulty of ions passing through the ion channels.

From the equation describing Ohm's Law, the obvious dependencies can be concluded: the voltage is proportional to the current or, similarly, the current is inversely proportional to the resistance. This relationship provides the basis for the voltage clamp technique and allows for the monitoring of the activity of ion channels in two different modes. The outward current is defined as the outward movement of the positive charge (potassium ions) and is, by convention, visualised as an upward deflection, while an inward current is defined as the

inward movement of the positive charge (sodium ions) and is represented as a negative deflection. The mode when voltage is kept at a known value and changes in current are recoded is termed as a voltage clamp, whereas when voltage changes are recorded while current is held at a known value is called current clamp. When the voltage clamp technique is used, the changes of current monitored in time will reflect the changes in the resistance of cell membrane, caused by the opening and closing of ion channels. The high-fidelity current measurements can only be obtained when the initial formation of a high-resistance (giga-ohm) seal between cell membrane and tip of the recording micropipette is established.

The high-resistance seal will allow for the monitoring of ion movement that occurs as a result of a change in the current caused by ion transfer through ion channels only. As a result, false current measurement caused by leakage of ions between the pipette and membrane directly into bath solution will be eliminated. The formation of such a seal increases the signal-to-noise ratio to an acceptable level. Problems associated with the signal-to-noise ratio vary considerably with channel density and basic biophysical properties of the channel under study. In contrast to sodium channels, the electrophysiological characterisation of calcium channels is more technically difficult due to the fact that calcium channel currents are generally low in amplitude and activate at more positive potentials at which membrane noise is increased. The patch clamp technique uses small glass pipettes that are made from borosilicate capillary tubes. This type of glass material is used due to its relatively low electrical noise and its low melting temperature, which is important for an easy and proper pipette pulling. The size of a pipette tip is important for the successful formation of a high-resistant pipette-membrane seal. There are several developed variations of the voltage clamp technique (Figure 12). The cell-attached configuration (Figure 12A) enables the measuring of a group of ion channels located within the diameter of the tip of the recording pipette. The activity of ion channels within the whole cell is measured by applying a whole-cell voltage clamp (Figure 12B). Furthermore, both inside-out and outside-out voltage clamp techniques are used when single channel measurements are being performed (Figure 12C,D). There is a significant difference between the two aforementioned patch clamp techniques. The inside-out configuration, where the interior of the cell membrane is facing

the bath solution (exterior of the lipid bilayer exposed to the internal pipette solution), allows for the investigation of the internal environment changing effect.
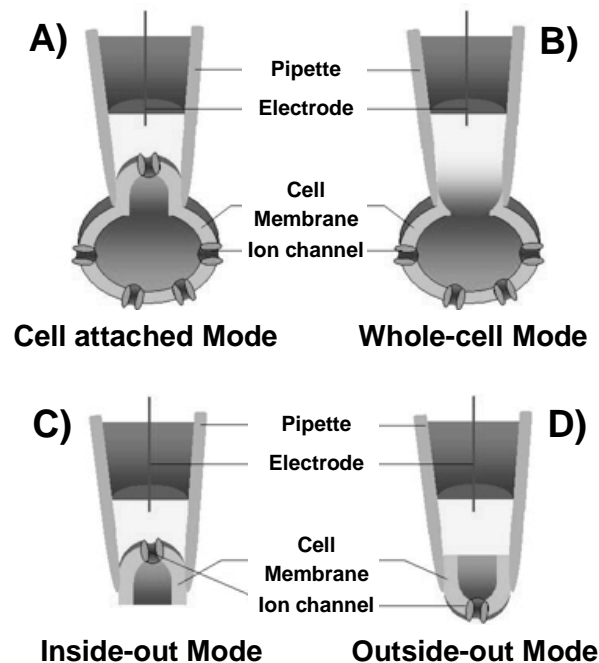
Figure 12: Different combinations of patch clamp technique.
Adapted from Bo Skaaning Jensen, NeuroSearch, Denmark.

The type of a voltage clamp technique used in the study of the voltage-gated sodium channel cloned from *Maricaulis maris* MCS10 (NaChMM) is a whole-cell combination. The pipette containing a conductive salt solution is attached on the top of a micromanipulator electrode, which allows the pipette to move precisely. The reference electrode is placed on the other side of the membrane, into the bath solution. As predicted by the Ohm's Law, as resistance increases, current decreases for a constant voltage. Hence, when the pipette enters the bath solution, a strong current signal appears (Figure 13A), as the resistance between the pipette tip and the bath solution is low. What is more, by lowering the pipette tip and directing it just above the cell, the current signal decreases across the pipette aperture (Figure 13B) as the resistance increases. Application of suction to the pipette further increases the resistance by creating a seal between the electrode and the membrane as well as by eliminating the current leakage across the pipette that leads to a low current signal (cell-attached patch clamp) (Figure 13C). Finally, the whole-cell patch configuration is obtained by applying a second suction that ruptures the patch of the membrane

(opens the cell) inside the tip of the electrode (Figure 13D). During this process, early gain giga-ohm seal can be disrupted and an "ion leakage" may occur (Figure 13E). Figure 13D presents the whole-cell voltage clamp with the retained giga-ohm seal.
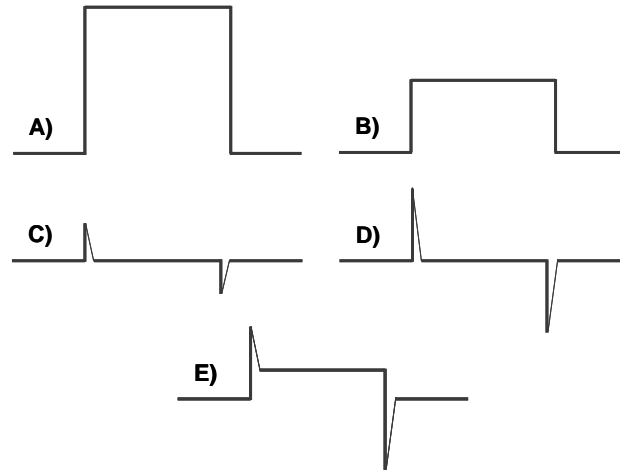
Figure 13: Current signals obtained during preparation of whole-cell voltage clamp.
A) Micropipette dipped in bath solution buffer – low resistance (~ 1 MΩ; B) Micropipette tip in close distance to the cell – increased resistance; C) Attached cell to micropipette – gigaohm seal (~ 8 GΩ); D) Open cell attached to the pipette – mega/gigaohm seal (~ 0.5 to 1 GΩ; E) Leaky cell – megaohm seal (~ 50 MΩ).

The conductance of an ion channel can be described according to the formula: $G = \dfrac{1}{R}$. Introduction of conductance G into Ohm's law will yield $G = \dfrac{I}{V}$. The conductance of a given ion channel can be determined from the slope of a graph plotting ion channel current as a function of membrane voltage (I-V curve). This approach provides information regarding the number of individual channels that are open within the studied membrane area. The current-voltage plot (I-V plot) is one of the indicators of the voltage-dependence of the investigated ion channel. The linearity of this function suggests that a conductance of current through the channel is not voltage-dependent (once opened, the conductance of the channel does not vary together with the changes in membrane potential). If the I-V curve for an ion channel is not linear, it suggests that the channel is voltage-dependent. An example of an I-V curve for the voltage-gated sodium channel (NaChBac) is presented in Figure 14C.
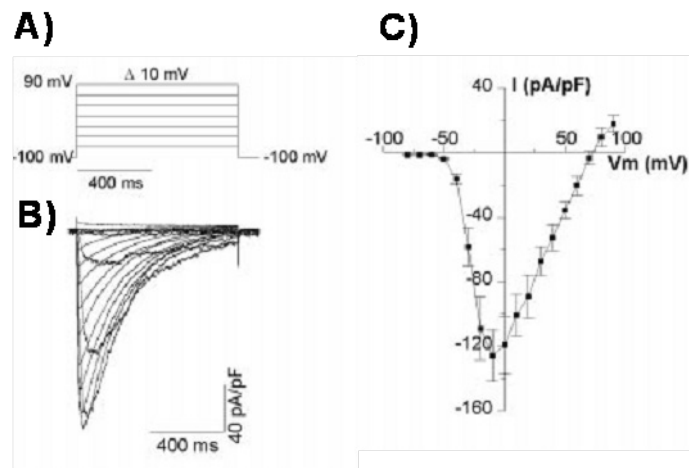
Figure 14: Example of an I-V curve.
Taken from Ren *et al.*, 2001; *A) wave stimulus – voltage pulse protocol; B) current recording C) I-V plot, where the peak of current is plotted against voltage pulses.*

The transport of Na^+ into the cell may be driven by the concentration of sodium ions and the negatively charged internal surface of the cell membrane that attracts positively charged sodium ions. The initialisation of the action potential at a particular point on the cell surface will cause an opening of voltage-gated sodium channels at this particular spot and a further depolarisation will progress along the cell membrane in a wave mode. The opened sodium channels depolarise membrane slightly ahead, which results in an opening of new voltage-gated sodium channel proteins and, in turn, a progressive increase in the transport of Na^+. Finally, within a fraction of a millisecond, the explosion of sodium influx takes place. In comparison to K^+ or Cl^-, the permeability of the cell membrane at the depolarised region is extremely large for Na^+ ions. The constant influx of Na^+ results in a subsequent equilibration of the cell membrane potential – E_{Na} (only for Na^+). The Na^+ ions are balanced on both sides of the cell membrane and a further sodium transport is stopped. The knowledge about the sodium concentrations inside and outside the cell enables calculation of the equilibrium potential (E_{Na}) by means of Nernst equation.

A simple scheme of voltage-gated channel behaviour is presented in Figure 15. Three conformations of an ion channel protein are depicted: open, closed, and inactivated (Kornreich, 2007). The transfer between the closed state and the open state is initiated by a cell membrane depolarisation/repolarisation.

The change from the activated state into the inactivated state occurs upon a continuous membrane depolarization. The recovery from inactivation describes the transfer of channel protein conformation from its inactivated state to its resting state. The three models of gating presented in Figure 15 can be used in an analysis of the data collected during the conducted experiments. Those models enable retrieving information about transition rates between the aforementioned states and additionally allow for the description of a channel preference for one of the conformations: closed, open, inactivated.
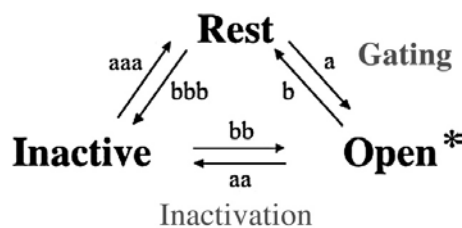
Figure 15: Simple Markov model representing the transition of an ion channel among its opened, closed, and inactivated conformations.
Taken from Kornreich, 2007; (*) represents a state that passes current.

Yet, while this three-state model may be sufficient to explain the biophysical properties of certain ion channels, more complex models containing numerous channel states and rate constants were proposed to characterize the function of others (Hille, 2001). The exact knowledge of these changes in the ion channel protein states is important, as certain drugs may have a greater binding affinity for a given channel conformation, which makes drug efficiency dependent on the amount of time the channel spends in that conformation.

1.5.1. Electrophysiological characteristics of Na_v *vs* NaChBac

Activities of eukaryotic and prokaryotic voltage-gated sodium channels were extensively studied by means of electrophysiological methods. The kinetics of Na_v activation, inactivation and recovery from inactivation are ~ 10-100 times faster than those of NaChBac (Yue et al., 2002). By comparison, the activation time of NaChBac was reported to be ~ 13 ms, with the activation midpoint of -24 mV (Ren et al., 2001), while the activation time of Na_v1.7 and Na_v1.8 channels present in rat dorsal root ganglion are 1.1 ms (activation midpoint: -28 mV) and

3.6 ms (activation midpoint: -1.2 mV), respectively (Vijayaragavan et al., 2004) . It was demonstrated that the human $Na_v1.8$ has two mechanisms of inactivation, slow and fast, the exact values of which have not however been presented yet (Zhao et al., 2007). While the slow inactivation has a voltage midpoint of -75 mV, the fast inactivation has a voltage midpoint of -34.4 mV (Zhao et al., 2007). To date, only one mechanism of inactivation has been discovered in prokaryotic voltage-gated sodium channels (Irie et al., 2010). The inactivation speed of NaChBac is 166 ms, with the inactivation midpoint of -40 mV (Ren et al., 2001). The two mechanisms of inactivation of Na_v are extensively studied and relatively well understood. Due to the absence of an obvious cytoplasmic inactivation gate in NaChBac, it is more likely that the fast inactivation mechanism does not exist in bacterial targets. The N-terminus of each domain in NaChBac was suspected to be responsible for the fast inactivation process. This idea was however abolished when no changes in inactivation kinetics were observed during the investigation of tandem dimers and tetramers (covalent linkages between homologous domains of NaChBac) of NaChBac (Pavlov et al., 2005). Moreover, Pavlov and co-workers introduced mutations in the selectivity filter of the pore region (S195E, S195D and S192E). While the mutation S192E did not show any effects on the NaChBac kinetics, the other two mutations influenced the midpoint of inactivation by 20 mV and the time of inactivation shortened. The data also reveal that the S192 localised in the pore region is engaged in the inactivation process, which is why the inactivation may involve a mechanism similar to that of the C-type inactivation in potassium channels (Pavlov et al., 2005; Liu et al., 1996). While the recovery from the inactivation of $Na_v1.8$ expressed in tsA201 was reported to be both fast (2.7 ms) and slow recovery (29.8 ms) (Zhao et al., 2007), the recovery from the inactivation for NaChBac was determined to be 0.66 s (at -100 mV) (Ren et al., 2001).

1.6. Aims of this study

This work will examine the production, crystallogenesis and X-ray analysis of an important class of membrane proteins, namely, the prokaryotic voltage-gated sodium channels, with the view to understand the mechanism of action of their counterparts in eukaryotic cells.

As membrane protein production and crystallisation are not predictable, a comprehensive screening approach based on the selection of voltage-gated sodium channels from three different organisms was started. The aim is to increase the likelihood of one of the chosen targets to lead to the obtaining of milligram quantities of homogenous and highly pure proteins required for functional and structural studies.

2. Materials and Methods

2.1. Materials

2.1.1. General equipment

Minispin microcentrifuge (Eppendorf)

Hettich Rotanta 460R centrifuge (DJB Labcare Ltd.)

Hettich Universal 32R centrifuge (DJB Labcare Ltd.)

Optima L-100 XP preparative ultracentrifuge (Beckman Coulter)

Electroporator (Medical Supply Co. Ltd.)

Q-Cycler PCR machine (Quantarus Ltd.)

Horizontal electrophoresis apparatus (Continental Lab Products CLP)

SDS-PAGE apparatus and Semi-dry blotting system (ATTO Corporation)

ÄKTAprime and ÄKTAexplorer 100 (GE Healthcare)

Typhoon Imaging System (GE Healthcare)

Sonicator HD 2200 Sonoplus (Wenk LabTec GmbH)

Chirscan spectropolarimeter (Applied Photophysics)

Axopatch 200B amplifier (Molecular Devices)

Micropipette puller (Sutter instrument)

Gel Doc Imaging System (Genius Genie)

ND-1000 spectrophotometer (NanoDrop Technologies, US)

2.1.2. Oligonucleotides

The primers, used in the cloning process, were designed and analysed with the Integrated DNA Technologies software. Oligonucleotides were purchased from Eurofins MWG Operon, Ebersberg, Germany.

2.1.2.1. Primers used in preparation of prokaryotic constructs

<u>Oligonucleotides used in the amplification of gene encoding for Na$^+$ channel from *B. halodurans*:</u>

(I) pTrcHis2A/NaChBac_for

       ***Nco*I**
5'-ACT**CCATGG**TAATGAAAATGGAAGCTAGACAGAAACAGAACAGC-3'

(II) pTrcHis2A/NaChBac_rev

       Xho*I**   ***Thrombin cleavage site
5'-ATT**CTCGAG**A*AGAACCTCTTGGTACTAG*TTTCGATTGTTTAAGCAAGCT

TTTTAGC-3'

(XI) pET15b(+)/NaChBac_for

    *Nde*I

5'-GC**CATATG**AAAATGGAAGCTAGACAGA-3'

(XII) pET15b(+)/NaChBac_rev

    *Bam*HI

5'-C**GGATCC**TCATTATTTCGATTGTTTAAGC-3'

<u>Oligonucleotides used in the amplification of gene encoding for Na⁺ channel from *S. pomeroyi:*</u>

(III) pTrcHis2A/NaChSP_for

    *Nco*I

5'-AAT**CCATGG**TAATGCAAAGAATGCAGGCCTTT-3'

(IV) pTrcHis2A/NaChSP_rev

    *Xho*I   *Thrombin cleavage site*

5'-ATT**CTCGAG**A*AGAACCGCGTGGCACCAG*CTTTTTGGTTTCACCAAG-3'

<u>Oligonucleotides used in the amplification of gene encoding for Na⁺ channel from *M. maris:*</u>

(V) pTrcHis2A/NaChMM_for

    *Nco*I

5'-AAT**CCATGG**TAATGAAGGCTTTTGTCGAAAGCGCG-3'

(VI) pTrcHis2A/NaChMM_rev

    *Xho*I   *Thrombin cleavage site*

5'-ATT**CTCGAG**T*ACTACCTCTTGGTACTAA*CTCCGACCTGTCAGCG-3'

(XIII) pET15b(+)/NaChMM_for

    *Nde*I

5'-GC**CATATG**AAGGCTTTTGTCGAAAGCGCG-3'

(XIV) pET15b(+)/NaChMM_rev

    *Bam*HI

5'-C**GGATCC**TCATTACTCCGACCTGTCAGCG-3'

<u>Oligonucleotides used in the amplification of shorter versions of gene encoding for Na⁺ channel from *M. maris:*</u>

(VII) pTrcHis2A/NaChMMΔ18C_for = (V)

    *Nco*I

5'-AAT**CCATGG**TAATGAAGGCTTTTGTCGAAAGCGCG-3'

(VIII) pTrcHis2A/NaChMMΔ18C_rev

    *Xho*I   *Thrombin cleavage site*

5'-ATT**CTCGAG**T*ACTACCTCTTGGTACTAA*CGAGCGCTGAACCAGG-3'

(IX) pTrcHis2A/NaChMMΔ58C_for = (V)

    *Nco*I

5'-AAT**CCATGG**TAATGAAGGCTTTTGTCGAAAGCGCG-3'

(X) pTrcHis2A/NaChMMΔ58C_rev

       *Xho*I   *Thrombin cleavage site*
5'-ATT**CTCGAG**T*ACTACCTCTTGGTACTAA*CTTGGCCTGCAGGCTG-3'

2.1.2.2. Primers used in preparation of eukaryotic constructs

<u>Oligonucleotides used in the amplification of EGFP gene:</u>

(XV) pEGFP-C1/EGFP_for

      *Eco*RI
5'-CG**GAATTC**CGCCACCATGGTGAGCAAGG-3'

(XVI) pEGFP-C1/EGFP_rev

      *Bam*HI
5'-CCG**GGATCC**TTACTTGTACAGCTCGTCCATGCC-3'

(XXI) pcDNA3.1(+)/EGFP-Zeo_for

       *Bsa*BI
5'-CATA**GATAAGGATC**GTTCGCATGGTGAGCAAGGGCGAGGAGC-3'

(XXII) pcDNA3.1(+)/EGFP_over_lap

5'-GCACTGGTCAACTTGGCGTCCATGCCGAGAGTGATC-3'

<u>Oligonucleotides used in the amplification of zeocin gene:</u>

(XXIII) pcDNA3.1(+)/Zeo_over_lap

5'-GATCACTCTCGGCATGGACGCCAAGTTGACCAGTGC-3'

(XXIV) pcDNA3.1(+)/EGFP-Zeo_rev

      *Asu*II
5'-ATAA**TTCGAA**CCCCAGAGTAATGCTCAGTCCTGCTCCTCGGC-3'

<u>Oligonucleotides used in the amplification of gene encoding for Na⁺ channel from *B. halodurans*:</u>

(XXV) pcDNA3.1(+)/EGFP-Zeo/NaChBac_for

      *Eco*RI
5'-CCC**GAATTC**GCCACCATGAAAATGGAAGCTAGACAG-3'

(XXVI) pcDNA3.1(+)/EGFP-Zeo/NaChBac_rev

      *Xho*I
5'-CCG**CTCGAG**CGTTCATTTCGATTGTTTAAGCAAGC-3'

<u>Oligonucleotides used in the amplification of gene encoding for neuromodulin signal sequence:</u>

(XXIX) pcDNA3.1(+)/EGFP-Zeo/Neu-NaChMM_for

      *Hin*dIII
5'-CCC**AAGCTT**GCCACCATGCTGTGCTGTATGAGAAG-3'

(XXX) pcDNA3.1(+)/EGFP-Zeo/Neu_over_lap

5'-CGCGCTTTCGACAAAAGCCTTCATGATCTTTTGGTCCTCATCATT-3'

Oligonucleotides used in the amplification of gene encoding for Na⁺ channel from *M. maris:*

(XVII) pEGFP-C1→N1/NaChMM_for

*Age*I
5'-ATTT**ACCGGT**CGCCACCATGAAGGCTTTTGTCGAAAGCGC-3'

(XVIII) pEGFP-C1→N1/NaChMM_rev

*Eco*RI
5'-AACCAGCAAGC**GAATTC**TCCGACCTGTCAGCGTCCTTCTC-3'

(XIX) pEGFP-C1/NaChMM_for

*Xho*I
5'-CCG**CTCGAG**CGATGAAGGCTTTTGTCGAAAGCG-3'

(XX) pEGFP-C1/NaChMM_rev

*Eco*RI
5'-CG**GAATTC**CTACTCCGACCTGTCAGCGTCCTTCTCG-3'

(XXVII) pcDNA3.1(+)/EGFP-Zeo/NaChMM_for

*Hin*dIII
5'-CCC**AAGCTT**GCCACCATGAAGGCTTTTGTCGAAAGC-3'

(XXVIII) pcDNA3.1(+)/EGFP-Zeo/NaChMM_rev

*Xho*I
5'-CCG**CTCGAG**CTACTCCGACCTGTCAGC-3'

(XXXI) pcDNA3.1(+)/EGFP-Zeo/NaChMM_over_lap

5'-AATGATGAGGACCAAAAGATCATGAAGGCTTTTGTCGAAAGC-3'

(XXXII) pcDNA3.1(+)/EGFP-Zeo/Neu-NaChMM_rev = (XXVIII)

*Xho*I
5'-CCG**CTCGAG**CTACTCCGACCTGTCAGC-3'

2.1.3. Enzymes

A wide selection of restriction enzymes has been used in this study. Most of the enzymes, including *Asu*II, *Bam*HI, *Eco*RI, *Hin*dIII, *Nco*I, *Nde*I and *Xho*I, were purchased from Roche Applied Science; these work at 37°C. The *Age*I (37 °C) and *Bsa*BI (60°C) restriction enzymes were purchased from New England BioLabs. As the *Bsa*BI enzyme is a *dam* methylation-sensitive enzyme, the plasmid DNA was propagated in *E. coli* K12 ER2925 strain. The enzymes used in the ligation and PCR gene amplification (T4 DNA Ligase and Phusion High-Fidelity DNA Polymerase) were purchased from New England BioLabs.

2.1.4. Bacterial strains and mammalian cell line

2.1.4.1. Plasmid propagating *Escherichia coli* strains

The following *E. coli* strains were used for plasmid propagation:

– TOP10 containing streptomycin resistance [<u>*Genotype:*</u> F$^-$ mcrA Δ(mrr-hsdRMS-mcrBC) φ80lacZΔM15 ΔlacX74 nupG recA1 araD139 Δ(ara-leu)7697 galE15 galK16 rpsL(Str^R) endA1 λ$^-$];

– DH5α containing nalidixic acid resistance [<u>*Genotype:*</u> F$^-$ endA1 glnV44 thi-1 recA1 relA1 gyrA96 deoR nupG Φ80d*lacZ*ΔM15 Δ(*lacZYA-argF*)U169, hsdR17(r$_K^-$ m$_K^+$), λ$^-$];

– K12 ER2925 containing chloramphenicol resistance. This strain is deficient in *dam* and *dcm* methylation. Therefore, it was especially useful in propagation of pcDNA3.1(+) vector which was further subjected to restriction digestion with *dam* sensitive *Bsa*BI endonuclease [<u>*Genotype:*</u> ara-14 leuB6 fhuA31 lacY1 tsx78 glnV44 galK2 galT22 mcrA dcm-6 hisG4 rfbD1 R(zgb210::Tn10)TetS endA1 rpsL136 dam13::Tn9 xylA-5 mtl-1 thi-1 mcrB1 hsdR2].

2.1.4.2. Protein expressing *Escherichia coli* strains

The *E. coli* BL21(DE3) strain and its derivatives listed below contain a T7 promoter, transcription from which can only occur upon IPTG induction All strains are deficient in Lon and OmpT proteases, which reduce the degradation of overexpressed proteins. The *E. coli* strains used for protein expression with their corresponding genotypes are as follows:

– BL21(DE3) [<u>*Genotype:*</u> F$^-$ *ompT gal dcm lon hsdS$_B$*(r$_B^-$m$_B^-$) λ(DE3) [lacI lacUV5-T7 gene 1 ind1 sam7 nin5];

– C41(DE3) [<u>*Genotype*</u>: F$^-$ *ompT hsdS$_B$*(r$_B^-$m$_B^-$) *gal dcm* (DE3)];

– C43(DE3) [C41(DE3) derivative];

– BL21star(DE3) [<u>*Genotype:*</u> F$^-$ *ompT hsdS$_B$*(r$_B^-$m$_B^-$) *gal dcm* rne131];

– BL21(DE3) CodonPlus-RIL is chloramphenicol resistant and contains a plasmid encoding for *argU*, *ileY*, and *leuW* tRNAs. These tRNAs recognize the codons: AGA/AGG (arginine), AUA (isoleucine), CUA (leucine), respectively. [<u>*Genotype:*</u> F$^-$ *ompT hsdS$_B$*(r$_B^-$m$_B^-$) *dcm*+ Tetr *gal* λ(DE3) *endA* Hte [*argU ileY leuW* Cam^R]];

– Rosetta (DE3) is chloramphenicol resistant and contains a plasmid encoding for tRNA molecules, which recognise the following rare codons: AGA/AGG (arginine), GGA (glycine), AUA (isoleucine), CUA (leucine), and CCC (proline). [*Genotype:* F$^-$ *ompT hsdS*$_B$(r$_B^-$ m$_B^-$) *gal dcm* (DE3) pRARE2 (Cam^R)].

2.1.4.3. Mammalian cell line

tsA201 mammalian cell line is a sub-clone of a human embryonic kidney (HEK293) cell line stably-transfected with the SV40 large T-antigen. The tsA201 cell line has been used in a variety of functional expression assays. It also has been reported to produce high levels of recombinant proteins due to its lower sensitivity to the toxic effect of foreign protein production.

2.1.5. Antibiotics and antibodies

The antibiotics and antibodies were purchased from Sigma-Aldrich. The following antibiotics were used at the indicated working concentrations: ampicillin (100 μg/mL), kanamycin (50 μg/mL), chloramphenicol (34 μg/mL), streptomycin (50 μg/mL). The monoclonal Anti-polyHistidine-peroxidase antibody was used at a 1:3000 dilution.

2.1.6. Detergents

The high-purity detergents: n-dodecyl-β-D-maltopyranoside (DDM), n-undecyl-β-D-maltopyranoside (UDM), n-decyl-β-D-maltopyranoside (Goldman et al.), Cymal-6, n-nonyl-β-D-glucopyranoside (NG), n-octyl-β-D-glucopyranoside (OG), Anzergent 3-14, Fos-Choline-12 were purchased from Anatrace.

Sodium dodecyl-sulfate (SDS) and Tween 20 were purchased from Sigma-Aldrich.

2.1.7. Protein and DNA ladders

The Quick-Load^{TM} 100 bp DNA Ladder; Quick-Load^{TM} 1 kb DNA Ladder; Prestained Protein Marker, Broad Range (6-175 kDa); Prestained Protein Marker, Broad Range (7-175 kDa) were purchased from New England Biolabs. The Prestained Protein Ladder Prep0925 was purchased from Bioman Scientific.

2.2. Methods

2.2.1. Cultivation of *Bacillus halodurans* C-125, *Silicibacter pomeroyi* DSS-3 and *Maricaulis maris* MCS10 for genomic DNA extraction

Bacillus halodurans C-125 was obtained from the German Collection of Microorganisms and Cell Cultures (Deutsche Sammlung von Mikroorganismen und Zellkulturen, DSMZ). It was grown in the Alkaline *Bacillus* medium at 37 °C and 250 rpm, overnight (Nielsen, 1995). [autoclaved 900 mL containing: 10 g of peptone, 5 g of yeast extract (YE), 1 g of K_2HPO_4 dissolved in 0.9 mL of dH_2O; filter sterilised 100 mL containing: 10 g of glucose, 10 g of Na_2CO_3]

Silicibacter pomeroyi DSS-3 was kindly supplied by Dr Wendy Ye (University of Georgia, Athens, GA). It was grown in ½ YTSS medium at 30 °C, 250 rpm in dark, overnight (Gonzalez *et al.*, 2003). [2.5 g/L tryptone, 4 g/L YE, 20 g/L sea salts]

Maricaulis maris MCS10 was kindly supplied by Professor of Microbiology John Smit (University of British Columbia, Canada). It was grown in the modified SPYEM broth at 30 °C and 200 rpm for 3 days (Abraham *et al.*, 1999). [1:44 ratio of 50x PYE and 3 % sea salts solution (autoclaved separately); 50x PYE contained: 100 g/L peptone and 50 g/L YE]

2.2.2. DNA preparative work

Centrifugation steps were performed with Minispin microcentrifuge, although the Hettich Rotanta 460R centrifuge was used when temperature control was required, the.

Unless specified otherwise, all procedures involving commercially available kits and chemicals were performed according to manufacturers' recommendations.

2.2.2.1 Genomic DNA purification

The genomic DNA purification was performed using the Tris-saturated phenol-chloroform extraction (Cheng and Jiang, 2006). The yield and purity of the DNA were assessed spectrophotometrically by measuring the absorbances at 260 and 280 nm and calculating the A260/A280 ratio.

A 1-mL overnight cell culture suspension was centrifuged at 15,000 g for 1 min. The supernatant was removed and the cell pellet was washed twice with 400 µL STE buffer [10 mM Tris pH 8, 100 mM NaCl, 1 mM EDTA]. Cells were then pelleted at 15,000 g for 1 min following resuspension in 200 µL of TE buffer [10 mM Tris pH 8, 1 mM EDTA]. For cell lysis, 150 µL of Tris-saturated phenol (pre-warmed to room temperature) was added and gently mixed by inverting the tube (to avoid shearing of genomic DNA). This was followed by centrifugation at 15,000 g for 5 min at 4 °C to separate the aqueous phase from the organic phase. 150 µL of the upper aqueous phase was transferred to a clean 1.5 mL tube and 50 µL of TE buffer was added and mixed with 150 µL of chloroform. Another centrifugation step was performed for 5 min at 15,000 g and 4 °C. The lysate was purified by chloroform extraction until a white interface was no longer present (this procedure was repeated three times). Finally, the upper 150 µL aqueous phase was transferred to a clean 1.5 mL tube and 50 µL of TE buffer and 5 µL of 10 mg/mL RNase were added. The mixture was incubated at 37 °C for 10 min and 100 µL of chloroform was added to the tube, mixed and centrifuged for 5 min at 15,000 g and 4 °C. The 150 µL upper aqueous phase containing purified DNA was transferred to a clean 1.5 mL tube and used directly for the subsequent experiments or stored at -20 °C.

2.2.2.2. PCR reaction

PCR reactions (50 µL) were performed in the Q-Cycler PCR machine using Phusion High-Fidelity DNA Polymerase with the supplied HF reaction buffer. The complete reaction mixture contained 5 ng of template DNA (genomic or plasmid DNA). The thermal-time profiles of the PCR reactions were designed by considering the oligonucleotide melting temperatures.

2.2.2.3. DNA enzyme digestion

A 5 µg of DNA was subjected to a restriction digestion in a volume of 50 µL using 2.5 U of restriction enzyme and the supplied buffer. The incubation time varied from 2 h (for analysis of clones) to overnight (for cloning purposes).

2.2.2.4. Purification of DNA after enzymatic reactions

The PCR products and DNA, which were previously subjected to digestion reactions, were purified using the QIAquick Gel Extraction Kit (QIAGEN). It can be used by applying two different protocols: gel extraction protocol or cleanup protocol.

The extraction from the agarose gel was performed only if more than one DNA fragment was synthesised during the PCR reaction and in between the gene sub-cloning procedures. In other cases, a simple cleanup was performed.

2.2.2.5. Ligation

The ligation reactions were performed with the T4 DNA Ligase at the room temperature. The molar ratio of vector to insert in the reaction mixture was 1:3 and total amount of DNA did not exceed 0.5 µg.

2.2.2.6. Ethanol precipitation

DNA was transferred to a mixture containing a one-tenth volume of 3 M sodium acetate buffer (pH 5.2) at 4 °C and a two-and-a-half volumes of ice cold ~ 100 % ethanol for incubation at -20 °C for 90 min. The sample was then centrifuged for 30 min at 20,000 g and 4 °C. The ethanol was then removed and 200 µL of ice cold ~ 70 % ethanol was added, followed by a 5-min centrifugation at 4 °C and 20,000 g. Finally, the ethanol was removed and the remaining minute amounts were evaporated at 37 °C in a water bath.

2.2.2.7. Preparation of the electrocompetent *E. coli* cells

The electrocompetent cells were prepared as described by (Dower *et al.*, 1988) with modifications. All washing procedures listed below were performed on ice.

A single colony of *E. coli* was inoculated into 5 mL of 2x TY medium [16 g/L Tryptone, 5 g/L NaCl, 10 g/L YE] in a 100-mL flask and incubated at 37 °C and 275 rpm, overnight. Subsequently, 2.5 mL of the culture was inoculated into 250 mL of 2x TY and incubated on a shaking platform (250 rpm) at 37 °C. The bacterial culture was removed when the OD^{600} reached 0.5 and was transferred to sterile, pre-chilled 750 mL centrifuge bottle and incubated on ice for 20 min. Cells were then centrifuged at 3,000 g for 15 min at 4 °C. The

supernatant was discarded and cell pellet was resuspended by gentle agitation in 100 mL of ice-cold sterile distilled water followed by centrifugation at 3,000 g for 15 min at 4 °C. The supernatant was discarded and the cell pellet was resuspended by gentle agitation in 50 mL of ice-cold 1 mM HEPES pH 7.4 buffer and centrifuged at 3,000 g for 15 min at 4 °C. The cells were then gently washed with 10 mL of 1 mM HEPES/10 % glycerol pH 7.4 solution and centrifuged at 3,000 g for 15 min at 4 °C. The cell pellet was then gently resuspended in 0.5 mL of sterile 25 % glycerol, and 50 µL aliquots were prepared in sterile pre-chilled microcentrifuge tubes while being kept on a water-ice bath. The cells were used immediately for transformation or were snap-frozen with liquid nitrogen and stored at -80 °C.

2.2.2.8. Transformation by electroporation

The transformation was performed with an electroporator using 1 mm electroporation cuvette (Eppendorf). The plasmid mixture, competent cells and electroporation cuvette were incubated on ice, while SOC broth [20 g/L Tryptone, 0.5 g/L NaCl, 5 g/L YE, 2.44 g/L $MgSO_4$, and filter-sterilized 20 mM glucose] was incubated at 37 °C prior to the experiment. The ligation mixture (after ethanol precipitation) or purified plasmid was transformed into *E. coli* cells by adding approximately 15 ng of DNA into 50 µL of electrocompetent cells. The whole mixture was then transferred into an electroporation cuvette and placed in the apparatus. After an impulse of 1,800 V was applied, the transformed cells were washed out from the cuvette with 1 mL of pre-warmed SOC broth and incubated 37 °C for 1 h. The cells were streaked on LA plates [10 g/L Tryptone, 5 g/L NaCl, 5 g/L YE, 15 g/L agar] containing the appropriate antibiotic and incubated at 37 °C overnight.

2.2.2.9. Glycerol stock preparation

A 0.5-mL of bacterial culture of OD^{600} = 0.6 was mixed with 0.5 mL of 50 % sterile glycerol and snap-frozen with liquid nitrogen and stored at -80 °C.

2.2.2.10. Purification of vector/plasmid

The isolation of vector/plasmid was performed with QIAprep Spin Miniprep Kit purchased from QIAGEN. Briefly, the plasmid DNA released from

lysed bacterial cells is able to bind to the silica in the presence of chaotropic agents. The purifications were always performed from 5-mL overnight cultures.

2.2.2.11. Preparation of plasmids

Prokaryotic expression vectors pTrcHis2A and pET15b(+) were kindly provided by Dr Takeshi Shimizu of Chiba University (School of Medicine, Japan) and Professor Slawomir Milewski (Gdansk University of Technology, Poland), respectively. The mammalian expression vectors pEGFP-C1, pcDNA3.1(+), pcDNA3.1/Zeo(+), pECFP-Mem were obtained from Professor Christoph Fahlke (Hannover Medical School, Germany).

The integrity of all prokaryotic and eukaryotic constructs was confirmed through DNA sequencing (Eurofins MWG Operon).

2.2.2.11.1. Prokaryotic constructs

2.2.2.11.1.1. Cloning into pTrcHis2A vector

The pTrcHis2A (Invitrogen) expression vector with the C-terminal fusion peptide encoding for *myc* epitope and $(His)_6$-tag is a pBR322 derivative. It includes the *trc* (*trp-lac*) promoter, which allows a high level of protein expression in *E. coli* (Brosius *et al.*, 1985; Mulligan *et al.*, 1985). It also contains the ampicillin resistance gene for selection.

The NaChBac, NaChSP and NaChMM genes encode for the voltage-gated sodium channel proteins from the different bacterial species. The NaChMMΔ18C and NaChMMΔ58C are the genes encoding for the truncated versions of NaChMM channel proteins lacking 18 and 58 residues at the C-termini, respectively. All these genes were PCR-amplified from their respective genomic DNA template and cloned into the pTrcHis2A vector using the *Nco*I and *Xho*I restriction sites.

1. The gene encoding for NaChBac was amplified with the primers:

    (I) pTrcHis2A/NaChBac_for//(II) pTrcHis2A/NaChBac_rev.

2. The gene encoding for NaChSP was amplified with the primers:

    (III) pTrcHis2A/NaChSP_for//(IV) pTrcHis2A/NaChSP_rev.

3. The gene encoding for NaChMM was amplified with the primers:

    (V) pTrcHis2A/NaChMM_for//(VI) pTrcHis2A/NaChMM_rev.

4. The gene encoding for truncated NaChMMΔ18C was amplified with the primers:

   (VII) pTrcHis2A/NaChMMΔ18C_for//(VIII) pTrcHis2A/NaChMMΔ18C_rev.

5. The gene encoding for truncated NaChMMΔ58 was amplified with the primers:

   (IX) pTrcHis2A/NaChMMΔ58C_for//(X) pTrcHis2A/NaChMMΔ58C_rev.

All the reverse primers included a thrombin cleavage site for the removal of the $(His)_6$-tag located at the C-termini of recombinant proteins.

2.2.2.11.1.2. Cloning into pET15b(+) vector

The pET15b(+) (Addgene) expression vector contains an N-terminal $(His)_6$-tag sequence followed by the thrombin cleavage site and three cloning sites (Bjork *et al.*, 2006). It also includes a T7 promoter for recombinant protein expression and pBR322 origin of replication with the ampicillin resistance selection marker.

The NaChBac and NaChMM genes were amplified from the genomic DNA template using the following set of primers, respectively:

(XI) pET15b(+)/NaChBac_for//(XII) pET15b(+)/NaChBac_rev,

(XIII) pET15b(+)/NaChMM_for//(XIV) pET15b(+)/NaChMM_rev.

Furthermore, the blunt-ended PCR products were directly inserted into the pCR-BluntII-TOPO vector (Invitrogen) yielding TOPO/NaChBac and TOPO/NaChMM plasmids. This pre-cloning step was introduced for a further highly efficient digestion with restriction enzymes and subcloning the desired genes into the pET15b(+) vector at the *Bam*HI-*Nde*I restriction sites.

2.2.2.11.2. Eukaryotic constructs

2.2.2.11.2.1. Cloning of NaChMM into pEGFP-C1

The pEGFP-C1 (Clontech) vector encodes for a red-shifted variant of the wild-type green fluorescent protein (GFP) (Chalfie *et al.*, 1994; Prasher *et al.*, 1992), which has been optimized for a brighter fluorescence and a higher expression in mammalian cells. The genes cloned into the MCS were expressed under the CMV promoter as a fusion at the C-terminus of the enhanced green fluorescent protein (EGFP) that provides for the microscopical localisation of the fusion protein *in vivo*. This vector contains the kanamycin resistance marker for

selection in prokaryotic cells and the neomycin resistance marker for establishing stable eukaryotic cell lines.

The NaChMM gene was amplified with the set of primers: (XIX) pEGFP-C1/NaChMM_for//(XX) pEGFP-C1/NaChMM_rev using the genomic DNA as the template. The PCR product was cloned into pEGFP-C1 vector at the *Xho*I-*Eco*RI restriction sites yielding the pEGFP-C1/NaChMM plasmid encodes for the recombinant protein where the EGFP is N-terminally fused with the NaChMM.

2.2.2.11.2.2. Modification of pEGFP-C1 vector and cloning of NaChMM

The pEGFP-C1 vector was modified to introduce the EGFP fusion at the C-terminus of the NaChMM protein. In order to achieve this, two amplification reactions were performed. The EGFP gene was amplified with the following set of primers: (XV) pEGFP-C1/EGFP_for//(XVI) pEGFP-C1/EGFP_rev using pEGFP-C1 vector DNA as the template. Similarly, the NaChMM gene was amplified with the set of primers: (XVII) pEGFP-C1→N1/NaChMM_for/ /(XVIII) pEGFP-C1→N1/NaChMM_rev using thegenomic DNA as the template. Furthermore, the EGFP gene was removed from the pEGFP-C1 vector using the *Age*I and *Eco*RI restriction enzymes and replaced by the NaChMM gene. The amplified EGFP was cloned into the MCS of pEGFP-C1 vector using the *Eco*RI and *Bam*HI endonucleases yielding the pEGFP-C1→N1/NaChMM plasmid, which encodes for the recombinant protein with an EGFP fusion at the C-terminus of the NaChMM.

2.2.2.11.2.3. Modification of pcDNA3.1(+) vector

The pcDNA3.1(+) (Invitrogen) expression vector is a pcDNA3 derivative. It includes two promoters: (i) a CMV promoter that provides a high-level expression of recombinant proteins in a wide range of mammalian cells (Boshart *et al.*, 1985) and (ii) an SV40 early promoter, which allows for episomal replication in cell lines that are latently infected with SV40 or that express the SV40 large T antigen (e.g. COS–7) (Fiers *et al.*, 1978). This vector contains the ampicillin resistance marker for selection in prokaryotic cells and the neomycin resistance marker for the establishment of stable eukaryotic cell lines.

The pcDNA3.1(+) vector was modified by removing the neomycin resistance and introducing an easy-to-detect EGFP selection marker. However, the features of a stable cell line had to be preserved; therefore, the zeocin resistance gene was also introduced under the direction of the SV40 promoter. In order to achieve that, two amplification reactions were performed.

1. The EGFP gene was amplified using pEGFP-C1 vector DNA as a template with the following set of primers:

   (XXI) pcDNA3.1(+)/EGFP-Zeo_for//(XXII) pcDNA3.1(+)/EGFP_over_lap.

2. The zeocin gene was amplified using the pcDNA3.1/Zeo(+)vector DNA as a template (Invitrogen) with the following set of primers:

   (XXIII) pcDNA3.1(+)/Zeo_over_lap//(XXIV) pcDNA3.1(+)/EGFP-Zeo_rev.

3. An overlap PCR was performed, resulting in the fusion of zeocin to the N-terminus of EGFP (EGFP-Zeo). The following set of primers was used in the overlap PCR reaction:

   (XXI) pcDNA3.1(+)/EGFP-Zeo_for//(XXIV) pcDNA3.1(+)/EGFP-Zeo_rev.

The newly-created EGFP-Zeo gene has been cloned in the place of neomycin resistance in the pcDNA3.1(+) vector at the *Bsa*BI-*Asu*II restriction sites resulting in the construction of pcDNA3.1(+)/EGFP-Zeo plasmid which encodes for EGFP-Zeo selection marker under SV40 promoter.

2.2.2.11.2.4. Cloning of NaChBac into modified pcDNA3.1(+) vector

The NaChBac gene was amplified with the (XXV) pcDNA3.1(+)/EGFP-Zeo/NaChBac_for//(XXVI) pcDNA3.1(+)/EGFP-Zeo/NaChBac_rev primers using the genomic DNA as the template. The PCR product was cloned downstream the CMV promoter of the pcDNA3.1(+)/EGFP-Zeo vector at the *Eco*RI-*Xho*I restriction sites. This resulted in the creation of pcDNA3.1(+)/EGFP-Zeo/NaChBac plasmid encoding for the native NaChBac independently expressed from EGFP-Zeo protein.

2.2.2.11.2.5. Cloning of NaChMM into modified pcDNA3.1(+) vector

The NaChMM gene was amplified with the (XXVII) pcDNA3.1(+)/EGFP-Zeo/NaChMM_for and (XXVIII) pcDNA3.1(+)/EGFP-Zeo/NaChMM_rev primers using the genomic DNA as the template. The PCR product was cloned downstream the CMV promoter into the

pcDNA3.1(+)/EGFP-Zeo vector at the *Hin*dIII-*Xho*I restriction sites, resulting in the creation of pcDNA3.1(+)/EGFP-Zeo/NaChMM plasmid that encodes for the native NaChMM sodium channel independently expressed from the EGFP-Zeo protein.

2.2.2.11.2.6. Cloning of Neu-NaChMM into modified pcDNA3.1(+) vector

To create the fusion of neuromodulin signal sequence with NaChMM, two PCR amplification reactions were performed:

1. The neuromodulin signal sequence was amplified using the pECFP-Mem vector DNA as the template (Clontech) with the following set of primers:
   (XXIX) pcDNA3.1(+)/EGFP-Zeo/Neu-NaChMM_for//
   (XXX) pcDNA3.1(+)/EGFP-Zeo/Neu_over_lap.
2. The NaChMM gene was amplified using the genomic DNA as the template with the following set of primers:
   (XXXI) pcDNA3.1(+)/EGFP-Zeo/NaChMM_over_lap//
   (XXXII) pcDNA3.1(+)/EGFP-Zeo/Neu-NaChMM_rev.
3. An overlap PCR was performed resulting in the fusion of neuromodulin signal sequence to the N-terminus of NaChMM (Neu-NaChMM). The following set of primers was used in the overlap PCR reaction:
   (XXIX) pcDNA3.1(+)/EGFP-Zeo/Neu-NaChMM_for//
   (XXXII) pcDNA3.1(+)/EGFP-Zeo/Neu-NaChMM_rev.

The created Neu-NaChMM gene was cloned under the CMV promoter into the pcDNA3.1(+)/EGFP-Zeo vector at the *Hin*dIII-*Xho*I restriction sites resulting in the creation of pcDNA3.1(+)/EGFP-Zeo/Neu-NaChMM plasmid that encodes for the recombinant Neu-NaChMM independently expressed from EGFP-Zeo protein.

2.2.2.12. Agarose electrophoresis

The DNA analyses were performed according to Sambrook (2001) using the horizontal electrophoresis apparatus. The 0.8 % and 1.3 % gels were prepared with Low EEO Agarose (MELFORD) and 1x TAE pH 8 buffer with the addition of either ethidium bromide (1:10,000) or SYBR Safe DNA gel stain (1:30,000) (Invitrogen). The DNA samples were prepared by the addition of 6x sample loading buffer (0.25 % bromophenol blue, 40 % sucrose) to a 1x final

concentration. The electrophoretic runs were performed at 8 V/cm in 1x TAE buffer. The 50x TAE pH 8 buffer contained: 242 g/L of Trizma base, 100 mL/L of 0.5 M EDTA, 49 mL/L of glacial acetic acid.

2.2.3. Protein experimental work

2.2.3.1. Protein expression conditions

All the media were sterilised by autoclaving (125 °C, 10 min) and stored at 4 °C unless stated otherwise. The bacterial cells were grown with shaking at 250 rpm shaking at all times. Each expression trial was initiated by the inoculation from the glycerol stock and pre-culturing overnight in LB medium [10 g/L Tryptone, 5 g/L NaCl, 5 g/L YE, 100 µl/ml ampicillin]. The samples analysed through SDS-PAGE were collected according to the optical density of cell culture (volume of collected sample in respect to $OD^{600} = 1$).

The comparison of final total protein levels was based on expression levels estimated by the SDS-PAGE and Western-blot of the whole cell extract and also by the final amount of produced biomass (measurements of final optical density at 600 nm).

2.2.3.1.1. Protein expression using terrific broth

The initial expression of NaChBac protein was performed in the terrific broth (TB) [11.8 g/L Peptone, 23.6 g/L YE, 9.4 g/L K_2HPO_4, 2.2 g/L of KH_2PO_4]. 1 mL of overnight culture was inoculated into 50 mL of TB containing ampicillin. The NaChBac protein production was initiated at $OD^{600} = 0.6$ using **0.5 mM** and **1 mM** IPTG for comparison. The expression was performed for 4 h.

A 1-mL overnight bacterial culture containing the plasmid encoding for the NaChMM protein was inoculated into 50 mL of TB containing ampicillin. Protein production was induced by the addition of 1 mM IPTG at the $OD^{600} = $ **0.6**, **1** and **1.2**. The expression was performed for 4 h.

The overnight cultures of *E. coli* BL21(DE3) strains containing plasmids encoding genes for NaChBac, NaChSP and NaChMM prokaryotic voltage-gated sodium channel proteins were inoculated at the ratio 1:50 (v/v) into TB or or TB+G (terrific broth containing 1.5 % of glucose), in the presence of ampicillin.

Protein production was induced with 1 mM. The production of NaChBac protein was initiated at OD^{600} = 0.6, while the production of NaChSP and NaChMM proteins was initiated at OD^{600} = 1.2. Following the addition of IPTG, the culture growth temperature was adjusted to 25 ºC and 37 ºC, and expression was continued at these temperatures for 4 h. Samples were collected hourly for the SDS-PAGE analysis.

2.2.3.1.2. Protein expression using auto-inducing medium

The overnight cultures of *E. coli* BL21(DE3) strains containing the different plasmids encoding genes for NaChBac, NaChSP and NaChMM were inoculated at the ratio 1:50 (v/v) into the modified ZYP-5052 auto-inducing medium (Naumann et al.) (Studier, 2005) containing ampicillin. After 3-h incubation at 37 °C, the temperature was either lowered to 25 °C or kept at 37 °C. The protein production was performed for the following 45 h. Samples were collected every 12 h for SDS-PAGE analysis. [1 L of AUM consisted of (i) 928 mL of ZY (10 g N-Z amine and 5 g YE), (ii) 1 mL of 1 M $MgSO_4$, (iii) 20 ml of 50x 5052 (250 g/L glycerol, 25 g/L glucose, 100 g/L lactose) and (iv) 50 mL of 20x NPS (66 g/L $(NH_4)_2SO_4$, 136 g/L KH_2PO_4, 142 g/L Na_2HPO_4)]

2.2.3.1.3. Expression in different *E. coli* hosts

The investigation of expression levels in different *E. coli* hosts was performed by applying stable growing conditions. While NaChBac and NaChSP were produced in the AUM at 25 °C, the expression of NaChMM protein was performed in the TB at 25 °C (cell culture was induced with 1 mM IPTG at OD^{600} = 1.2). The *E. coli* strains were grown in the presence of ampicillin. Samples were collected every 12 h (NaChBac and NaChSP protein expression) and 1 h (NaChMM protein expression) for the SDS-PAGE analysis.

2.2.3.2. Electrophoresis and Western-blotting analysis

2.2.3.2.1. SDS-PAGE

The sodium dodecyl sulphate polyacrylamide gel electrophoresis (SDS-PAGE) was performed as described by Laemmli (1970). The 16 % gels were used for standard protein separations, and 12 % gels were used in the analysis of cross-linking experiments. The gels were stained post-electrophoresis with the

coomassie-based staining solution InstantBlue (Expedeon). The resolving gels were prepared by mixing the following stock solutions: 40 % of acrylamide/bis-acrylamide 29:1 (Sigma-Aldrich), 1.5 M Tris/HCl pH 8.8, 10 % SDS solution, 10 % APS solution and N,N,N′,N′-tetramethylethylenediamine (TEMED) (Sigma-Aldrich). The stacking gels were prepared using the same stock solutions except 1.5 M Tris/HCl pH 8.8, which was replaced by 1 M Tris/HCl pH 6.8. The electrophoretic runs were performed in 1x SDS-PAGE running buffer [5x SDS-PAGE running buffer: 72 g/L glycine, 15.14 g/L Trizma base, 5 g/L SDS, pH 8.3]. The samples were prepared by the addition of 1x SDS-PAGE sample loading buffer (in whole cell extract analysis) or by the addition of 5x SDS-PAGE sample loading buffer [30.28 g/L Trizma base, 20 % β-mercaptoetanol, 10 % SDS, 0.1 % bromophenol blue, 50 % glycerol, pH 6.8] to a 1x final concentration (purified protein samples).

2.2.3.2.2. Western-blotting

The Western-blotting analysis (Burnette, 1981) was performed using the semi-dry method. The $(His)_6$-tagged proteins were transferred onto nitrocellulose membrane (0.2 μm; Bio-Rad) using the transfer buffer [3 g/L Trizma base, 11.3 g/L Glycine, 100 mL/L methanol, pH 8.3]. The protein transfer, performed at 80 mA for 1 h, was followed by a 1-h incubation of the blotting membrane in 5 % skimmed milk solution to block non-specific antibody binding and further 1-h incubation in 30 mL of antibody solution [0.3 g BSA, 12.5 μL Tween 20, 10 μL anti-polyHis antibody]. Finally, the immunological reaction was developed with 3,3',5,5'-tetramethylbenzidine (TMB) (Sigma-Aldrich). The skimmed milk and antibody solutions were prepared in the 1x TBS buffer [5x TBS: 30 g/L Trizma base, 44 g/L NaCl, 11 g/L $CaCl_2$, pH 7.6]; the extensive washes of the blotting membrane after the incubation step were performed with 1x TBS buffer.

2.2.3.3. Protein purification

The purification process was fully automated using the ÄKTAprime and ÄKTAexplorer 100 systems. The recombinant proteins were quantified by measuring the absorbance at 280 nm and using the molecular weight and extinction coefficient in calculations (Fasman, 1992) (buffers without imidazole were considered a necessity as imidazole has a strong absorbance at 280 nm).

The final samples were typically concentrated to ~ 10 mg/mL using a Vivaspin concentrator (Sartorium Stedim Biotech, 100 kDa MWCO), aliquoted and flash-frozen for storage at -80 °C.

2.2.3.3.1. Membrane isolation

After completion of the selected targets' expressions, the cells were harvested by centrifugation and resuspended in the lysis buffer (1x PBS pH 7.4, 10 mM $MgCl_2$, protease inhibitors (Sigma-Aldrich) – 1 tablet/20 g of cell pellet, 0.2 mg/mL lysosyme, 25 μg/mL DNase); [10x PBS pH 7.4: 2 g/L KCl, 80 g/L NaCl, 14.4 g/L Na_2HPO_4, 2.4 g/L KH_2PO_4]. A 1-g wet cell pellet was resuspended in 5 mL of lysis buffer. The cell lysis mixture was then sonicated with a processing frequency of 20 kHz on ice. The bacterial cell wall was disrupted by applying a pulsation of 1 s and amplitude of 30 %. The sonication time varied with the volume of sonication mixture and it was 30 min/50 mL of cell lysis mixture. Membrane protein isolation procedure was completed using two different protocols: (i) Solubilisation of membrane proteins, which included the addition of 1 % DDM into the disrupted cell mixture followed by an overnight incubation at 4 °C with stirring and (ii) isolation of membranes, which involved extensive centrifugation steps as follows: the disrupted cells were centrifuged at 4 °C, 10,000 g for 30 min to remove unbroken cells, cell debris and possible inclusion bodies. The supernatant was then ultracentrifuged at 4 °C, ~ 200,000 g for 1 h to pellet the cell membranes. The pellet containing cell membranes was resuspended in 1x PBS buffer pH 7.4 and solubilised overnight with 1 % DDM at 4 °C under stirring. The unsolubilised materials were removed by centrifugation at 10,000 g for 30 min. The supernatant was then filtered through a 0.45-μm filter before the addition of 20 mM imidazole prior to affinity purification.

The extraction of NaChMM recombinant protein from the cell membranes was performed with different detergents at the following concentrations: 10 % DM, 3 % UDM, 3 % Cymal-6, and 1 % Anzergent 3-14, and in this case the first procedure of membrane protein extraction was applied.

2.2.3.3.2. Affinity chromatography

In order to bind $(His)_6$-tagged voltage-gated ion channel proteins (1 mg of recombinant protein/1 mL of nickel charged resin), the solubilised membrane proteins with the added 20 mM imidazole and 1 % DDM were loaded onto a column packed with Ni Sepharose 6 Fast Flow resin (GE Healthcare). The affinity resin was previously equilibrated with 1x PBS buffer pH 7.4 containing 500 mM NaCl, 20 mM imidazole and 0.05 % DDM. The solubilised membrane was applied at a rate of 1 mL/min with the following washing and elution steps of 2.5 column volumes performed at a rate of 2 mL/min with 60 mM imidazole and 100 mM imidazole. The recombinant proteins were eluted with the buffer containing 250 mM imidazole. The fractions containing voltage-gated ion channel proteins were combined, concentrated with a Vivaspin concentrator (100 kDa MWCO) and subjected to gel filtration chromatography or desalting with a PD10 column (GE Healthcare). The removal of high salt buffer and imidazole was crucial for an efficient $(His)_6$-tag removal by thrombin digestion (Thrombin Clean Cleave Kit; Sigma-Aldrich).

The purity of NaChMM protein after affinity purification was established according to the protein band intensities visualised on the SDS-PAGE. The intensities of protein bands were measured with CurveScan Version 1.03.000 and the peak area after applying 20 % cut off was calculated using "OriginPro 8". This was followed by the percentage calculation of of NaChMM protein and contaminants at each elution step.

The NaChMM recombinant protein was also purified using different detergents at the following concentrations: 0.02 % of DDM, 0.2 % DM, 0.06 % UDM, 0.06 % Cymal-6, 0.05 % Anzergent 3-14.

The regeneration of the Ni Sepharose 6 Fast Flow resin was performed regularly to maintain sufficient recombinant protein binding. The first step including stripping the nickel ions from the resin was achieved by a washing step with 20 mM NaP_i pH 7.4, 500 mM NaCl and 50 mM EDTA (one resin volume), followed by an extensive wash with water (three resin volumes) and a further application of 1 M NaOH and incubation for 2 h. Finally, NaOH was removed by an extensive rinsing with water and the resin was nickel recharged using 100 mM $NiSO_4$ solution (about one resin volume) followed by a water wash (three resin volume).

2.2.3.3.3. Size exclusion chromatography (SEC)

The size exclusion chromatography was performed with the HiLoad Superdex 200 prep grade XK 16/60 (GE Healthcare) column equilibrated with the desired buffer (Figure 16). A 2.5-mL protein sample was injected onto the column and eluted with a flow rate of 1 mL/min. The collected fractions were analysed by a 16 % SDS-PAGE and the selected samples were pooled and concentrated with Vivaspin (100 kDa MWCO).
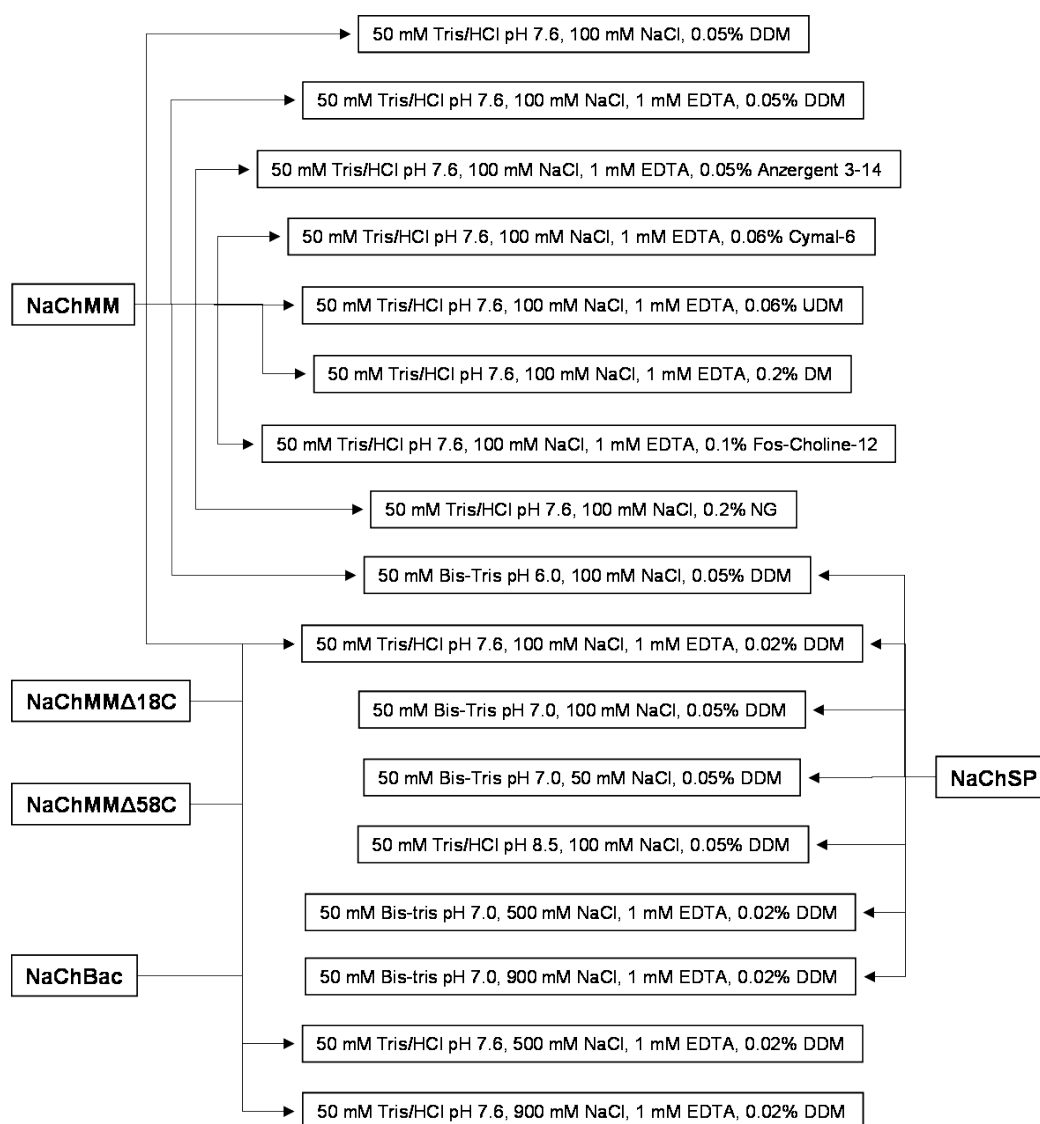
Figure 16: Scheme representing the different buffers used in gel filtration chromatography of NaChBac, NaChSP, NaChMM, NaChMMΔ18C and NaChMMΔ58C recombinant proteins.

2.2.3.3.4. Ion exchange chromatography

The anion exchange chromatography was performed when detergent exchange was required. The purified NaChMM protein sample in 50 mM Tris/HCl pH 7.6, 100 mM NaCl and 0.05 % DDM was diluted 100 times with the same buffer, but in the absence of NaCl to reduce the sample conductivity. This was then applied onto the prepacked MonoQ 5/50 GL column (GE Healthcare), which was previously equilibrated with 50 mM Tris/HCl, pH 7.6 and 0.05 % DDM. The bound NaChMM protein was washed (10 column volumes) with 50 mM Tris/HCl pH 7.6, containing 0.2 % NG and the protein was then eluted with the same buffer containing 500 mM NaCl. The protein sample was further desalted using a PD10 desalting column (GE Healthcare) into the same buffer, containing 100 mM NaCl and concentrated with Vivaspin (100 kDa MWCO). The anion exchange chromatography was performed at a constant flow rate of 1 mL/min. The same procedure was applied when detergent was exchanged into 0.1 % Fos-Choline-12; however, the buffers additionally contained 1 mM EDTA.

2.2.3.3.5. Removal of (His)$_6$-tag

The protein was digested with thrombin in 50 mM Tris/HCl pH 7.6, 100 mM NaCl, 1 mM EDTA, 0.02 % DDM and an additional 10 mM CaCl$_2$. One-hundred µL of thrombin-agarose suspension was pre-washed with 50 mM Tris/HCl pH 8 and 10 mM CaCl$_2$ and applied for cleavage of 1 mg protein in 1 mL (Thrombin Clean Cleave Kit; Sigma-Aldrich). The time (1 h, 2 h, 4 h, 6 h, 24 h) and temperature (4 ℃ and RT) of thrombin digestion was preliminarily investigated. However, further experiments were performed by incubation of the protein-thrombin resin mixture at 4 ℃ with agitation overnight.

After the completed digestion, the thrombin resin was recovered by applying the mixture onto a column, separating the protein solution and the thrombin resin. The eluate was subjected to an affinity chromatography (1 mL of nickel resin, gravity flow) in order to remove any undigested recombinant protein and other impurities. The resulting protein sample was concentrated using a Vivaspin (100 kDa MWCO) and applied onto a gel filtration column as a final polishing step.

The sample buffer for NaChMM cleavage varied in detergent types and their concentrations: 0.02 % DDM, 0.2 % DM, 0.06 % UDM, 0.06 % Cymal-6, 0.05 % Anzergent 3-14. Moreover, the sample buffer used for $(His)_6$-tag removal from NaChSP recombinant protein was 50 mM Bis-tris pH 7, 500 mM NaCl, 1 mM EDTA, 10 mM $CaCl_2$, 0.02 % DDM.

The thrombin resin was regenerated by extensive washing steps, first with 50 mM Tris/HCl pH 8, 500 mM NaCl and second with 50 mM Tris/HCl pH 8. Finally, thrombin resin was resuspended in a 1:2 resin-to-buffer ratio in 20 mM Tris/HCl pH 8, 50 % glycerol and stored at -20 °C.

2.2.3.4. Biochemical characterisation

2.2.3.4.1. Cross-linking experiments

Five µg of pure NaChMM protein (0.25 mg/mL) in 20 mM HEPES pH 7.4, 100 mM NaCl, 1 mM EDTA containing the selected detergent (0.05 % DDM, 0.06 % UDM, 0.2 % DM, 0.06 % Cymal-6 and 0.05 % Anzergent 3-14) was cross-linked with glutaraldehyde (Sigma-Aldrich). The protein solution was incubated with 0.3 % of glutaraldehyde at room temperature. The reaction was quenched after 15 min by the addition of 2 µL of 1 M Tris pH 7.6 and incubated for 10 min followed by the addition of 3 µL of 5x SDS sample loading buffer. Samples were then analysed on 12 % SDS-PAGE.

The cross-linking reaction with formaldehyde was performed for 15 min, and did not require quenching with 1 M Tris buffer pH 7.6 but the 5x SDS sample loading buffer was directly added and samples were analysed by 12 % SDS-PAGE.

2.2.3.4.2. BN-PAGE

The recombinant NaChMM protein purified in DDM, DM, UDM, Cymal-6, Anzergent 3-14 was analyzed in a non-denaturing polyacrylamide gel (Swamy *et al.*, 2006). The 4 % stacking and the 11 % resolving blue native (BN) gels were prepared using the following stock solutions: 1 M ε-aminocaproic acid, 1 M Bis-tris pH 7.0, 40 % acrylamide solution ratio 29:1, 10 % APS and TEMED (Eichacker, 2006). The cathode buffer [15 mM Bis-tris, pH 7, 50 mM Tricine and 0.002 % CBB] and anode buffer [50 mM Bis-tris pH 7] were applied in different compartments of the electrophoretic chamber. The protein sample

was prepared by mixing with 10x sample loading buffer [100 mM Bis-tris pH 7, 5 % CBB, 500 mM ε-aminocaproic acid, 25 % glycerol] to a 1x final concentration. Bovine serum albumin (Absalom et al.) was used as a molecular weight marker: monomer (66 kDa), dimer (132 kDa) and trimer (198 kDa). Five μg of BSA and each of the analysed NaChMM samples were loaded on the gel. The electrophoresis was performed at the constant 100 V for ~ 6 h at 4 °C. The gel was de-stained with a mixture of 20 % methanol and 10 % acetic acid.

2.2.3.4.3. Circular dichroism

The α-helical secondary structure of NaChMM protein was analysed through circular dichroism (CD) spectroscopy using a Chirascan spectropolarimeter equipped with a 150 W Xenon arc lamp and Julabo AWC 100 water-circulation system for temperature control. Prior to the analysis of influence of different detergents on the secondary structure, the samples were diluted 10 times with 10 mM KP_i pH 7.6, in the presence of the detergent (0.05 % DDM, 0.2 % DM, 0.06 % UDM, 0.06 % Cymal-6, 0.05 % Anzergent 3-14). The spectra were recorded with a 1-nm bandwidth and a 2-s time-per-point at 20 °C, over the wavelength range from 260 nm to 180 nm. Four scans were collected for each of 1 mg/mL protein sample and its corresponding baseline in the same 0.01 cm path length Suprasil cuvette. Using the Pro-Data Chirascan processing software, the averaged baseline spectra were subtracted from the corresponding averaged protein spectra and smoothed with a Savitsky-Golay filter with a factor of 4. Spectra were converted into mean residue ellipticity, using a mean residue weight value of 112.4. The deconvolution and statistical analysis of the CD spectra were performed using the CDNN algorithm (Bohm *et al.*, 1992).

2.2.3.4.4. MALDI-TOF-MS and N-terminal sequencing

The matrix-assisted laser desorption/ionization time-of-flight – mass spectrometry (MALDI-TOF-MS) and N-terminal sequencing were performed by Alphalyse A/S (Denmark). Both analytical processes required 3 mg/mL of NaChMM sample in 5 mM Tris/HCl pH 7.6 and 0.8 % OG. In MALDI-TOF-MS analysis, NaChMM sample was deposited on a metal target and co-crystallized with a light-absorbing sinapinic acid matrix. A laser beam was directed at the

dried sample matrix resulting in desorption and ionisation of sample molecules. The desorbed and ionized masses were measured in a time-of-flight (Di Cera et al.) mass analyzer. The mass of the NaChMM was calculated as the average mass of the intact non-protonated protein. The mass spectra were calibrated using the external calibration standards. The N-terminal sequence of NaChMM was determined by N-terminal sequencing based on the Edman degradation chemistry. The analysis was carried out in an ABI Procise 494 sequencer on an acid-etched glass fibre disk with conversion to a PTH-AA residue and identified by HPLC chromatography.

2.2.3.5. Crystallisation

The crystallisation experiments were performed with the sitting-drop vapour diffusion method, which is simple and extremely scalable for screening and optimisation. In total, 11 different protein samples (Figure 17) were subjected to the crystallisation screening process. These samples differed in the:

- ♦ protein concentrations (5 , 10 and 30 mg/mL);
- ♦ detergent type (DDM, UDM, DM, Cymal-6, Anzergent 3-14, NG, DDM:DM = 1:1, Fos-Choline-12);
- ♦ detergent concentration (0.02 % DDM, 0.05 % DDM);
- ♦ $(His)_6$-tagged and non $(His)_6$-tagged NaChMM.
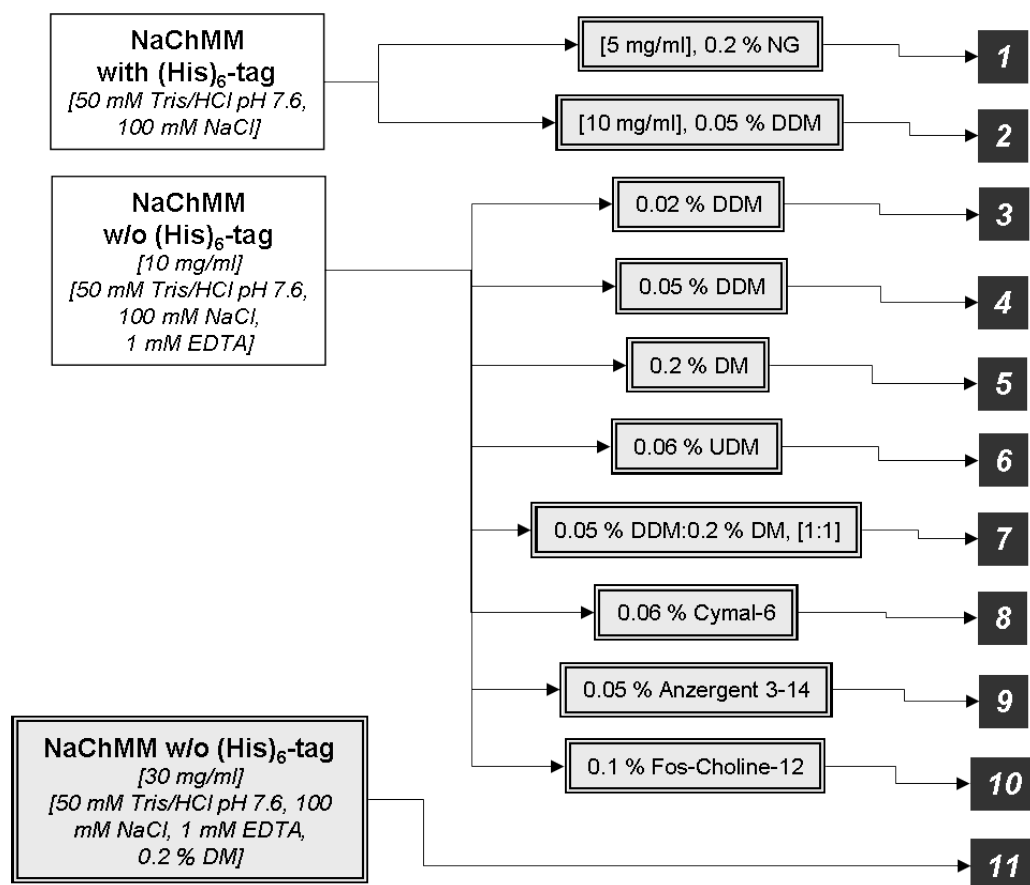
Figure 17: Characteristics of NaChMM protein samples subjected to crystallisation screening.
To simplify further description of crystallisation screening process, a single number code, which corresponds to a unique sample, was introduced.

The crystallisation screens used in this study are listed below (Table 2).

Table 2: List of crystallisation screens used in this study.

Letter	Screen Name	Company	No of conditions
(A)	Crystal Screen		48
(B)	Crystal Screen 2		48
(C)	Natrix		48
(D)	Index		96
(E)	SaltRx		96
(F)	PEG/Ion	(Hampton Research)	48
(G)	PEG/Ion 2		48
(H)	MembFac		48
(I)	Crystal Screen Lite		50
(K)	Detergent Screen HT		96
(L)	Wizard I		48
(M)	Wizard II	(Emerald BioSystems)	48
(N)	Wizard III		48
(O)	MemStart		48
(Q)	MemSys		48
(P)	ProPlex	(Molecular Dimensions Limited)	96
(R)	PACT premier		96
(S)	JCSG-*plus*		96
(T)	MemGold		96
(U)	JBScreen Cryo	(Jena Bioscience)	96
(W)	ModifMemGold	(In home prepared, see Appendix	96
(X)	PEG Screen	I: Crystallisation screens)	96

2.2.3.5.1. Manual crystallisation experiments

Nine protein samples were subjected to crystallisation screening with five different crystallisation screens (D, H, I, W, X) (Figure 18). The experiments were performed by mixing 1 µL of protein sample with 1 µL of crystallisation reagent using MVD/24 crystal growth chambers.
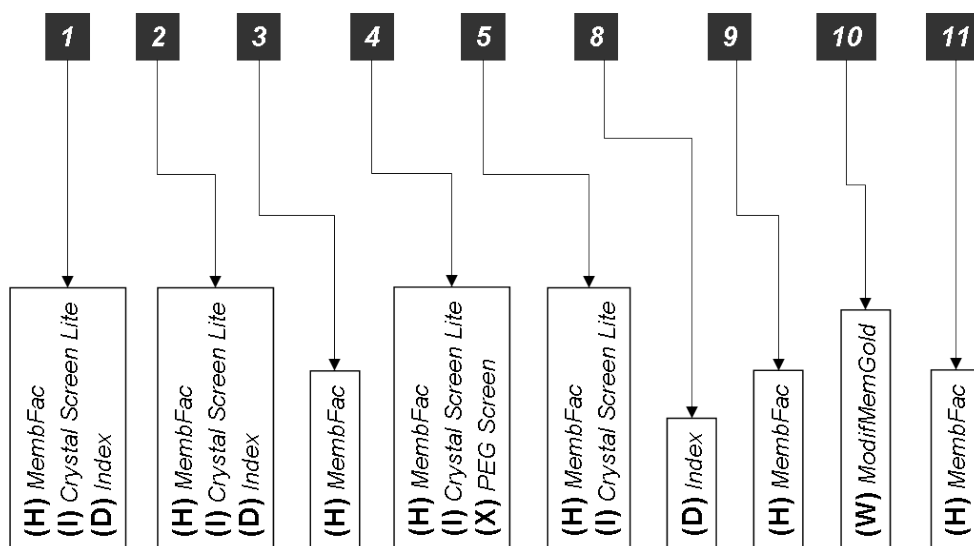
Figure 18: **Scheme summarising the manual crystallisation screening process.**
Unique samples (1-5 and 8-13) used in crystallisation with various crystallisation screens.

2.2.3.5.2. Automated crystallisation experiments

The experiments were performed using the Mosquito Nanodrop crystallisation robot located in the Imperial College London and pre-prepared crystallisation plates. Access to the crystallisation facility was kindly provided by Dr Jeremy Moore. Six different NaChMM samples were used in the crystallisation screening with seventeen standard crystallisation screens and a detergent screen (K) (Table 2) (Figure 19). The screening was performed on the MRC/96 double-well crystal growth chambers by mixing 50 nL of protein sample with 50 nL of crystallisation reagent. The detergent screening was performed by mixing 250 nL of protein sample and 250 nL of crystallisation reagent prior to the addition of 50 nL of detergent.
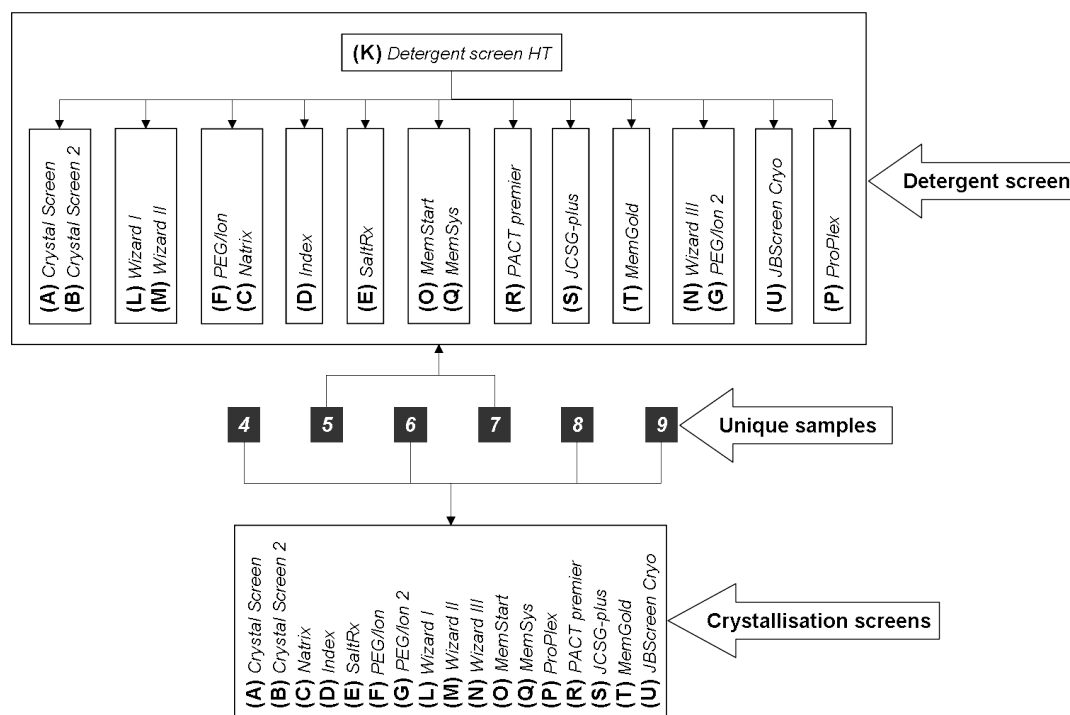
Figure 19: Scheme summarising the automated crystallisation screening process.
Unique samples (4-9) used in crystallisation with various crystallisation screens and detergent screen.

2.2.3.6. Mammalian electrophysiology

2.2.3.6.1. Transfection

Transient transfection of the tsA201 cell line was achieved by the calcium phosphate method (Sambrook, 2001). Ten μg of pcDNA3.1(+)/EGFP-Zeo/NaChMM plasmid DNA was mixed with 10 μL of carrier salmon sperm DNA (1:10 solution; Sigma-Aldrich) and 500 μL of 250 mM $CaCl_2$ was added.

This mixture was then added drop-by-drop with vigorous shaking every 3-4 drops into a 1.5-mL tube containing 500 μL of 2x HEBS buffer [40 mM HEPES pH 7.05, 274 mM NaCl, 12 mM dextrose, 10 mM KCl, 1.4 mM Na_2HPO_4]. The prepared transfection mixture was incubated for 20 to 30 min at RT. Prior to the addition of transfection mixture onto the Petri dish containing a layer of tsA201 cells, the old cultivation medium was removed and replaced by a new Dulbecco's modified Eagle's medium (DMEM; Invitrogen) (Dulbecco and Freeman, 1959) complemented with 10 % fetal bovine serum (FBS), and supplemented in L-glutamine and penicillin/streptomycin (P/S). The transfection

mixture was then dispensed drop-by-drop on the top of the layer of tsA201 cells and the Petri dish was swayed for proper distribution of transfection mixture. The transfected cells were incubated at 37 °C with 5 % CO_2 for 18 h.

2.2.3.6.2. Cell preparation

Eighteen hours after transfection, cells were detached from the dish surface by 1-min incubation in 25 % Trypsin-EDTA (Invitrogen) at 37 °C and split using a plastic dispenser. Furthermore, 3 to 6 drops of the split tsA201 cells were added into fresh 3 mL of DMEM modified medium, swayed and incubated for 18 h at 37 °C with 5 % CO_2 in order to settle and recover from trypsin treatment.

2.2.3.6.3. Laser Scanning Confocal Microscopy (LSCM)

The samples analysed with LSCM were prepared according to the Sections *2.2.3.6.1.* and *2.2.3.6.2.* However, 2 µg of pEGFP-C1→N1/NaChMM plasmid was transfected and the incubation times after the transfection and cell splitting were 12 and 6 hours respectively. The imaging was performed with a Leica DM IRB confocal laser scanning microscope equipped with a TCS SP2 AOBS scan head. The cells were illuminated through an oil immersion objective lens (63x/1.4) while the NaChMM-EGFP fusion protein was excited with an Ar laser at 488 nm. The fluorescence intensities of the EGFP fusion protein (emission peak at 510 nm) was measured at 514 nm.

2.2.3.6.4. Activity assay

The standard whole-cell patch-clamp recordings were performed after 36 h from transfection using an Axopatch 200B amplifier. The measurements were performed from fluorescent, transfected tsA201 cells using borosilicate glass pipettes with a resistance of 1-2.2 MΩ. The fluorescence was monitored with Zeiss Axiovert 25 inverted fluoresce microscope using GFP filter. The series resistances were adequately compensated by an analog procedure to reduce voltage errors. This procedure results in a calculated voltage error below 5 mV in all the analyzed cells. The currents were filtered at 2 kHz and digitized with a sampling rate of 50 kHz using a Digidata (Molecular Devices) analog-to-digital converter. The extracellular solution contained 160 mM NaCl, 2 mM KCl, 1.5

mM CaCl$_2$, 1 mM MgCl$_2$, 10 mM glucose and 10 mM HEPES pH 7.4, whereas the intracellular solution contained 25 mM NaCl, 5 mM MgCl$_2$, 5 mM KCl, 105 mM CsF, 10 mM EGTA, and 10 mM HEPES pH 7.4. All measurements were conducted at 22 ± 2 °C. The holding potential was -85 mV at all times. The whole recorded data were analyzed with a combination of pClamp10 (Molecular Devices) and OriginPro 8 SR1 softwares. All current amplitudes were measured with the applied leak-subtraction procedure.

2.2.3.6.4.1. Activation curve

To analyze the voltage dependence of channel activation, the sodium conductance (G_{Na}) was calculated using following relationship $G_{Na} = I/(V_R - V_M)$, where the peak current data for each cell were divided by the respective driving force, plotted against the test potential V_M, normalised to the I_{max} and fit to a single Boltzmann equation of the following form:

$$G_{Na} = \frac{G_{max}}{1 + \exp\left(\dfrac{V_h - V_M}{k}\right)},$$

where G_{max} is the maximum G_{Na}, V_h is the voltage at which 50 % of the NaChMM are activated, and k is the slope of the curve.

2.2.3.6.4.2. Steady-state inactivation curve

The steady-state inactivation was measured by applying a double-pulse protocol, consisting of a 2,500 ms pre-pulse ranging from -160 to 50 mV (in 10 mV increments), followed by a test pulse to -10 mV. The data sets (a plot of peak I_{Na} during the -10 mV test pulse vs. pre-pulse voltage) were first normalised with respect to I_{max}, then fitted with the summation of two Boltzmann equations of the following form:

$$I_{Na} = \frac{f_1}{1 + \exp\left(\dfrac{V_M + V_{h1}}{k_1}\right)} + \frac{f_2}{1 + \exp\left(\dfrac{V_M + V_{h2}}{k_2}\right)},$$

where f_1 and f_2 are the fractions of the first and second components of inactivation, respectively. V_h is the potential at which half of the I_{Na} was inactivated, and k is the slope factor for each component. The sum of both fractions is the calculated maximum I_{Na} ($f_1 + f_2 = I_{max}$).

2.2.3.6.4.3. Recovery from inactivation

To examine the rate of channel recovery from inactivation, a protocol was designed comprising a 50 ms pre-pulse to -85 mV, followed by a test pulse to -10 mV, and then returning to -85 mV for a variable time period (250, 500, 750, 1000, 1500, 2000, 2500, 3000, 4000, 6000, 9000, and 12000 ms) before the application of a second test pulse to -10 mV. The I_{Na} amplitude from the second -10 mV pulse was divided by the amplitude of the corresponding first test pulse to obtain the fraction of I_{Na} recovered after the recovery time. The data were fit with a double-exponential equation of the following form:

$$\frac{I_{Na^{p2}}}{I_{Na^{p1}}} = f_1\left[1 - \exp\left(-\frac{t}{\tau_1}\right)\right] + f_2\left[1 - \exp\left(-\frac{t}{\tau_2}\right)\right],$$

where the $I_{Na}{}^{p2}/I_{Na}{}^{p1}$ is the fraction of current recovered, f_1 and f_2 are the respective fractions of the fast and slow recovery components, t is the recovery time, and τ_1 and τ_2 are the time constants for each recovery component.

3. Results and Discussion

3.1. Target selection

To date, seven prokaryotic voltage-gated sodium channels have been analysed by means of electrophysiological methods (Ren *et al.*, 2001; Koishi *et al.*, 2004; Ito *et al.*, 2004; Irie *et al.*, 2010). However, only NaChBac has been expressed heterologously, purified and characterised biochemically (Nurani *et al.*, 2008). The evolutionary relationship of those proteins including NaChMM has been evaluated and shows that NaChMM appears to be less related to *Bacillus species* (Figure 20). However, as a marine bacterium, it evolved from common ancestors as well as a group of marine microorganisms presented in the phylogenetic tree below.
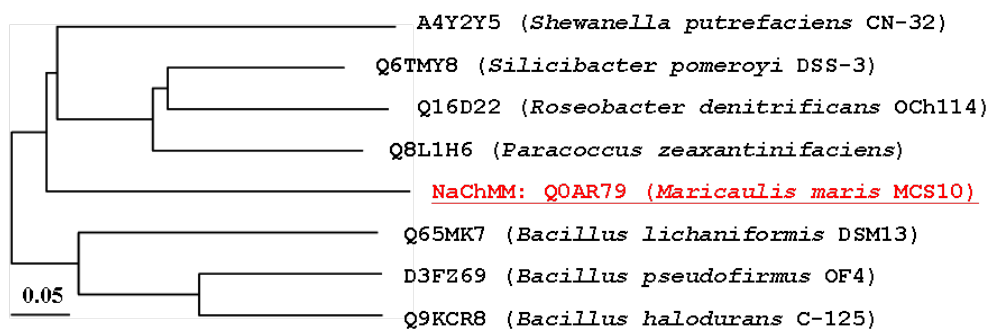
Figure 20: Phylogenetic tree of known and characterised prokaryotic voltage-gated sodium channels.
NaChMM – prokaryotic voltage-gated sodium channel (red); full length amino acid sequence alignment was analysed by means of neighbourhood joining (PAUP).

During this study, three channel proteins were selected in order to increase the likelihood of stable and sufficient protein production, necessary for its further extensive and detailed biochemical, biophysical and structural investigation.

The first of the selected targets was NaChBac voltage-gated sodium channel, present in *Bacillus halodurans* C-125 (Ren *et al.*, 2001). This target is mostly investigated *in vivo* and, as previously mentioned, it is the first target purified as a recombinant protein (Nurani *et al.* 2008). The second of the selected targets, NaChSP voltage-gated sodium channel from *Silicibacter pomeroyi* DSS-3, was described by Koishi and group (2004). Eleven prokaryotic proteins that

are structurally related to NaChBac were investigated by the authors using expression in mammalian cell lines However, only two from selected homologues, including NaChSP, were producing voltage-activated inward currents.

At the start of this thesis, in order to find the homolog prokaryotic voltage-gated sodium channel proteins that have not been described until then, a standard BLASTP was performed using the whole amino acid sequence of NaChBac. Based on that analysis, a third target protein (NaChMM) was selected. According to UniProtKB protein data base, the NaChMM voltage-gated sodium channel present in *Maricaulis maris* MCS10 is classified as an ion channel protein. The sequence comparison presented in Figure 21 shows highly conserved arginine residues situated every third amino acid in α4. These residues have been assigned to be involved in the voltage sensing. Similarly, the highly conserved amino acids, which are located in the pore region (P) and which have been described to be responsible for ion selectivity, are also present in all three target proteins. This leads to a strong assumption that NaChMM is, indeed, a voltage gated ion channel.
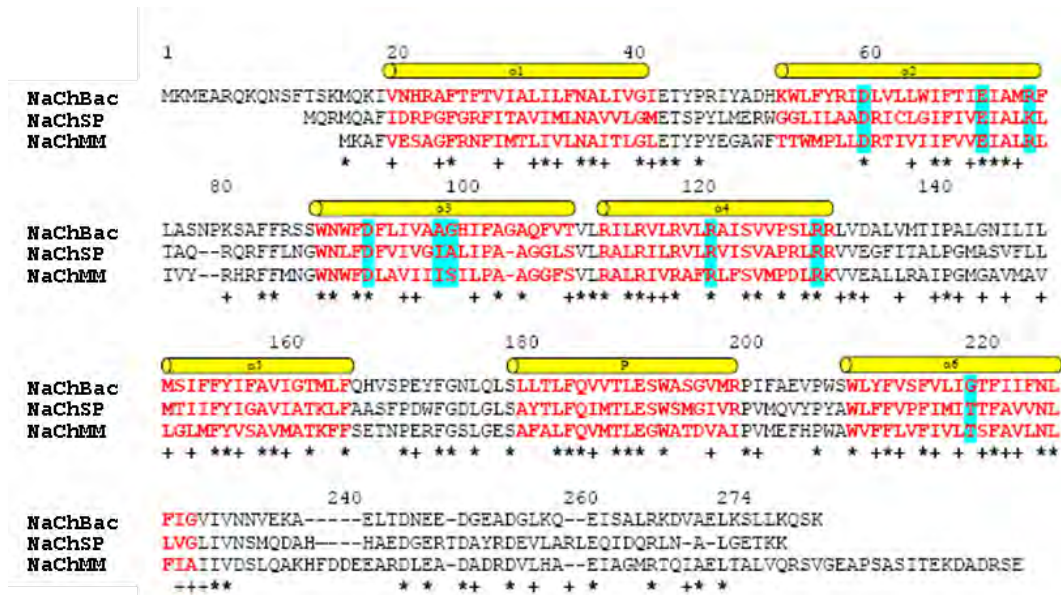
Figure 21: Sequence alignment of the voltage-gated sodium channel from three distantly related organisms: *B. halodurans* (NaChBac), *S. pomeroyi* (NaChSP) and *M. maris* (NaChMM).

The predicted transmembrane helices α1 - α6 and the pore region P, are highlighted in red. Highly conserved and similar amino acid residues are marked with asterisks and plus signs, respectively. Positively charged residues (blue) on segment α4 are the main contributors to voltage-sensing, whilst negatively charged residues (blue) on the α2 and α3 segments are believed to participate to the process of opening and closing. G219 has been identified, as a critical residue involved in activation of NaChBac channel; however, it is not conserved in other organisms.

The reasons for selecting the three aforementioned prokaryotic voltage-gated sodium channels are as follows:

1) The similarity of amino acid sequences of NaChBac, NaChSP and NaChMM has been established: the sequence of NaChMM shares 49 % and 36 % identity with NaChSP and NaChBac, respectively; and the sequence of NaChBac shares 40% identity with NaChSP.

2) NaChBac (Ren *et al.*, 2001) and NaChSP (Koishi *et al.*, 2004) were characterised by *in vivo* activity assay, showing Na⁺-selectivity; however, their kinetics and voltage dependence was significantly different.

3) NaChMM shows an isoelectric point of 5 *vs.* ~ 9.4 for NaChBac and NaChSP (Table 3), a feature that could be exploited during crystallogenesis.

4) The positively and negatively charged residues D58 (α2) R120 (α4), E68 (α2) with R129 (L45), and D91 (α3) with R72 (α2), which are responsible for the voltage-sensing, are highly conserved, whilst other key residues, such as A(98) and G(99), which are supposed to interact with D58 (α2) in NaChBac, as well as the key residue G219 (α6), which is involved in channel activation, are respectively mutated to I(98), S(99) and T219 (Figure 21).

5) NaChMM has a very short cytoplasmic N-terminus but an extended C-terminus, which might play a role in a different behaviour of the protein, effecting its expression and stability. In comparison, the NaChSP has short N- and C-termini.

6) Each sodium channel protein is present in distantly related bacteria species. Even though these bacteria differ substantially, they also share certain characteristic features. All three bacteria species are rod-shaped, mesophilic and motile. In contrast to *B. halodurans*, the *S. pomeroyi* and *M. maris* are Gram-negative and grow in an aquatic habitat. Moreover, *B. halodurans* and *M. maris* have facultative oxygen requirements, while *S. pomeroyi* is an aerobe. Each of the bacterial strains has a unique feature, while *B. halodurans* is classified as alkaliphilic bacterium, and therefore grows poorly at neutral pH and very well at pH > 9.5 (Nielsen, 1995), *S. pomeroyi* is capable of degrading a number of sulphur compounds (i.e. madimethylsulfoniopropionate – DMSP), which contributes to the global sulphur cycle (Gonzalez *et al.*, 2003). *M. maris,* in turn, forms a biofilm, volatilises mercury and plays an important role in biogeochemical cycling of organic nutrients in the marine environment (Abraham *et al.*, 1999).

Table 3: Comparison of physical parameters of prokaryotic voltage-gated sodium channel proteins.

	No of aa	MW [g/mol]	pI	Ext. coefficient [M^{-1}cm^{-1}]	Instability index
NaChBac	274	31456.3	9.45	47440	45.86 (us)
NaChSP	258	28969.5	9.20	36440	28.72 (s)
NaChMM	278	31227.6	5.02*	44460	26.45 (s)*

Values were computed by means of "ProtParam" online tool and using corresponding amino acid sequences; (*) indicates extreme difference in isoelectric point and increased stability of NaChMM protein.

It is common for heterologous membrane protein production that the amount of expressed membrane protein can not be predicted (Daley *et al.*, 2005). Moreover, recombinant production of similar membrane proteins may vary drastically (Huang *et al.*, 2003). With the goal of obtaining a highly pure homogenous protein, an extensive optimisation procedure of recombinant production of voltage-gated sodium channels and their purification, as well as the subsequent biochemical and biophysical characterization were presented in this research. Furthermore, with the aim of elucidation of 3D molecular structure, its crystallogenesis was probed.

3.2. Optimisation of heterologous protein expression

The low number of known transmembrane protein structures reflects the unstable nature and difficulties related to handling of membrane proteins. In contrast to soluble proteins, membrane proteins are difficult to produce, purify and crystallise. Very often the bottleneck lies in the limited yield of recombinant production (Wagner *et al.*, 2006).

There are different parameters that may affect protein expression levels, stability and membrane integrity (Korepanova *et al.*, 2005; Vasina and Baneyx, 1996; Schein, 1989; Kurland and Gallant, 1996). Therefore, the optimisation of membrane protein production was performed by manipulation of cell growth temperature, expression broth, expression time, inducer concentration, induction time and *E. coli* expression host (Table 4).

Table 4: Parameters analysed during optimisation of a heterologous expression of prokaryotic voltage-gated sodium channels.

Condition	Variation
Inducer concentration (IPTG)	0.5 mM and 1.0 mM
Expression initiation time	OD^{600} = 0.6, 1.0 and 1.2
Protein production temperature	25 °C and 37 °C
Expression media	terrific broth (TB), terrific broth with addition of glucose (TB+G), auto-inducing medium (Naumann et al.)
E. coli expression hosts	BL21 (DE3), C41 (DE3), C43 (DE3), BL21 star (DE3), BL21 codon plus (DE3) RIL, Rossetta

The genes encoding for NaChBac, NaChSP and NaChMM voltage-gated sodium channels were cloned into bacterial pTrcHis2A vector (under *trc* promoter) commonly used in production of prokaryotic membrane proteins (Wagner *et al.*, 2006). All three recombinant proteins have $(His)_6$-tag attached to the C-terminus, as presented in Figure 22.

| 2 aa | Prokaryotic voltage-gated sodium channel gene | Thrombin | 16 aa | *myc* epitope-tag | 4 aa | $(His)_6$-tag |
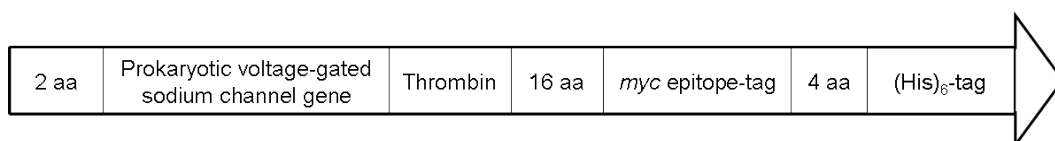
Figure 22: Schematic map of recombinant voltage-gated sodium channel.

Table 5 presents the comparison of the characteristic features of each recombinant voltage-gated sodium channel protein and native proteins. In contrast with NaChSP and NaChMM, the relatively high instability index of NaChBac can play a role in recombinant protein production.

Table 5: Characteristics of NaChBac, NaChSP and NaChMM sodium channel proteins (native and recombinant).

		No of aa	MW [g/mol]	pI	Ext. coefficient [M^{-1}cm^{-1}]	Instability index
NaChBac	Native	274	31456.3	9.45	47440	45.86 (us)
	recombinant	319	36516.9	9.02	48930	45.31 (us)
	without (His)$_6$-tag	280	32152.2	9.58	47440	45.20 (us)
NaChSP	Native	258	28969.5	9.20	36440	28.72 (s)
	recombinant	303	34030.1	7.94	37930	30.69 (s)
	without (His)$_6$-tag	264	29665.4	9.45	36440	28.42 (s)
NaChMM	Native	278	31227.6	5.02	44460	26.45 (s)
	recombinant	323	36302.3	5.37	45950	27.69 (s)
	without (His)$_6$-tag	284	31923.5	5.09	44460	26.52 (s)

Values computed using "ProtParam" online tool, calculations based on their amino acid sequence; (us) – unstable; (s) – stable.

3.2.1. Optimisation of IPTG concentration and different induction times

With the exception of the figure presenting a Western-blot, expression parameters were not available in the year 2007 (Ren *et al.*, 2001). Hence, IPTG concentrations was investigated with the induction set at the mid log phase (cell optical density of 0.6). During this experiment, two concentrations of IPTG were used for the induction of NaChBac protein production, while *E. coli* cells were cultivated in TB at 37 °C.
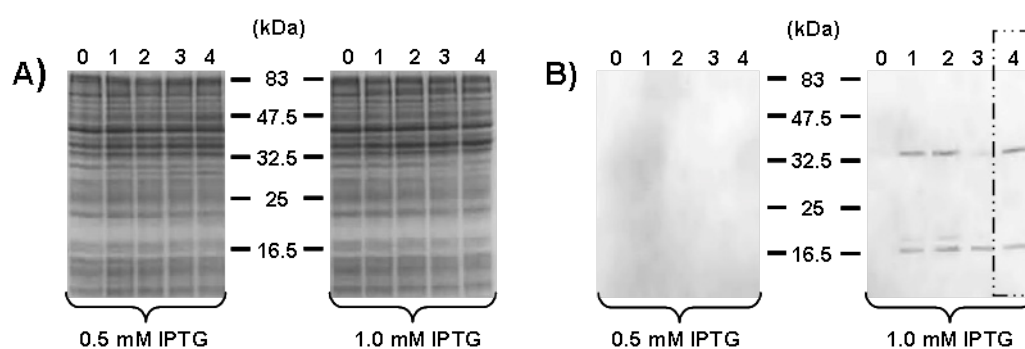
Figure 23: Expression of NaChBac in *E. coli* BL21(DE3).
A) SDS-PAGE and B) Western-blot; lane: 0 – without induction, lanes: 1, 2, 3, and 4 – 1, 2, 3, and 4 h after IPTG induction, respectively; broken line marks the best result.

Protein production is observed only in the case where 1 mM IPTG was used (Figure 23). Moreover, in addition to the full length NaChBac migrating in SDS-PAGE at a size of ~ 35 kDa, a second protein band is detected in Western-blot at about 17 kDa. This indicates that a partial degradation or, most probably, a site directed proteolysis has occurred.

The IPTG concentration and induction time for NaChSP expression was reported by Koishi and colleagues (2004). It therefore was not investigated.

Taking into account both previous results for NaChBac expression (Figure 23) and literature values for NaChSP production, 1 mM IPTG was applied in the optimisation of different times of induction of NaChMM expression (Figure 24). This experiment was performed by cultivating the cells in TB at 37 °C.
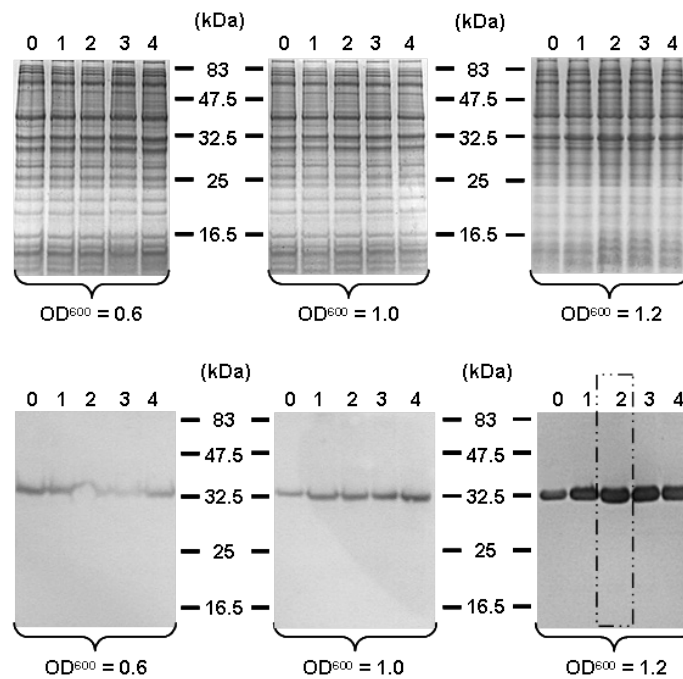
Figure 24: Expression of NaChMM in *E. coli* BL21(DE3).
SDS-PAGE (Eunson et al.) and Western-blot (bottom); lane: 0 – without induction, lanes: 1, 2, 3, and 4 – 1, 2, 3, and 4 h after induction, respectively; broken line marks the best result.

E. coli cultures were producing NaChMM protein regardless of initiation of protein production time, although the amounts were noticeably different (Figure 24). The addition of IPTG in early stages of cell cultures growth was not effective and only a small amount of NaChMM protein was produced. Higher levels of protein production were reached when induction was performed at a cell

culture optical density of 1.2. The improvement in NaChMM protein expression at late log phase, which is presented in Figure 24, can be explained by the fact that *E. coli* cells at this growth stage have already undergone a metabolic and growth shift, which lowers their response to foreign and toxic proteins (Galloway *et al.*, 2003).

3.2.2. Optimisation of protein production by varying expression media and incubation temperatures

The relatively fast mechanism of protein production in prokaryotes may cause mistargeting and misfolding of expressed protein (Wagner *et al.*, 2006). Lowering the temperature of bacterial cultivation will slow down the mechanism of recombinant protein production, which may result in an improvement of recombinant protein solubility (Vasina and Baneyx, 1996; Sorensen and Mortensen, 2005).

During this part of the study, different incubation temperatures and types of expression media were investigated. The transformed *E. coli* BL21(DE3) cells were subjected to expression at 25 °C and 37 °C in TB, TB+G and in AUM. Figure 25, 26 and 27 present expression results of, respectively, NaChBac, NaChSP and NaChMM.

The type of expression media or cultivation temperatures did not exert noticeable influence on the amount of produced NaChBac and NaChSP proteins, as presented in Figure 25 and Figure 26, respectively. By contrast, the levels of produced NaChMM protein in AUM increased at both tested temperatures (Figure 27).

The production of NaChBac and NaChSP in TB and TB+G (at 25 °C and 37 °C) resulted in protein degradation products, which were not observed in AUM at both temperatures (Figure 25). Surprisingly, NaChMM N-terminus degradation was detected by Western-blot in AUM (Figure 27).
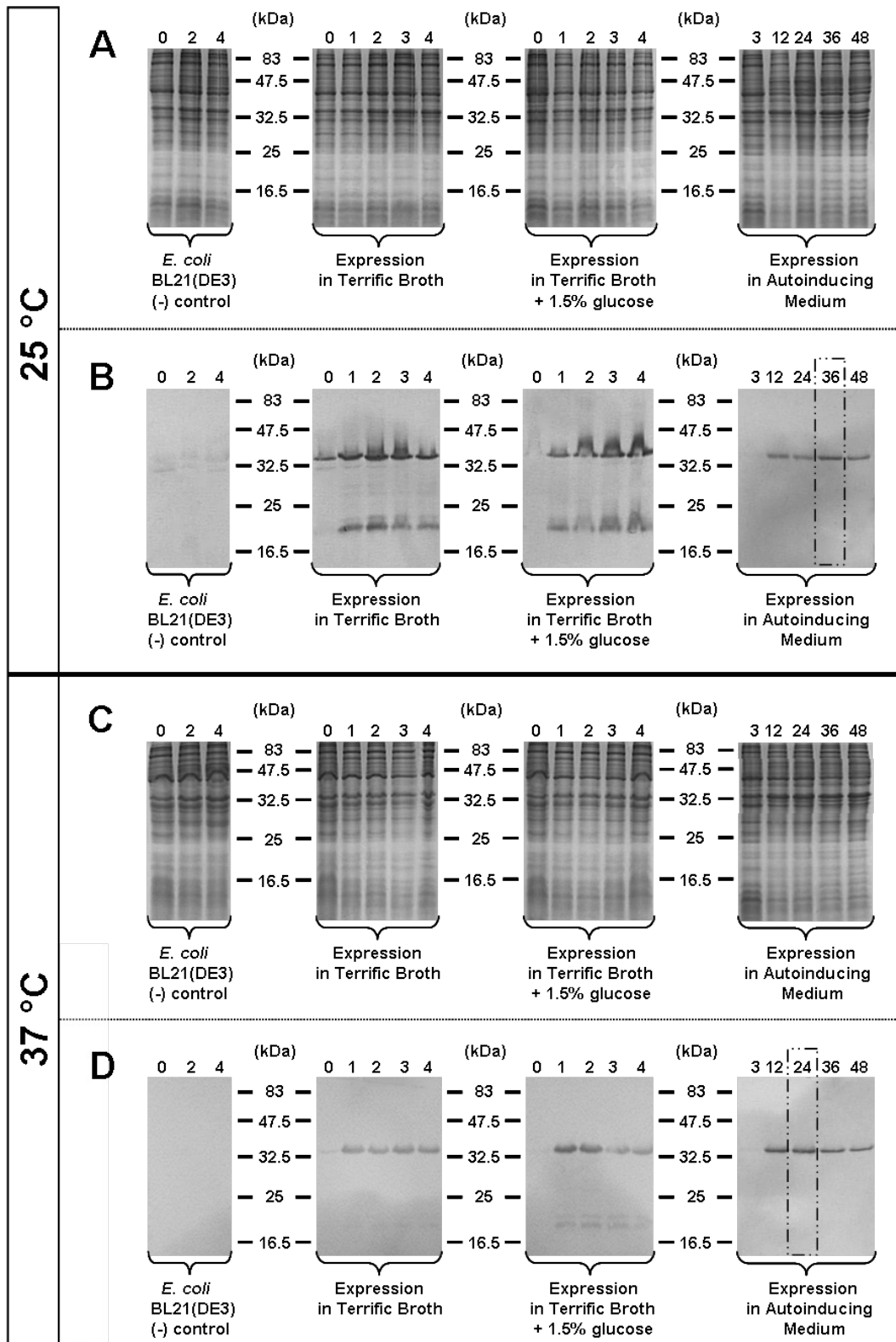
Figure 25: NaChBac expression in *E. coli* BL21(DE3) at 25 °C and 37 °C.
*SDS-PAGE (A and C) and Western-blot (B and D); non-transducted
E. coli BL21(DE3) strain grown in TB; lane: 0 – without induction;
lanes: 1, 2, 3, and 4 – 1, 2, 3 and 4 h after induction, respectively;
lanes 3, 12, 24, 36 and 48 for protein production in AUM – 3, 12, 24,
36 and 48 h after inoculation; broken lines mark the best results at
each temperature.*
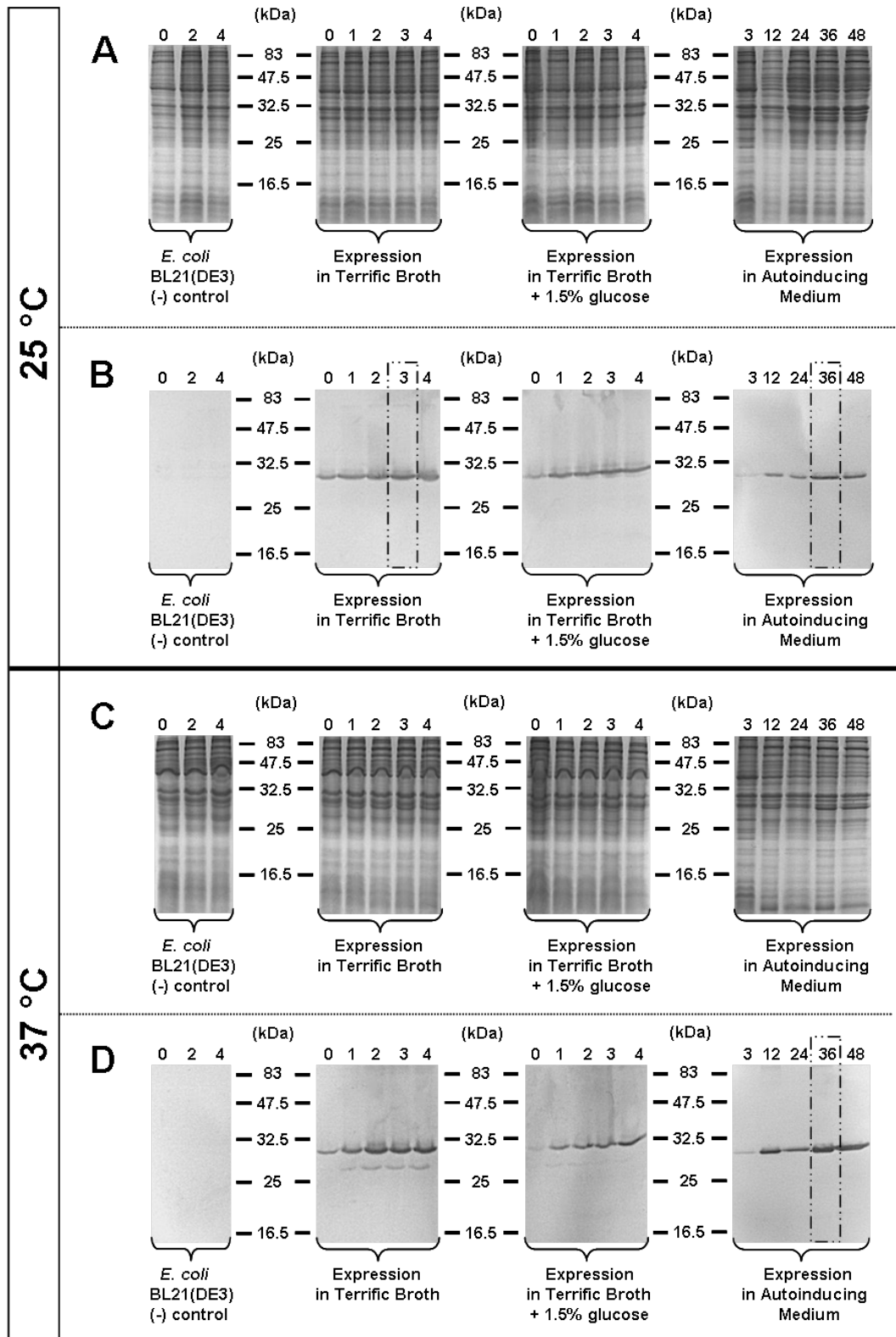
Figure 26: NaChSP expression in *E. coli* BL21(DE3) at 25 °C and 37 °C.
SDS-PAGE (A and C) and Western-blot (B and D); non-transducted E. coli BL21(DE3) strain grown in TB; lane: 0 – without induction; lanes: 1, 2, 3 and 4 – 1, 2, 3 and 4 h after induction, respectively; lanes 3, 12, 24, 36 and 48 h for protein production in AUM – 3, 12, 24, 36 and 48 h after inoculation; broken lines mark the best results at each temperature.
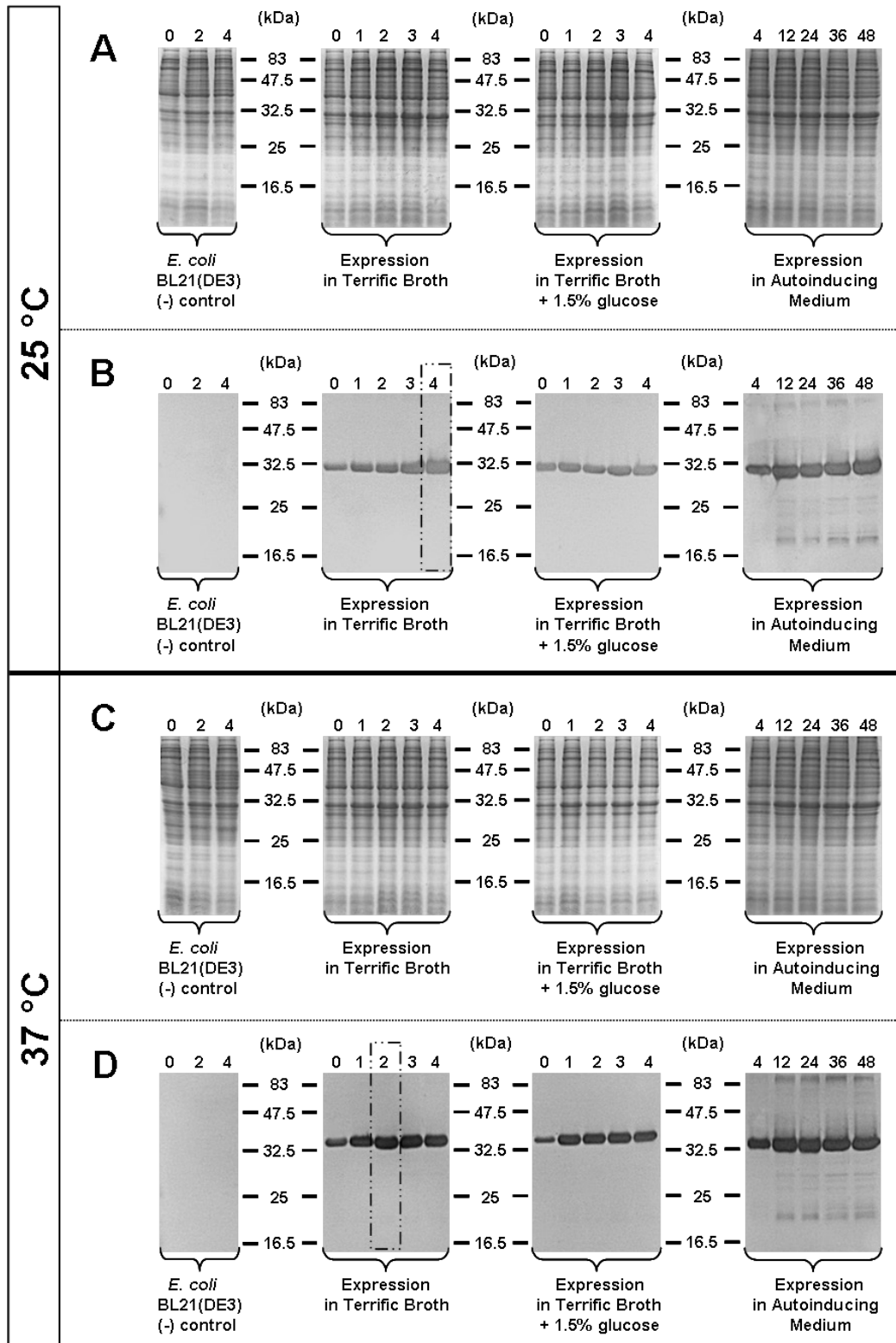
Figure 27: NaChMM expression in *E. coli* BL21(DE3) at 25 °C and 37 °C.
SDS-PAGE (A and C) and Western-blot (B and D); non-transducted E. coli BL21(DE3) strain grown in TB; lane: 0 – without induction; lanes: 1, 2, 3 and 4 – 1, 2, 3 and 4 h after induction, respectively; lanes 4, 12, 24, 36 and 48 h for protein production in AUM – 3, 12, 24, 36 and 48 h after inoculation; broken lines mark the best results at each temperature.

The amounts of *E. coli* cells after completed protein production were analysed by comparing their optical density values at 600 nm. The lowest OD^{600} values were recorded for cultivation in TB at 25 °C and the highest OD^{600} values were recorded for cultivation in AUM at 37 °C. The glucose introduced into TB increased levels of bacterial growth (Figure 28). The stabilisation of bacterial growth appeared after 3 h from IPTG induction and after 12 h when AUM was used.
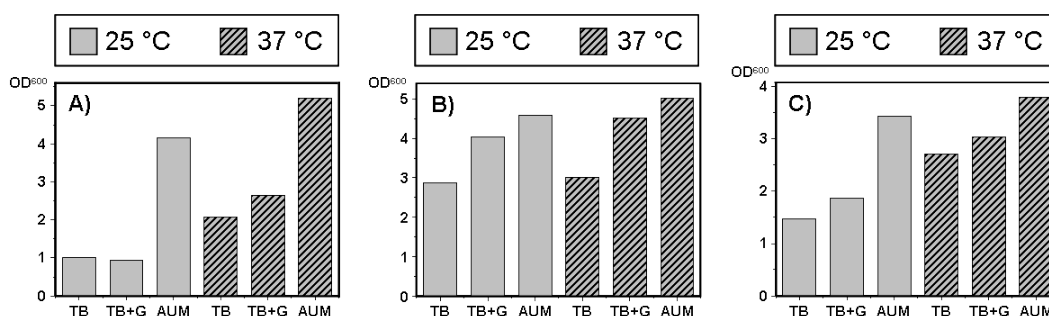
Figure 28: Yields of bacteria cells after completed expression of NaChBac (A), NaChSP (B) and NaChMM (C) proteins.
Optical density measured for bacterial cultures grown at 25 °C and 37 °C in TB, TB+G and AUM.

The highest amount of cells expressing NaChBac protein was observed when cultivation was performed in AUM (at 25 °C and 37 °C). The recorded optical density values were 4.2 (at 25 °C) and 5.2 (at 37 °C) (Figure 28A).

The amount of cells producing NaChSP protein was the most constant throughout the investigated conditions. However, similarly to *E. coli* producing NaChBac protein, the highest optical density values were recorded when bacteria expressing NaChSP were cultured in AUM at 25 °C ($OD^{600} = 4.6$) and at 37 °C ($OD^{600} = 5.0$) (Figure 28B).

The amount of *E. coli* cells producing NaChMM protein was again the highest when cultivation was performed in AUM and the optical density yielded 3.4 (at 25 °C) and 3.8 (at 37 °C) (Figure 28C).

3.2.3. Optimisation of heterologous protein production in different *E. coli* expression strains

Specialized expression hosts can greatly influence levels of membrane proteins' expression. The *E. coli* strains investigated in this study are widely used in membrane protein over-expression (Drew *et al.*, 2006, Eshaghi *et al.*, 2005).

Hence, the investigation of the influence of different expression hosts on the amount of produced protein (Figure 29) was performed applying the previously established conditions according to which the production of NaChBac and NaChSP was performed in AUM at 25 °C, while expression of NaChMM was performed in TB at 25 °C (induction with 1 mM IPTG at $OD^{600} = 1.2$ (see paragraph: <u>Summary – selection of parameters for efficient expression of NaChBac, NaChSP and NaChMM recombinant proteins</u> on page 81).
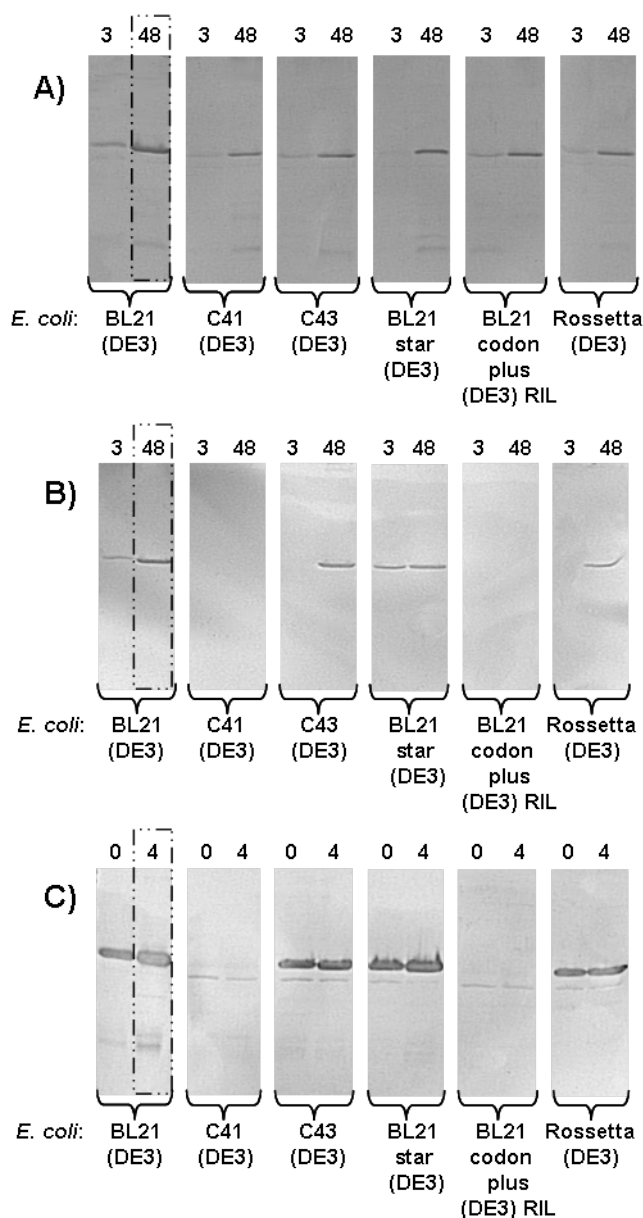
**Figure 29: Expression of NaChBac (A), NaChSP (B) and NaChMM (C) in 6
different *E. coli* strains analysed by Western-blots.**
*Lanes: 3 and 48 – 3 and 48 h after inoculation; 0 – without induction
and 4 – 4 hours after IPTG induction; broken lines mark the best
results.*

While NaChBac protein was produced in each of the tested strains,
NaChSP and NaChMM proteins were not expressed in C41(DE3) and BL21
codon plus (DE3)-RIL strains. The amounts of produced proteins and the final
optical densities of bacterial cultures were comparable for each recombinant
protein.

Summary – selection of parameters for efficient expression of NaChBac, NaChSP and NaChMM recombinant proteins

The optimal conditions for NaChBac, NaChSP and NaChMM production were established. The three factors considered during the selection of appropriate conditions for large scale protein production were as follows: the quality of expressed protein (non-degraded protein), the level of expressed protein and the yield of produced biomass. The presence of two populations of $(His)_6$-tagged protein (full length and degraded or cleaved protein) may lead to difficulties in their separation during purification, resulting in a non-homogeneous final protein sample. Therefore, the quality of produced protein has the strongest influence in establishing proper expression parameters. The optimal parameters for heterologous expression of prokaryotic targets are presented in Table 6.

Table 6: Final expression conditions established for the highest yields of NaChBac, NaChSP and NaChMM.

	NaChBac	NaChSP	NaChMM
E. coli **expression strain**	BL21(DE3)	BL21(DE3)	BL21(DE3)
Expression broth	AUM	AUM	TB
Time of induction OD^{600} (with 1 mM IPTG)	-	-	1.2
Time of protein production	24 h	24 h	4 h
Temperature of protein production	25 ℃	25 ℃	25 ℃

AUM – auto-inducing medium; TB – terrific broth.

AUM was selected for generating high yields of non-degraded NaChBac and NaChSP proteins, whilst TB was selected for NaChMM protein production.

The protein expression at 25 °C resulted in a lower cell mass and a slower protein production but, most importantly, it partially repressed proteolytic degradation; therefore, the expression at 25 °C was selected as the parameter for an efficient expression of all three target proteins in *E. coli* BL21(DE3).

The OD^{600} of 1.2 was established to be the most suitable for induction with 1 mM IPTG in order to achieve high levels of NaChMM expression. The highest level of produced protein was established for NaChMM and it was estimated that the ratio of produced NaChBac:NaChSP:NaChMM proteins is 1:1:3.

3.3. Recombinant protein purification

In order to study the structural and functional relationship of proteins and protein complexes, their specific activity and their mechanism of action, the milligram quantities of highly pure material are required. The selected targets were thus purified using a series of steps involving commonly used techniques, such as affinity and size exclusion chromatography. To establish the purification protocol, the following processes are taken into account: an extended purification time may lower protein stability, whilst a multi-step purification process will decrease pure protein yield.

Purification process for any his-tagged membrane protein consists of (i) preparation of membranes after cell lysis, (ii) solubilisation of membrane proteins using mild detergents and (iii) affinity chromatography (IMAC) followed by a gel-filtration.

3.3.1. Purification of NaChMM voltage-gated sodium channel

Cells containing NaChMM were disrupted using lysozyme followed by sonication. Membrane solubilisation was performed using mild detergents. The efficiency of sonication depends, among other parameters, on the volume of sonication mixture (Feliu *et al.*, 1998). Hence, over the course of experiments the ratio of cell pellet mass (grams) to volume of sonication mixture (millilitres) was respectively modified in the following way: 1:15, 1:12, 1:9, 1:6 to 1:3.

NaChMM purification requires extraction of the protein from the fragmented cell membranes. Two different approaches were therefore investigated: (i) Solubilisation of membrane proteins or (ii) Purification of membranes (see section 2.2.3.3.1.).

3.3.1.1. Investigation of parameters for affinity chromatography of NaChMM purification

3.3.1.1.1. Linear gradient affinity chromatography

Since the affinity of NaChMM protein to the nickel charged resin remains unknown, the initial trial of affinity chromatography purification of NaChMM was performed by applying a steep linear gradient of imidazole concentration.
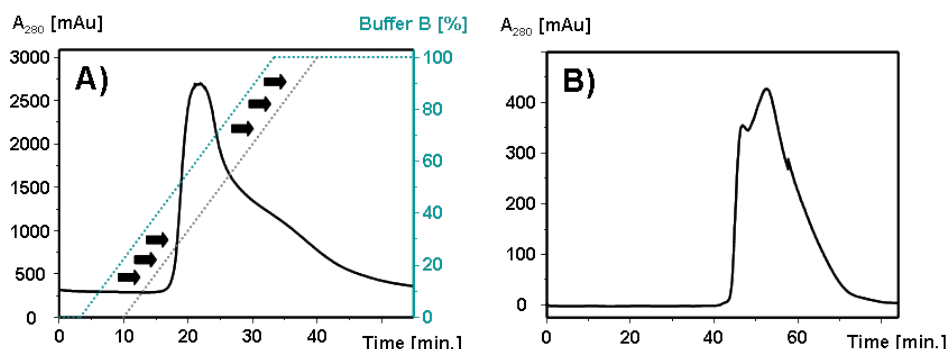
Figure 30: Linear gradient affinity chromatography (A) and subsequent SEC chromatography (B) of NaChMM voltage-gated sodium channel.
Grey broken line – shift of linear gradient curve caused by dead volume of used resin.

A short and fast linear gradient was found to be insufficient for the separation of (His)$_6$-tagged protein from impurities (Figure 30A,B). What is more, the elution profile of gel filtration chromatography (Figure 30B) shows a non-Gaussian distribution which indicates that the protein sample is either non-homogenous or it contains impurities.

Although the imidazole linear gradient is proven to be insufficient for purifying NaChMM, it was successfully used for a rough estimation of the imidazole concentration required for NaChMM elution. Due to the dead volume of used nickel resin, the elution profile curve of NaChMM is shifted in relation to the linear gradient curve (Figure 30A). The range of 250-350 mM imidazole was estimated to be the most suitable for NaChMM elution.

3.3.1.1.2. Step gradient affinity chromatography

The aim of the introduction of a step gradient purification was to improve the purity of NaChMM sample. A three-step elution was applied with 60 mM, 100 mM and 250 mM imidazole, followed by a gel filtration analysis of pooled fractions in both 100 mM and 250 mM imidazole steps. The 60 mM and 100 mM imidazole washing steps were introduced in order to wash-out impurities, whilst recombinant protein was eluted with 250 mM imidazole step. The results are presented in Figure 31.
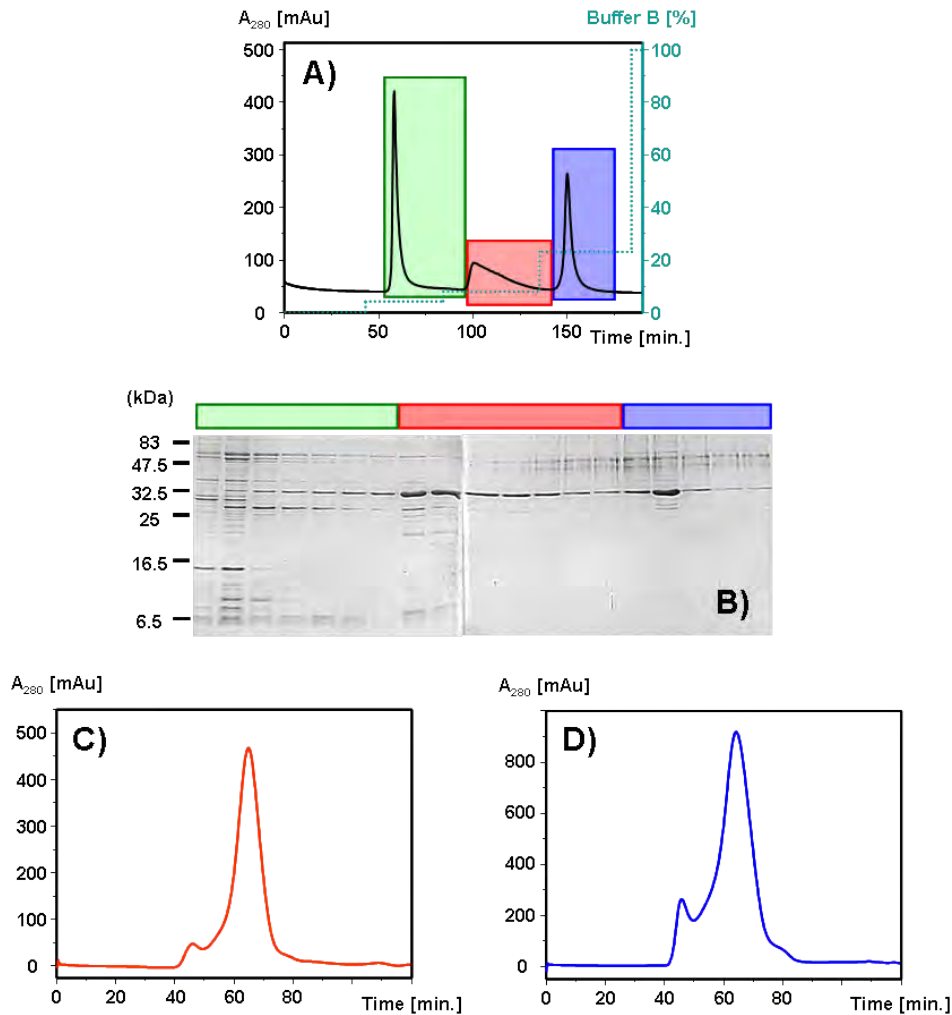
Figure 31: Purification of NaChMM voltage-gated sodium channel.
A) affinity chromatography elution profile; B) SDS-PAGE of fractions collected during affinity chromatography; C) size exclusion chromatography of pooled fractions eluted with 100 mM imidazole; D) size exclusion chromatography of pooled fractions eluted with 250 mM imidazole.

As proven by SDS-PAGE analysis of affinity purification, NaChMM is present in each elution step. The amount of NaChMM protein and contaminants as well as their ratio to one another differ along the imidazole step gradient (Figure 31B). The amount of contaminants in the pooled fractions containing 60 mM imidazole was established to be greater than 80 %. Yet, in samples containing 100 mM imidazole and 250 mM imidazole, they represent ~ 20 %. The presence of NaChMM protein in 100 mM and 250 mM elution steps indicates differences in its affinity to the nickel resin. This may be caused by different oligomeric state of NaChMM protein.

To investigate differences in the oligomeric state of NaChMM samples, gel filtration chromatography was performed (Figure 31C,D). The large peak eluting at 64 min suggests that both samples represent homogenous protein. The smaller peak eluting at 45 min is in turn most likely to represent aggregates. The only noticeable differences between the size exclusion elution profiles of both analysed protein samples are the amount of eluted protein and the ratio of homogenous NaChMM protein to the aggregates (Figure 31C,D).
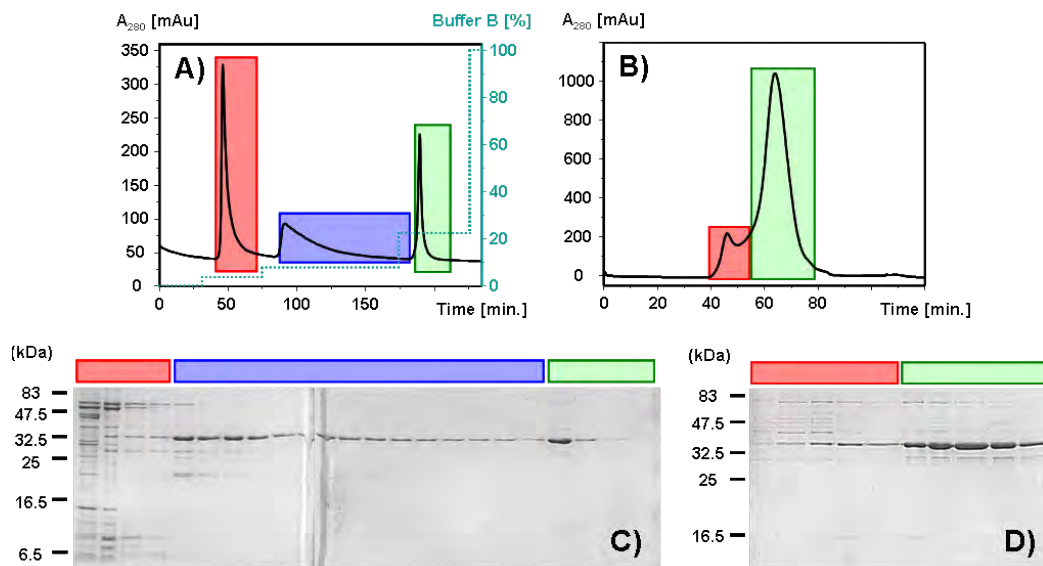
Figure 32: Purification of NaChMM voltage-gated sodium channel.
A) affinity chromatography elution profile; B) size exclusion chromatography of pooled fractions eluted with 100 mM and 250 mM imidazole (combined); C) SDS-PAGE of fractions collected during affinity chromatography; D) SDS-PAGE of fractions collected during size exclusion chromatography.

The results described previously suggest that NaChMM fractions eluting with 100 mM and 250 mM imidazole can be pooled prior to gel filtration. This was applied in subsequent experiments and the final gel filtration elution profile is presented in Figure 32B. The SDS-PAGE (Figure 32C) clearly implies that the 100 mM imidazole elution step can be omitted, however, with an advised simultaneous extension of the 60 mM imidazole wash. Furthermore, the aggregates were separated and the homogenous sample was subjected to further analysis.

Summary of (His)$_6$-tagged NaChMM purification

The most efficient cell disruption was accomplished when 1 gram of cell pellet was resuspended in 6 millilitres of lysis buffer.

The final yields of NaChMM protein, which was purified by means of two different approaches: (i) the solubilisation of membrane proteins or (ii) the purification of membranes, were compared and no significant difference was noticed. This indicates that the major amount of NaChMM protein is correctly folded and inserted into the cell membrane.

The following purification experiments allowed for the testing of various detergent concentrations in membrane solubilisation process (3 % to 1 %) and demonstrated that there is no significant difference in the final amount of purified protein. Therefore, 1 % solution of DDM was selected as a sufficient amount for membrane solubilisation.

The scaling-up of the purification process resulted in an increased proportional protein loss. It was discovered that the purification of NaChMM from large pellets (> 20 g) enhances the difficulty of the purification. It additionally resulted in the increase of the protein handling time that affected protein stability and led to the formation of aggregates and increased protein degradation. It was established that the cell pellet which provides optimal amounts of pure protein is 15 g (2.5 L of protein expression).

To summarise, the affinity chromatography purification of NaChMM involves a two-step gradient purification, where the protein is eluted in a 250 mM imidazole step with 85 % purity, yielding approximately 8 mg/L cell culture.

3.3.1.2. Investigation of EDTA stabilising effect on the NaChMM

To investigate NaChMM protein stability, the previously concentrated sample stored at -80 °C was subjected to SDS-PAGE and Western-blot analysis.
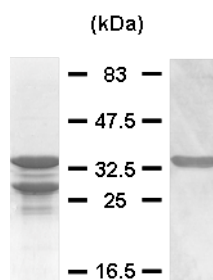
Figure 33: Degradation of NaChMM protein.
SDS-PAGE (left) and Western-blot (right).

SDS-PAGE analysis revealed a strong degradation of the protein sample. However, the Western-blot reaction of (His)$_6$-tagged NaChMM shows a response for full length NaChMM only, which indicates that the degradation of the protein occurs from the C-terminus (Figure 33).

This kind of protein degradation may occur spontaneously or may be caused by proteases (Kekow *et al.*, 2000). To eliminate a possible proteolitic degradation of NaChMM, 1 mM EDTA was permanently introduced into buffers used specifically in gel filtration chromatography. EDTA is reported to have a stabilizing effect and to limit protein degradation (Iizuka *et al.*, 1993; Janas *et al.*, 1994).

3.3.1.3. Optimisation of (His)$_6$-tag removal

The construction of recombinant NaChMM voltage-gated sodium channel resulted in a recombinant protein with a long (37 amino acids excluding thrombin recognition site) C-terminus tail (Figure 34) terminated with the (His)$_6$-tag that is required for efficient affinity chromatography purification. This long C-termini-tag may affect the activity of the protein, interfere in the crystal formation process and be partially responsible for rapid protein degradation. For these reasons, a thrombin cleavage site was initially introduced to eliminate the potentially unstable tag.
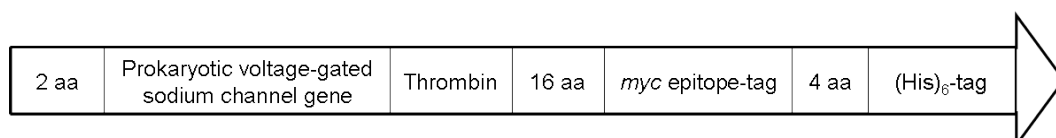
Figure 34: Scheme of organisation of recombinant NaChMM protein.
Thrombin recognition site introduced during PCR reaction.

The efficient thrombin cleavage depends on a variety of parameters, such as: pH of incubation buffer, salt content, temperature and time of incubation, reducing agents, thrombin:protein ratio and nature of cleaved protein (Di Cera *et al.*, 1991).

Since the buffering conditions (pH 7.6, salt content ~ 100 mM, no reducing agents present) used in the NaChMM digestion are classified as highly compatible with the thrombin requirements, the only factors investigated were incubation time and reaction temperature. Digestion of NaChMM protein was performed with thrombin-agarose (Sigma-Aldrich) at different incubation temperatures and different times (Figure 35).
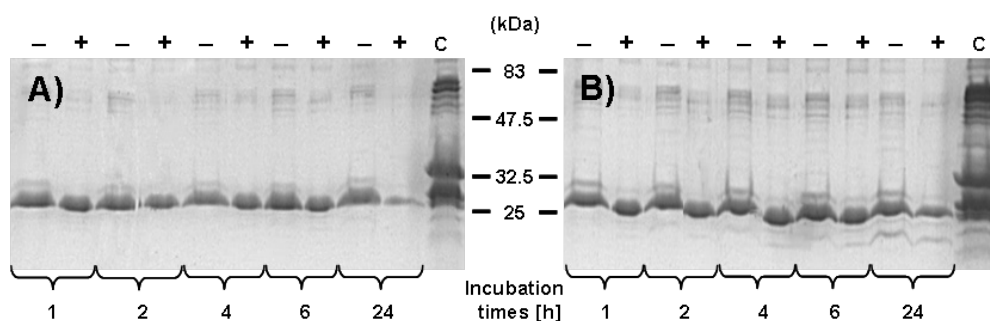
Figure 35: Thrombin digestion of NaChMM at 4 °C (A) and at room temperature (B) using different incubation times.
c – sample that was subjected to thrombin digestion; (-) sample without nickel resin treatment; (+) sample purified from a possible undigested protein and a free (His)$_6$-tag.

As presented in Figure 35, there is no significant difference registered in the digestion efficiency when time or temperature of incubation varied.

NaChMM was found to be more stable and less degradable at 4 °C and an overnight incubation was chosen for convenience. An additional affinity purification after (His)$_6$-tag removal was introduced in order to increase protein purity and to remove any remains of an undigested NaChMM.

Additional purification steps, including thrombin digestion and a second affinity chromatography purification, extended purification protocol time to a 3-day procedure. Interestingly, the (His)$_6$-tag removal step impaired protein degradation and led to obtaining a stable NaChMM.
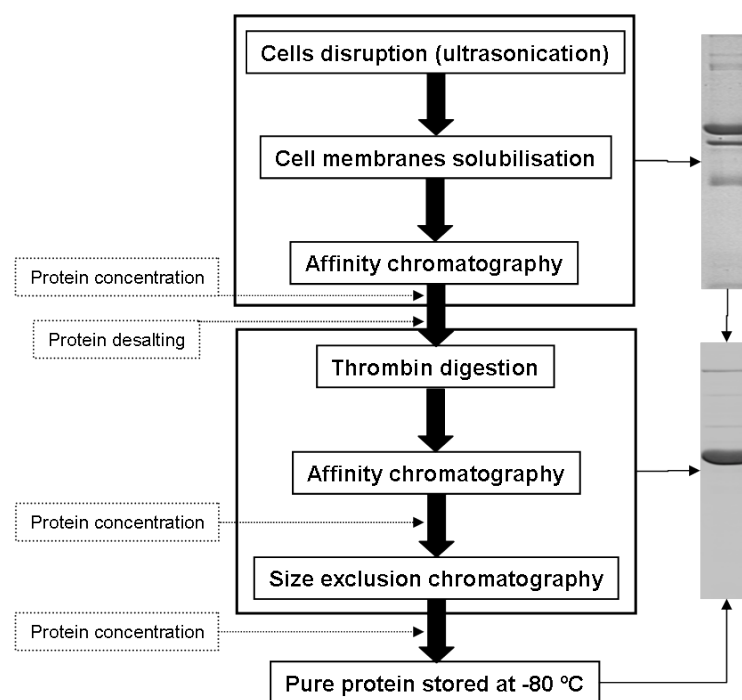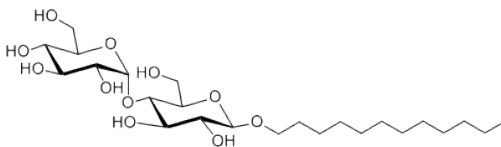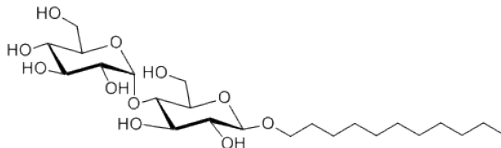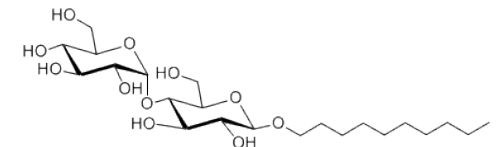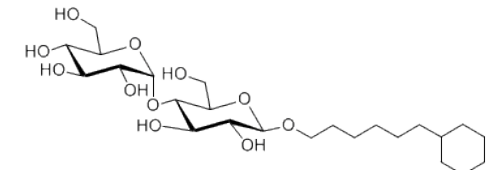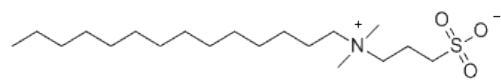
Figure 36: General scheme of recombinant protein purification protocol.
Representative SDS-PAGE results obtained after indicated purification processes.

The complete purification protocol for NaChMM was established (Figure 36), which included the step gradient affinity chromatography, followed by the (His)$_6$-tag removal, the second affinity purification and the final size exclusion chromatography as a protein "polishing" step. This protocol was adopted for NaChBac, NaChSP and truncated NaChMM proteins; however, certain adjustments in buffer solutions were introduced to obtain stable, non-precipitating and non-aggregating proteins.

3.3.1.4. Role of different detergents used in NaChMM purification

The type of detergent used in the purification process may affect protein stability, leading to its aggregation and activity loss. Hence, the stability of NaChMM protein in various types of detergents was investigated in order to select the most suitable detergent for protein purification. The established protocol for recombinant voltage-gated sodium channels purification (Figure 36) was used to asses influence of five different detergents on NaChMM protein stability, each varying in length and type of hydrophobic tail and polar head group (Table 7).

Table 7: List of detergents used in the solubilisation and purification process.

n-dodecyl-β-D-maltopyranoside (DDM)	
$C_{24}H_{46}O_{11}$ CMC in H_2O: 0.17 mM Ag. No (H_2O): 78 ÷ 149 MW: 510.6 g/mol	
n-undecyl-β-D-maltopyranoside (UDM)	
$C_{23}H_{44}O_{11}$ CMC in H_2O: 0.59 mM Ag. No (H_2O): ~ 71 MW: 496.9 g/mol	
n-decyl-β-D-maltopyranoside (Goldman et al.)	
$C_{22}H_{42}O_{11}$ CMC in H_2O: 1.8 mM Ag. No (H_2O): ~ 69 MW: 482.6 g/mol	
Cymal-6	
$C_{24}H_{44}O_{11}$ CMC in H_2O: 0.56 mM Ag. No (H_2O): ~ 91 MW: 508.5 g/mol	
Anzergent 3-14	
$C_{19}H_{41}NO_3S$ CMC in H_2O: 0.16 mM Ag. No (H_2O): 83 ÷ 130 MW: 363.6 g/mol	

Each detergent was introduced at the beginning of each of the separate purification processes at the point of extraction of the protein from the lipid bilayer and the purification was independently continued for every preliminarily chosen detergent. The same buffering conditions and equipment were used throughout each of the purification processes.
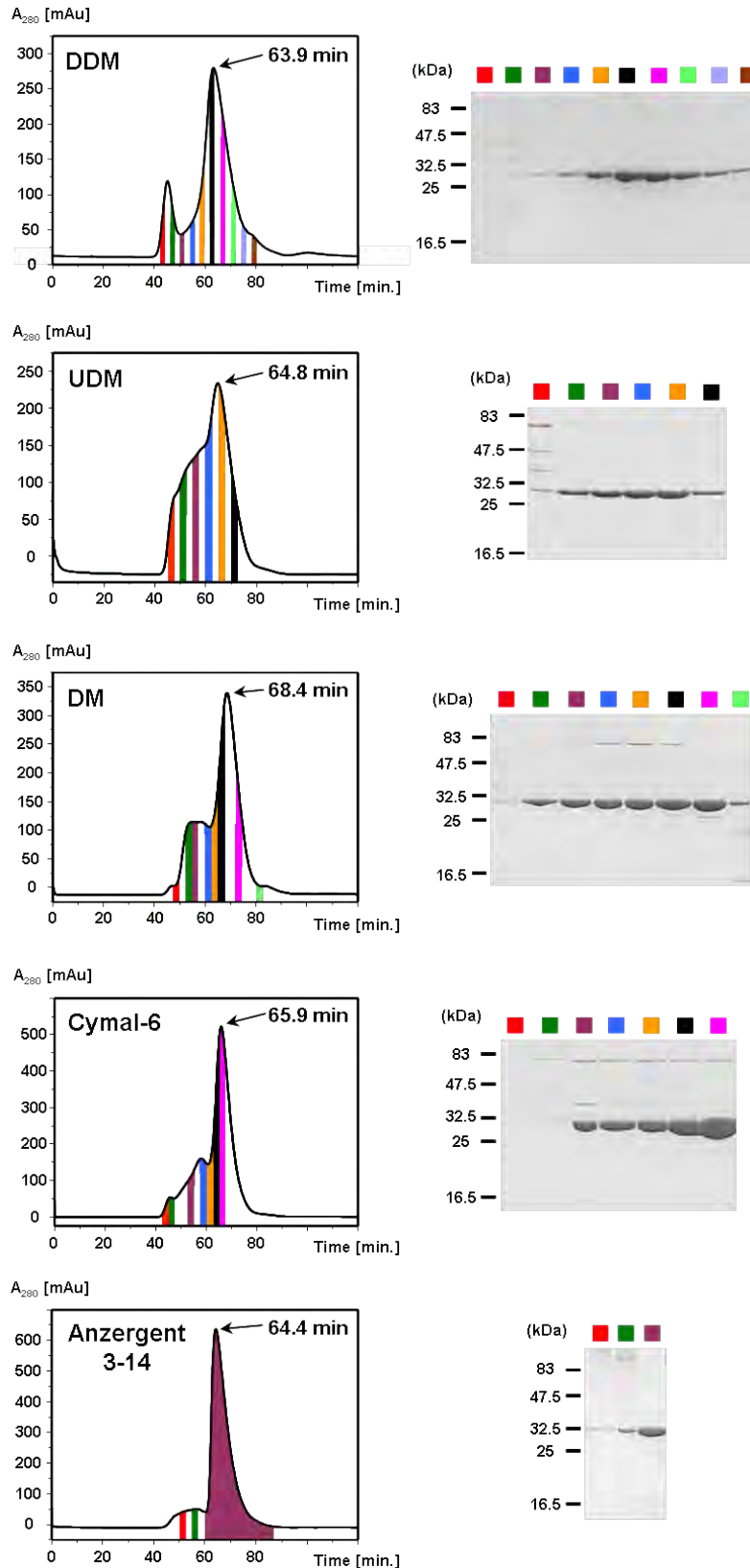
Figure 37: The size exclusion chromatograms of NaChMM purified in different detergents as indicated with accompanying SDS-PAGE analysis.

The colours above the gels correspond to the fractions collected during size exclusion chromatography.

The elution profiles of purified NaChMM (Figure 37) present tetrameric NaChMM (major peak), oligomers and aggregates in different ratios, depending on the detergent used.

The active and fully functional NaChBac prokaryotic voltage-gated sodium channel is reported to be homoteratameric (Nurani *et al.*, 2008), which is why the molecular weight of NaChMM is expected to be ~ 128 kDa. According to the standard curve presented below (Figure 38), NaChMM in the size of ~ 128 kDa will elute with the time of ~ 69 min. However, taking into account the detergent bound to NaChMM protein, it is expected to elute in less than 69 min.
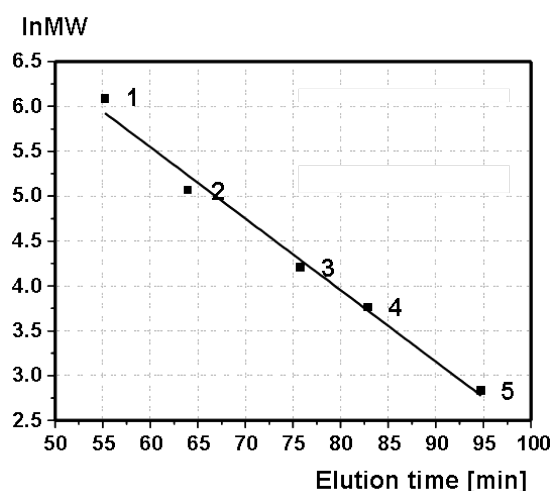
Figure 38: SEC calibration curve.
The ln of MW plotted against elution time of the globular soluble proteins chromatographed with HiLoad 16/60 Superdex 200 prep grade column (graph created using manufacturers' data); linear fitting equation: F(x) = -0.07971x + 10.33059; 1 – ferritin (440 kDa), 2 – IgG (158 kDa), 3 – albumin (67 kDa), 4 – ovalalbumin (43 kDa), 5 – myoglobin (17 kDa).

The elution times of the major peaks presented on the elution profiles in Figure 37 are 63.9 < 64.4 < 64.8 < 65.9 < 68.4 min for NaChMM protein purified in DDM, Anzergent 3-14, UDM, Cymal-6, DM, respectively. The shifts in the elution volumes of major peaks are potentially caused by differences in the amount of detergent bound to protein particle and the size of the resultant detergent micelle. The general summary of elution profiles is presented in Table 8.

Table 8: Summary of SEC elution profiles (presence and absence of different oligomeric forms).

NaChMM voltage-gated sodium channel purified in detergents:	Tetramers (elution volume, mL)	Oligomers (presence of protein eluted in the range of 50 mL to 60 mL)	Aggregates (presence of protein eluted at 45 mL)
DDM	63.9	Absent	Present
Anzergant 3-14	64.4	Absent	Absent
UDM	64.8	Present	Present
Cymal-6	65.9	Present	Absent
DM	68.4	Present	Absent

To analyse the oligomeric state, homogeneity and the secondary structure of NaChMM purified in different detergents, the major peaks were respectively subjected to cross-linking reaction, BN-PAGE and circular dichroism (see section 3.4.). The aforementioned samples were also subjected to an extensive crystallisation screening.

3.3.1.5. Purification of two truncated NaChMM proteins (NaChMMΔ18C and NaChMMΔ58)

In order to stabilise and improve the NaChMM protein crystallisation process, its secondary structure was searched for regions that could potentially prevent or disprove protein crystal formation.

The amino acid sequence comparison of NaChMM and NaChBac voltage-gated sodium channels, performed by means of "ClustalW" software, showed that NaChMM protein has an extended C-terminus (17 amino acids residues). What is more, the Regional Order Neural Network (RONN) software (Yang *et al.*, 2005) was used to predict the NaChMM protein disordered regions, due to which the last 18 amino acids at the C-terminus of NaChMM were classified as a mobile protein part that could cause potential difficulties in crystal formation. As a result, the truncated form NaChMMΔ18C was designed. Moreover, a second truncated version of NaChMM was created by removing 58 amino acids from the C-terminus and leaving the transmembrane part of the protein guarded only by small cytoplasmic N- and C-termini tails. Both variations of voltage-gated sodium channel, NaChMMΔ18C and NaChMMΔ58C, were cloned into pTrcHis2A vector, expressed and purified for

crystallisation experiments. The results of NaChMMΔ18C and NaChMMΔ58C purification are presented in Figure 39 and Figure 40, respectively.
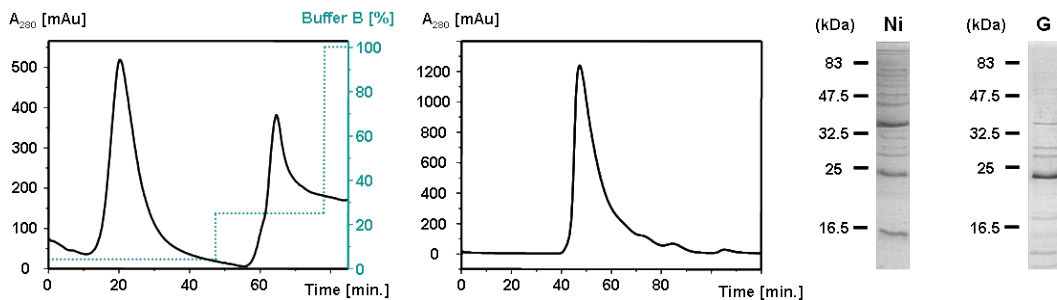
Figure 39: Purification of truncated NaChMMΔ18C.
Affinity chromatogram and gel filtration chromatogram followed by SDS-PAGE of protein sample after affinity purification (Ni) and protein sample after gel filtration purification (G).

The final amount of purified NaChMMΔ18C was established to be 0.5 milligram from a 1 L expression. The NaChMMΔ18C aggregated, what is visualised by the size exclusion chromatography elution profile in Figure 39.
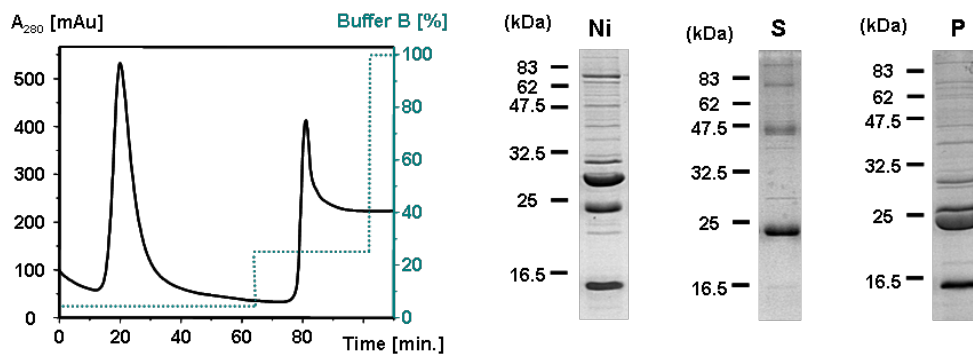
Figure 40: Affinity chromatography purification of truncated NaChMMΔ58C.
SDS-PAGE of protein sample after affinity purification (Ni), soluble protein sample after gel filtration purification (S) and precipitated protein sample treated with 8 M urea (P).

The NaChMMΔ58C appeared to be fully unstable and strongly precipitating after the $(His)_6$-tag removal (Figure 40), which is why gel filtration was not performed in this case. The most notable feature of NaChMMΔ58C is its extreme change in theoretical isoelectric point from ~ 6.8 to ~ 9.2 after its tag removal. This is suspected to be the reason for protein precipitation during thrombin digestion. The precipitating sample was centrifuged in order to separate precipitant "P" from supernatant "S", both of which were further analysed by

SDS-PAGE, what is presented in Figure 40. The analysed supernatant in lane "S" show a pure NaChMM representing four oligomeric populations (monomers, dimers, tetramers and, possibly, octamers). The continuous protein aggregation leads to further protein precipitation that affects the SDS-PAGE performance. SDS-PAGE denaturing conditions are not sufficient for a complete denaturation of NaChMMΔ58C sample, due to which different oligomeric forms are visible on the SDS-PAGE lane "S" (Figure 40).

The introduced truncations negatively affected the stability of NaChMM voltage-gated sodium channel protein, while the exact same purification conditions as for NaChMM (including buffering conditions) were used. Furthermore, the expression levels of NaChMMΔ18C and NaChMMΔ58C decreased drastically when compared to the production of full length NaChMM, which is why this approach was classified as insufficient for improvement of protein crystallisation.

3.3.2. Purification of NaChSP

Koishi and colleagues (2004) presented only the SDS-PAGE of affinity chromatography purification of NaChSP. Nevertheless, any further purification and protein characterisation steps were not reported in scientific literature. The purification protocol established for NaChMM was therefore adopted.

The extensive purification trials of NaChSP were leading to protein precipitation upon the removal of imidazole. A number of buffers with varying pHs (6, 7, 7.6, 8.5) and containing 100 mM NaCl were analysed. Stability of NaChSP sample was not, however, improved. Finally, different concentrations of NaCl were subjected for analysis. The purification process in the presence of 500 mM and 900 mM salts is depicted in Figure 41.

The NaChSP was preliminary subjected to a standard step gradient affinity chromatography (Figure 41A). This was followed by the exchange of NaChSP buffer into buffers containing 500 mM and 900 mM NaCl. Surprisingly, no precipitation occurred in either of the tested NaCl concentrations. In order to detect possible aggregates, both samples were thus analysed by gel filtration chromatography (Figure 41B).
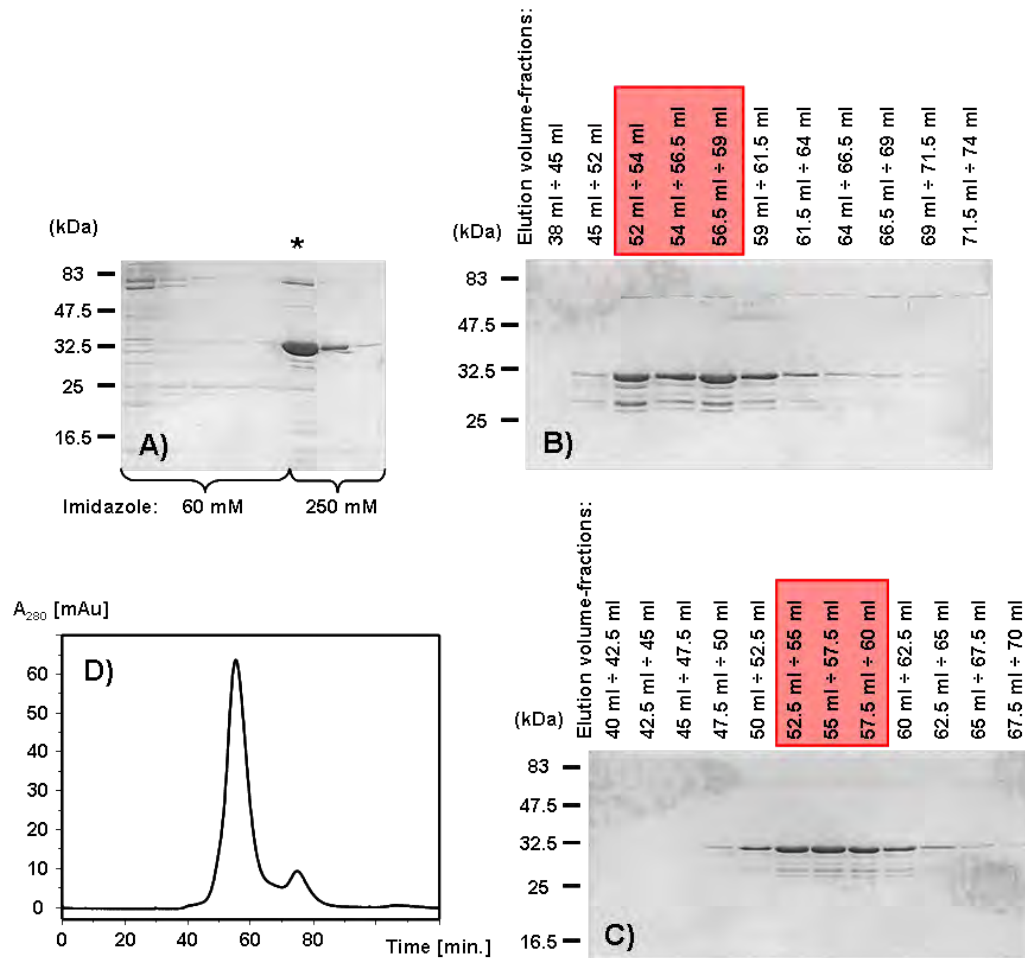
Figure 41: Purification of NaChSP using two different concentrations of NaCl.

A) SDS-PAGE of fractions collected during affinity purification; (*) fraction divided into two and separately analysed by SEC, the results of which are presented in figures B and C; B) SDS-PAGE of (His)$_6$-tagged protein fractions eluted during SEC with buffer containing 900 mM NaCl and C) 500 mM NaCl; D) final gel filtration elution profile of NaChSP without (His)$_6$-tag after pooling of fractions presented in figures B and C; NaChSP eluted with ~ 55 ml. Red boxes indicate the fractions of major NaChSP peak.

The gel filtration analysis presented in Figure 41B,C is clearly indicating that both NaChSP samples containing 500 mM and 900 mM NaCl are eluting with the same volume of ~ 55 mL. Hence, both samples were pooled and rechromatographed into 500 mM NaCl. The final gel filtration elution profile is presented in Figure 41D. The Gaussian peak (Figure 41D) representing pure NaChSP is migrating with the time of 55.4 min, which indicates a size of ~ 370 kDa that in turn suggests an octameric population of NaChSP.

The estimated amount of NaChSP purified from 1 litre expression was ~ 3 mg, which was a sufficient amount for both biochemical characterisation and crystallisation experiments.

3.3.3. Purification of NaChBac

In the beginning, and until 2008, when Nurani and colleagues (2008) presented biochemical characterisation of NaChBac, no information about NaChBac purification was available. Hence, similarly to NaChSP, the purification protocol established for NaChMM was also adopted for NaChBac. The purification by means of gel filtration buffer containing 100 mM NaCl is presented in Figure 42.
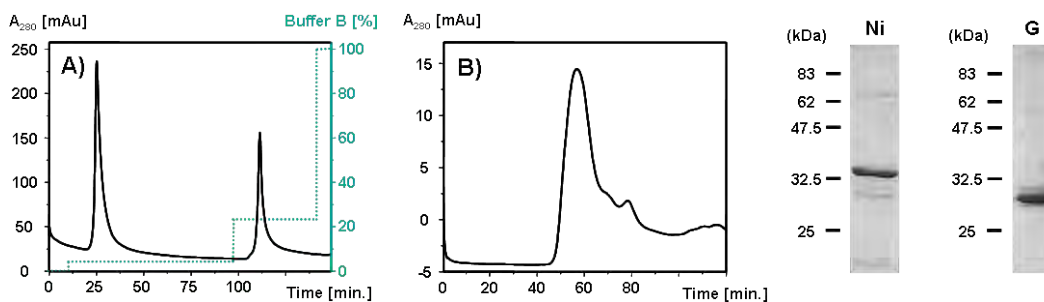
Figure 42: Purification of NaChBac.
Affinity chromatogram (A) and gel filtration chromatogram (B) followed by SDS-PAGE of protein sample after affinity purification (Ni) and protein sample after gel filtration purification (G).

In contrast to NaChSP, the NaChBac was found to be more stable. However, its slow progressive precipitation led to only a few micrograms of pure protein (Figure 42B), which was not sufficient for crystallisation trials. The influence of increased NaCl concentration was studied and the results are presented in Figure 43.
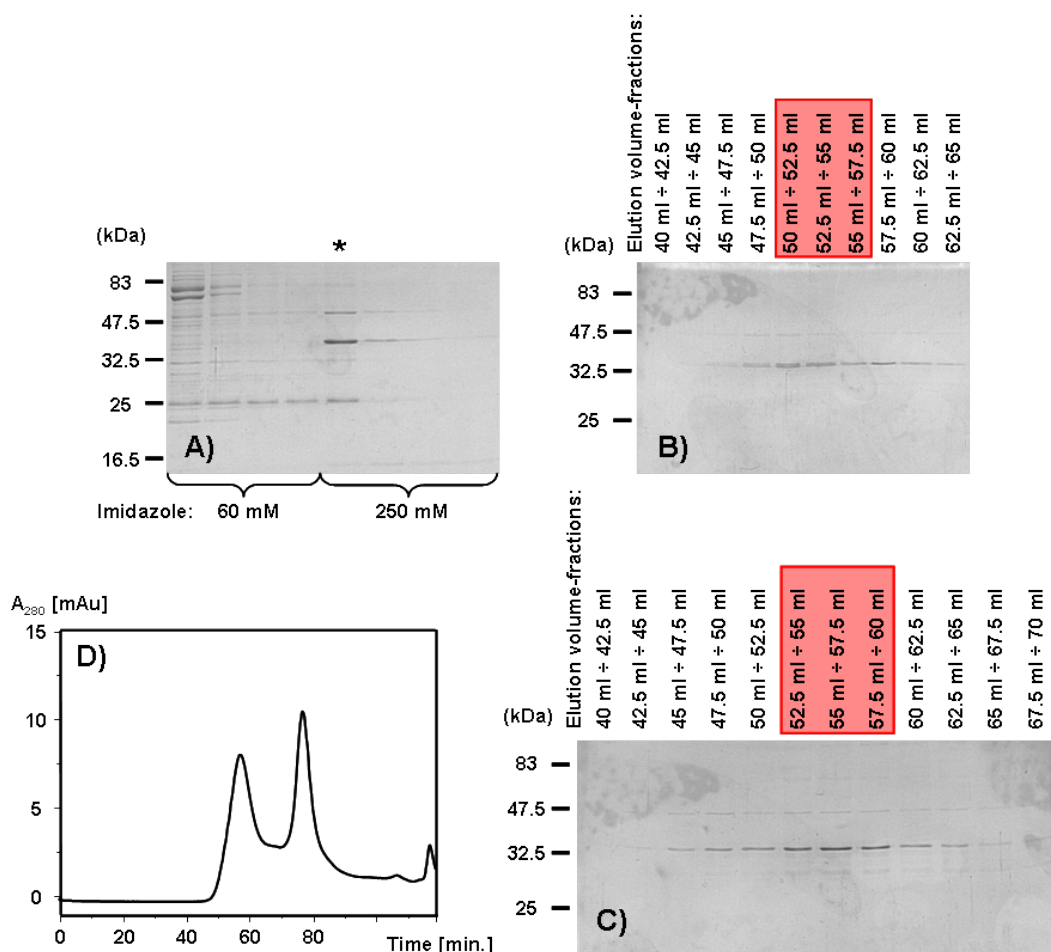
Figure 43: Purification of NaChBac using two different concentrations of NaCl.

A) SDS-PAGE of fractions collected during affinity purification; (*) fraction divided into two and separately analysed by SEC, the results of which are presented in figures B and C; B) SDS-PAGE of (His)$_6$-tagged protein fractions eluted during SEC with buffer containing 900 mM NaCl and C) 500 mM NaCl; D) gel filtration elution profile of NaChBac without (His)$_6$-tag after the pooling of the fractions presented in figures B and C; NaChBac eluted with ~ 55 ml. Red boxes indicate the fractions of major NaChBac peak.

As for NaChSP, the NaChBac was preliminarily subjected to a standard step gradient affinity chromatography (Figure 43A). After exchanging the buffer of NaChBac into two buffers containing 500 mM and 900 mM NaCl, respectively, the precipitation did not occur in either of the samples. In order to detect possible aggregates, both samples were thus analysed by gel filtration chromatography. The SDS-PAGE analysis presented in Figure 43B and C clearly indicates that the both NaChBac samples are migrating with the same volume of ~ 55 mL, which indicates possible octameric populations of NaChBac, the same

as for NaChSP. The final gel filtration analysis was performed (Figure 43D), yielding less than 0.5 mg of NaChBac from 1 L expression culture.

To summarise, the established NaChMM purification protocol was successfully adapted for two other target proteins (NaChSP and NaChBac). The full length NaChMM tetrameric voltage-gated sodium channel was the most stable protein that was purified in relatively large amounts and yielded ~ 6 mg from 1 L expression. The NaChBac and NaChSP were most probably purified in an octameric form, in the presence of high salts which prevent the protein from precipitation.

In 2008 a new expression and a purification approach was presented by Nurani and group. The NaChBac was cloned into pET15b(+) vector, which results in the expression of NaChBac with the N-terminal $(His)_6$-tag fusion. Therefore, to compare Nurani's approach with the one studied extensively in this research, the NaChBac and NaChMM genes were cloned into pET15b(+) expression vector, expressed and purified. The results for NaChBac and NaChMM are presented respectively in Figure 44 and Figure 45.
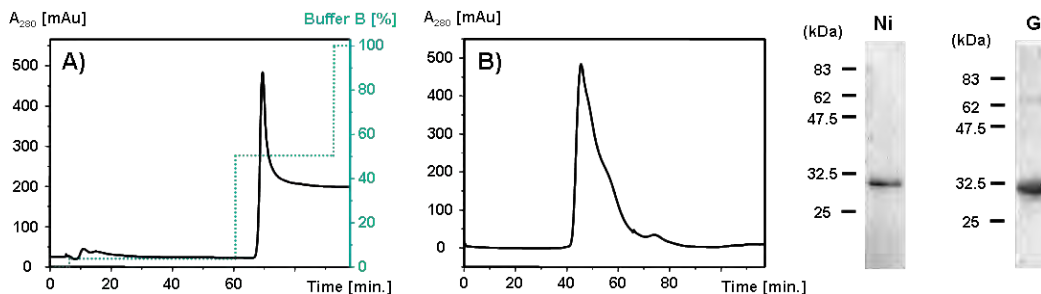
Figure 44: Purification of NaChBac.
Affinity purification (A) with corresponding SDS-PAGE – "Ni"; Gel filtration (B) with corresponding SDS-PAGE – "G".

The elution profiles of NaChBac and NaChMM gel filtrations detect significant protein aggregation. The modification of NaChMM by introduction of the $(His)_6$-tag at the N-terminus decreased the protein production levels. Moreover, the purification protocol used here did not result in obtaining of a pure NaChMM protein sample.
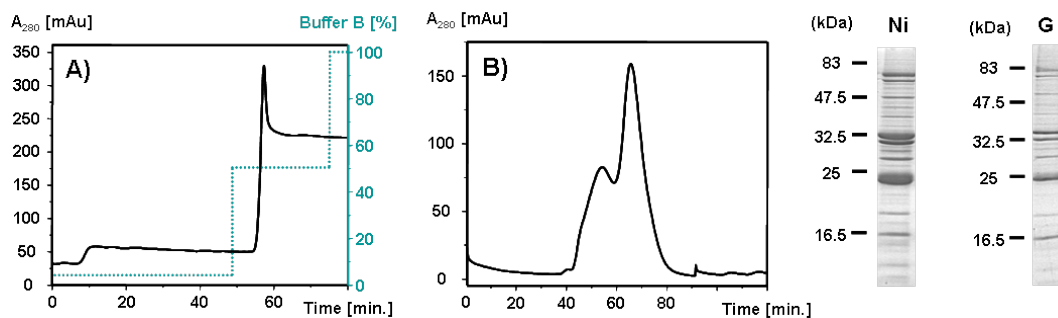
Figure 45: Purification of NaChMM.
Affinity purification (A) with corresponding SDS-PAGE – "Ni"; Gel filtration (B) with corresponding SDS-PAGE – "G".

Summary of purification of voltage-gated sodium channels NaChBac, NaChSP and NaChMM

As outlined in previous paragraphs, NaChBac, NaChSP and NaChMM were purified and showed different degrees of stability. In this study, it is clearly demonstrated that NaChBac and NaChSP are less stable. Yet, the final pure protein samples most probably consist of an octameric form of voltage-gated sodium channel protein. NaChMM voltage-gated sodium channel was produced in mg quantities in a pure and stable form.

The comparison of production levels of pure recombinant proteins and their stability is presented in Table 9.

Table 9: Comparison of different recombinant proteins, their stability and final amount.

	Amount of pure protein obtained from 1 l expression	Protein degradation	Protein aggregation	Protein precipitation
	Proteins produced using pTrcHis2A vector in *E. coli* BL21(DE3)			
NaChBac	Less than 0.5 mg	Fast	Medium	No
NaChSP	~ 3 mg	Fast	Medium	No
NaChMM	~ 6 mg	Slow	Low	No
NaChMMΔ18C	~ 3 mg	Slow	High	No
NaChMMΔ58C	-	Slow	-	Present
	Proteins produced using pET15b(+) vector in *E. coli* C41(DE3)			
NaChBac	~ 1 mg	None	High	No
NaChMM	~ 3 mg	-	Medium	No

Grey highlighted row – the most suitable protein, chosen for biochemical studies and crystallisation screening.

NaChMM was further analysed by several biochemical methods. Its crystalogenesis was investigated and its activity was studied by *in vivo* patch clamp assay.

3.4. Biochemical characterisation of NaChMM voltage-gated sodium channel

3.4.1. MALDI-TOF-MS, N-terminal sequencing

The MALDI–TOF mass spectrometry analysis of NaChMM revealed high purity of the protein sample, as only one major peak was labelled in the MALDI spectrum (Figure 46). The molecular mass (31821 Da) obtained for NaChMM is very close to the value calculated from the reported amino acid sequence (31924 Da). The 103 Da difference between the masses may indicate that the protein undergoes a modification during its expression. Moreover, enlargement of double-protonated molecular mass region suggests two forms of NaChMM that differ by 153 Da which corresponds to methionine mass.
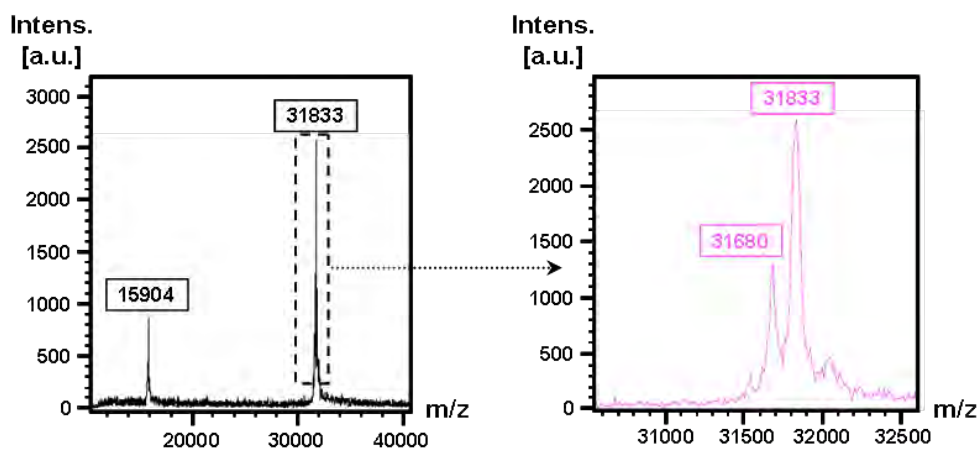
Figure 46: Mass spectrometry MALDI-TOF of NaChMM.
Single- and double-protonated (left) and magnification of the double-protonated NaChMM (right).

The N-terminal sequencing analysis confirms the processing of N-terminal methionine by *E. coli* and indicates that the ratio of protein with processed methionine to the full length is approximately 40:60 (Table 10).

Table 10: Results of N-terminal sequencing.

Cycle No	Peak ID	R. Time (min.)	C. Time (min.)	Height (mV)	pmol HT
1	**Met**	13.77	13.77	10.440	93.698
	Val	14.14	14.14	7.918	65.698
2	**Val**	14.14	14.14	10.278	85.282
	Met	13.77	13.77	7.169	64.344
3	**Met**	13.78	13.77	10.044	90.149
	Lys	17.99	17.96	9.777	76.693
4	**Lys**	17.98	17.96	12.545	98.409
	Ala	8.49	8.48	8.455	71.374
5	**Ala**	8.47	8.48	11.242	94.904
	Phe	17.22	17.21	6.899	46.708
6	**Phe**	17.24	17.21	8.715	59.002
	Val	14.15	14.14	7.593	63.004
Full length of N-terminus/Processed methionine					
Met-Val-Met-Lys-Ala-Phe/Val-Met-Lys-Ala-Phe-Val					

3.4.2. Cross-linking experiments

The heterologous expression of NaChMM protein and its further manipulations during purification procedure can affect the oligomeric state of NaChMM. In order to determine the oligomeric state of NaChMM, *in vitro* chemical cross-linking reaction, which is one of the strategies most commonly used for demonstration of protein-protein interactions, was therefore employed in this study.

The chemical cross-linking is involved in many proteomic methods, such as preparation of probes for western blotting and ELISA tests, including protein structural investigation (Weetall, 1974; Back *et al.*, 2003). What is more, it is widely used in the examination of transient or stable protein-protein interactions. The cross-linking technique uses chemical reagents which are capable of creating covalent bonds with specific functional groups (carboxyls, primary amines, sulfhydryls, carbonyls) that are found on proteins and other molecules.

The multimers forming the functional NaChMM sodium channel can only be covalently cross-linked when they are in a close physical interaction with one another. In order to determine whether NaChMM is present as a monomer or a dimer, or whether it forms a tetrameric complex *in vitro*, an analysis was

performed using two different cross-linkers: glutaraldehyde and formaldehyde that are commonly used in cross-linking reactions. Those reagents belong to a homo-bifunctional group of compounds and react mainly with ε-amine groups of lysine residues (Habeeb and Hiramoto, 1968; Richards and Knowles, 1968), creating stable inter- and intra-molecular cross-linkages.

The oligomeric state of pure protein *in vitro* depends on multiple parameters (Patzelt *et al.*, 2002), such as buffer type, pH or concentrations of both the protein and the cross-linker. Therefore, a wide range of NaChMM (0.25 mg/mL - 5 mg/mL) and cross-linker (0.1-1 % for formaldehyde and 0.3-5 % for gluteraldehyde) concentrations was used in the presented analysis. The pH of the performed cross-linking reaction was 7.4, which is an optimal pH for the protein stability. Moreover, the NaChMM was purified in 5 different detergents and the effect of each detergent on the oligomeric state of NaChMM was investigated. The cross-linked protein complexes were separated by a 12 % SDS-PAGE.

A preliminary study of various cross-linkers and their concentrations resulted in the selection of glutaraldehyde as the most suitable cross-linker for further investigation. Formaldehyde was sufficient to show formation of tetrameric NaChMM, but the amounts of formed dimeric and tetrameric populations of the protein were low when compared to the amount of monomer (Figure 47B). This indicates that some of the active groups lay far away from each other, preventing creation of additional covalent bonds which would otherwise increase dimeric and tetrameric species of NaChMM. Formaldehyde is most likely to limit the cross-linking reaction due to a very short spacer arm it forms. The increasing concentration of formaldehyde results in a slightly higher formation of tetramer species and also increases formation of intrabonds.
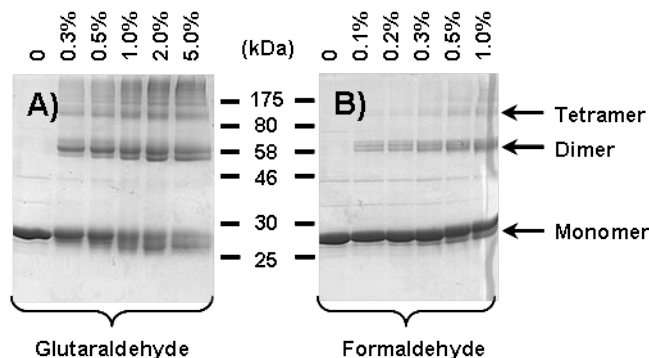
Figure 47: SDS-PAGE of NaChMM purified in DDM and cross-linked with glutaraldehyde (A) and formaldehyde (B).
The concentration of cross-liker used is indicated above gels.

By contrast, glutaraldehyde results in different monomer:dimer:tetramer ratios that fit to the statistical suggestions of Kapoor (2007). Based on theoretical and statistical analysis, the author states that when a cross-linking reaction is performed on tetrameric protein, the probability of intralinks formation in monomers is the highest. The formation of intralinks is followed by the creation of interlinks which results in dimeric, then trimeric and tetrameric species of protein sample, which results in the populations of each oligomeric state (monomer > dimer > trimer > tetramer) to decrease. However, when dimer interactions are preferred, their cross-linked population will be higher in relation to other monomeric, trimeric and tetrameric species.

The absence of trimeric species indicates that the dimer-dimer interaction (formation of tetramer) is stronger than the dimer-monomer interaction (Figure 47A). The presented results indicate that NaChMM forms a tetramer; however, to further assess the homogeneity of the protein, the cross-linking reaction of NaChMM with glutaraldehyde as a cross-linking agent at an optimised concentration of 0.3 % was performed (Figure 47A).

The probability of interactions between two protein subunits increases together with protein concentration. Therefore, at high concentrations, the protein may very often be present in the form of high oligomeric form (Payne, 1973). As the NaChMM forms tetramers, any shifts in the oligomeric equilibrium caused by the manipulation of protein concentrations could result in different tetramer:dimer:monomer ratios. This would help to establish the dependency of protein concentration versus its oligomeric state. To achieve this, a number of

various concentrations of NaChMM were subjected to cross-linking with glutaraldehyde. The results presented indicate that the oligomeric state of NaChMM is not concentration-dependent. The ratio between different forms is stable and comparable in each protein concentration (Figure 48).
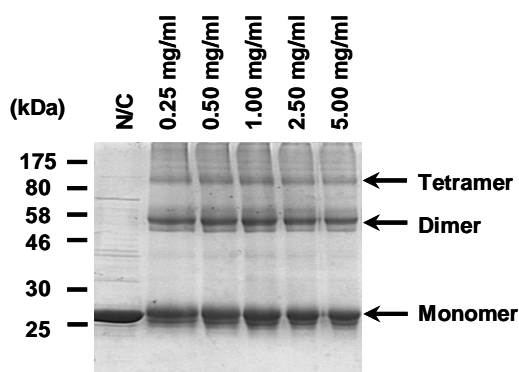
Figure 48: SDS-PAGE of NaChMM purified in DDM, cross-linked with glutaraldehyde.
N/C – non-cross-linked protein sample; the increasing concentrations of NaChMM used in chemical reactions are indicated on top of the gel.

Furthermore, different detergent application effects were analysed, as the type and concentration of a detergent can affect the oligomeric state of the protein (Heuberger *et al.*, 2002). The NaChMM was purified in 5 different detergents and the final elution profiles of their size exclusion chromatography are presented in section 3.3.1.3. In addition to the NaChMM sample eluted in the main peak in each detergent, the fractions that indicate an aggregation of the protein were also subjected to the cross-linking reaction (Figure 49).
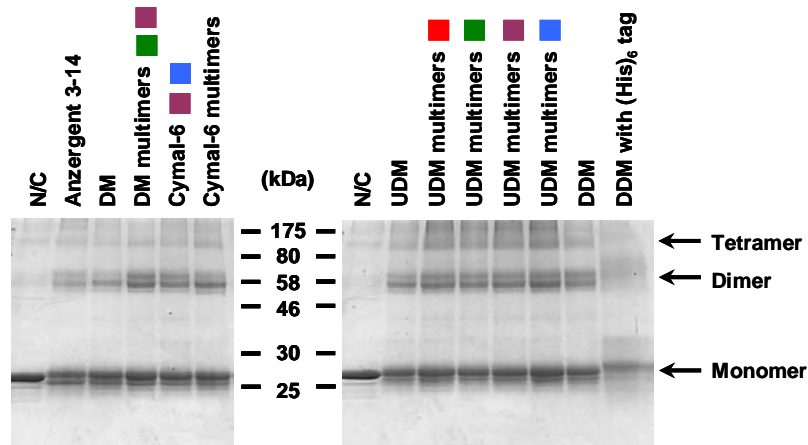
Figure 49: SDS-PAGE of pure NaChMM purified in 5 different detergents and cross-linked with glutaraldehyde.
N/C – non-cross-linked protein; the detergent used in buffer for protein stabilisation is indicated on top of the gel; the colours correspond to fractions used for cross-linking experiment (see section 3.3.1.3.).

Surprisingly, no significant correlation between the variation of a detergent and the oligomeric state of NaChMM was observed. The exact same pattern of monomer and higher molecular mass bands, corresponding to a dimer, tetramer and higher oligomers, was formed in each sample (main protein peak and aggregates).

The results presented in this section support our hypothesis that NaChMM forms tetrameric complexes. However, due to the positions of the lysines and the orientation of their side chains within the monomers, their intra- and intermolecular interactions do not favour the cross linking reaction of the tetramers only but also lead to formation of dimmers and higher oligomers.

3.4.3. BN-PAGE

BN-PAGE is a widely used method for the analysis of the composition, the oligomeric state and the molecular mass of soluble proteins. It can also be applied to analyse the membrane protein complexes. Nevertheless, due to the nature of membrane proteins, difficulties may arise during the experiment (Heuberger *et al.*, 2002). The mobility of protein molecules in the electric field is achieved by substituting detergent molecules with negatively charged Coomassie Brilliant Blue (CBB) dye.

Membrane proteins have an affinity for binding detergent or CBB dye (Heuberger *et al.*, 2002). Therefore, the apparent molecular mass established from BN-PAGE is often different than the calculated molecular weight. What is more, membrane proteins may aggregate upon the replacement of the detergent with the CBB dye, which appears as a ladder of bands at the top of the gel. The accurate determination of the molecular mass of a membrane protein can only be established when the amount of bound CBB dye and detergent per protein molecule is known. Heuberger and colleagues (2002) performed a parallel analysis of transporter proteins by BN-PAGE and analytical ultracentrifugation (Patzelt et al.), which led to the estimation of a conversion factor of 1.8 for the recalculation of the theoretical molecular weight into the experimental one. The factor was established from BN-PAGE migration pattern with respect to the migration of soluble protein standards.

The samples of NaChMM voltage-gated sodium channel purified in different detergent were subjected to BN-PAGE analysis for determination of its oligomeric state. The same samples of NaChMM analysed with SDS-PAGE show a single protein band migrating at a size of monomeric NaChMM form (see section 3.3.1.4.).
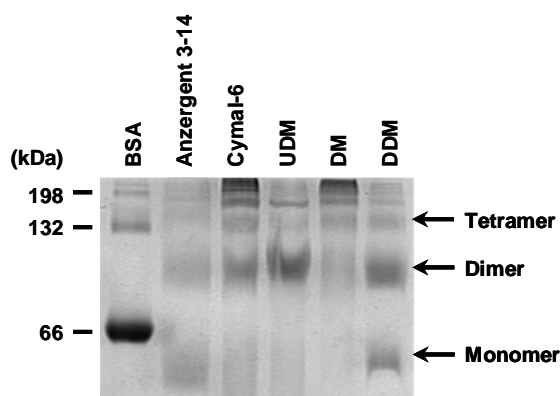
Figure 50: BN-PAGE of pure NaChMM purified in 5 different detergents.
From lane 1-5 are Anzergent 3-14, Cymal-6, UDM, DM, and DDM respectively.

The BN-PAGE experiment indicates that NaChMM is present as a heterogeneous protein mixture. Monomers, dimers and tetramers can be observed in Figure 50. The ratios of different oligomeric forms differ, depending on the type of detergent present in the sample. The NaChMM purified in the presence of 0.06 % UDM or in the presence of 0.06 % Cymal-6 reveals a tendency for

dimerisation, while the NaChMM purified in 0.05 % DDM reveals a significant amount of monomeric NaChMM species.

3.4.4. Circular dichroism analysis of NaChMM

The secondary structure of NaChMM was investigated by means of circular dichroism which was established as a standard tool in structural investigations of membrane proteins.

The NaChMM purified in different detergents (DDM, DM, UDM, Anzergent 3-14, Cymal-6) resulted in spectra with negative signals at ~ 222 and ~ 210 nm and a positive signal at ~ 192 nm (Figure 51), which are characteristic for proteins containing α-helical structures (Wallace *et al.*, 2003). The proportions between the negative peaks were similar in all samples.
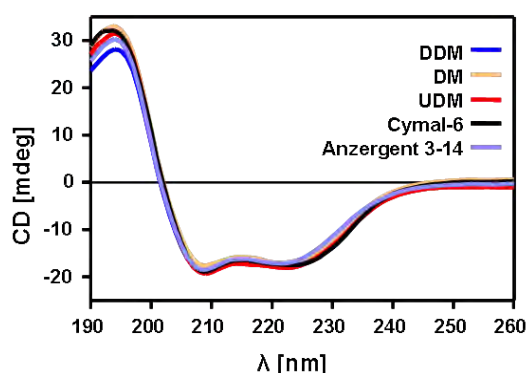
Figure 51: CD spectra of NaChMM purified in 5 different detergents.

Based on its amino acid sequence, the theoretical content of α-helices in NaChMM was calculated, which resulted in 70 %, 79 % and 58 %, when analysed with JPred, PHDsec and PSI-BLAST algorithms, respectively. The composition of secondary structure elements of NaChMM purified in various detergents, based on the CD spectra (Figure 51), was established by CDNN software and the results are presented in Table 11.

Table 11: Secondary structure elements of NaChMM purified in different detergents.

Type of secondary structure	DDM	DM	UDM	Cymal-6	Anzergent 3-14
Helix	55 %	62 %	64 %	63 %	55 %
Anti-parallel	2 %	1 %	1 %	1 %	2 %
Parallel	5 %	4 %	4 %	4 %	5 %
Beta-turn	14 %	12 %	12 %	12 %	14 %
Random Coil	19 %	18 %	15 %	16 %	19 %
Total	95 %	97 %	96 %	96 %	95 %

The α-helical content of NaChMM was found to vary between 55 % and 65 % in different detergents. The difference of 9 % in helical secondary structures can indicate the loss of one of the α-helices, with a parallel increase in random coil structures. The content of α helices is lower for the detergents including long hydrophobic tails (DDM and Anzergent 3-14) and it increases when the hydrophobic tails of the detergents used are shorter (DM, UDM and Cymal-6).

The CD analysis confirms that NaChMM expressed in *E. coli*, which was extracted and purified in a variety of detergents, preserve the helical structure characteristic for members of the voltage-gated ion channels family.

Summary of biochemical characterisation of NaChMM voltage-gated sodium channels

NaChMM mass was investigated by MALDI-TOF-MS and revealed a 103 Da difference between the calculated and the experimental mass. Moreover, two populations of the protein were discovered, one with and one without the first methionine, which was additionally confirmed by the N-terminal sequencing. The experiment conducted to establish the oligomeric state of the protein did not give a straight answer. In addition, the cross-linking experiments performed on NaChSP (potential octamer) resulted in the same pattern of protein bands as for NaChMM, which indicates that this method is not suitable for establishing the oligomeric state of NaChMM. The circular dichroism analysis confirmed α-helical structure of NaChMM.

3.5. Crystallisation trials

The crystallisation condition, in which protein crystals diffracting to a high resolution can be grown, is unpredictable. As a result, to increase the likelihood of generation of well-shaped crystals that could be subjected to X-ray structural analysis, twenty two different crystallisation screens (Table 12) and eleven NaChMM samples (Figure 52) were used to probe the crystallogenesis of the NaChMM voltage-gated sodium channel.

In Figures 53, 54 and 55 that present crystallization hits, the code in the top left corner of each photograph indicates the sample number (s.), type of crystallisation screen (c.s.) and the number of crystallization condition.

Table 12: List of crystallisation screens used in this study.

Letter	Screen Name	No of conditions
(A)	Crystal Screen	48
(B)	Crystal Screen 2	48
(C)	Natrix	48
(D)	Index	96
(E)	SaltRx	96
(F)	PEG/Ion	48
(G)	PEG/Ion 2	48
(H)	MembFac	48
(I)	Crystal Screen Lite	50
(K)	Detergent Screen HT	96
(L)	Wizard I	48
(M)	Wizard II	48
(N)	Wizard III	48
(O)	MemStart	48
(Q)	MemSys	48
(P)	ProPlex	96
(R)	PACT premier	96
(S)	JCSG-*plus*	96
(T)	MemGold	96
(U)	JBScreen Cryo	96
(W)	ModifMemGold	96
(X)	PEG Screen	96
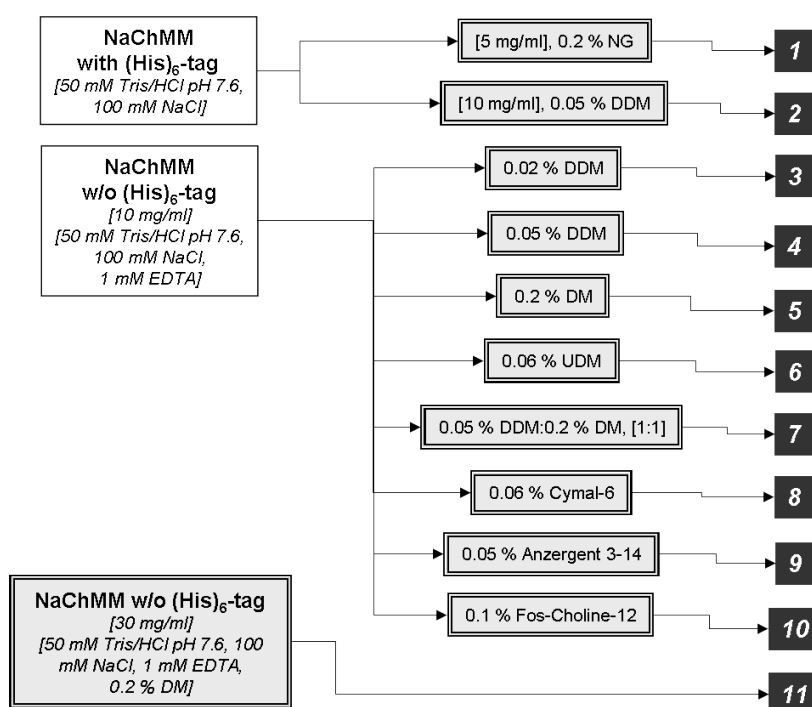
Figure 52: Characteristics of NaChMM protein samples subjected to crystallisation screening.
To further simplify the description of the crystallisation screening process, a single number code that corresponds to a unique sample was introduced.

Three different protein concentrations were used for NaChMM crystallisation screening: 5 mg/mL, 10 mg/mL and 30 mg/mL. In most cases, trials using the highly concentrated sample (30 mg/mL) resulted in a precipitation of the protein and, therefore, the sample was labelled as not suitable for further analysis. NaChMM at concentration of 5 and 10 mg/mL were henceforth used in subsequent crystallisation trials.

Seven protein samples containing different detergents (DDM, DM, UDM, Cymal-6, Anzergent 3-14, NG and Fos-Choline-12, and mixture DDM:DM-1:1) were subjected to crystallisation trials. Crystallisation trials with protein solubilised either in a buffer containing Fos-choline-12 or a buffer containing a mixture of DDM:DM (1:1) did not lead to formation of any crystal-like structures. Most of the crystal hits for NaChMM samples purified in other detergents were observed in the presence of polyethylene glycols (PEGs) used as precipitating agents.

The preliminary crystallisation hits resulting in <u>irregular bulky structures</u> were obtained for the NaChMM sample purified in DDM, using MembFac and Crystal Screen Lite crystallisation screens. These experiments were followed by investigation of pH and PEG variations using NaChMM samples purified in different detergents. The process resulted in the formation of <u>crystal-like structures with regular edges</u> for NaChMM sample in the presence of UDM or Cymal-6 (Figure 53).
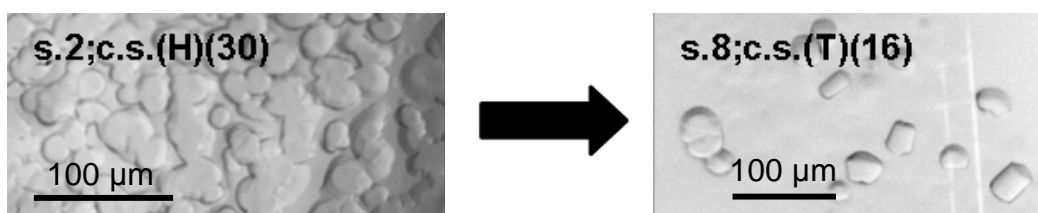
Figure 53: Irregular bulky structures before optimisation and crystal-like structures with regular edges after optimisation.

The nano-scale crystallisation process of NaChMM in DM conducted in the presence of additives, MEGA-10 detergent or fluorinated octyl maltoside detergent, resulted in the growth of <u>needle-shaped crystal-like structures</u> (Figure 54). However, the up-scaling of the experiments performed at a micro-scale proved to be difficult and the crystal-like structures could not be reproduced.
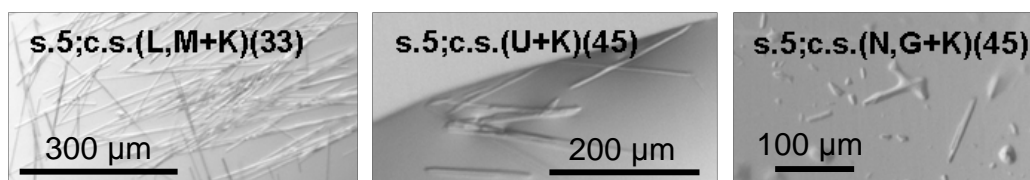
Figure 54: Needle-shaped crystal-like structures.

A number of crystal-like structures was also observed after a long time of incubation (several months), which is summarised in Figure 55. Due to the amount of crystal-like shapes produced, their size and, mainly, their irregularity, they were not subjected to X-ray diffraction experiments.
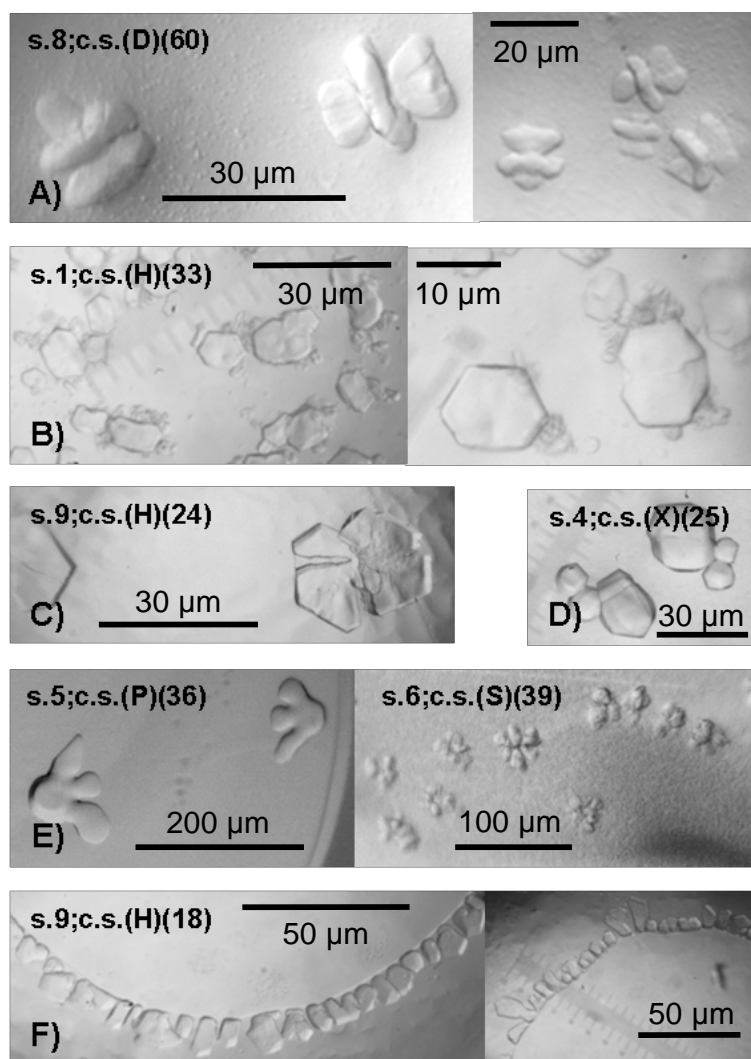
Figure 55: Unique crystal-like structures obtained during crystallisation trials.

A) Crystal-like sandwich-butterfly-shaped structures of NaChMM in Cymal-6 grown in the following unique crystallisation condition: at a pH of 8.5, with CoCl$_2$ and in the presence of polyviylpyrrolidone K 15 as a precipitating agent; B) Crystal-like hexagonal plates structures obtained with (His)$_6$-tagged NaChMM samples in NG in a unique crystallisation condition, at a pH of 7.5 and PEG 400; C) Crystal-like flower plates structures with sharp edges obtained with NaChMM in Anzergent 3-14, in the following crystallization conditions: at a pH ~ 7, with high concentrations (~ 1 M) of ammonium or sodium phosphate salts; D) Crystal-like irregular structures with twin spheres attached obtained with NaChMM in 0.05 % DDM, in an unique crystallisation condition at a low pH and in the presence of 10 % PEG 1,000; E) Crystal-like flower structures with dull edges obtained with NaChMM in DM or UDM, in the presence or absence of salts and PEG 400 or PEG 4,000; F) Crystal-like plates structures with sharp edges grown on a phase separation surface obtained with NaChMM in 3-14, in a unique crystallisation condition at a pH of 5.6 with Li$_2$SO$_4$, and PEG 6,000.

3.6. Mammalian electrophysiology

Voltage patch clamp technique was shown as the method of choice for *in vivo* analysis of voltage-gated ion channels. Hence, in order to confirm NaChMM function as a voltage-gated sodium channel, the analysis of its activity was undertaken by means of this technique. The gene encoding for NaChMM was thus cloned into a mammalian expression vector that can be used in a transient transfection. An enhanced green fluorescent protein (EGFP) was used for the identification of expressing cells (Heim *et al.*, 1995).

Four constructs were designed and generated for the expression of NaChMM in mammalian cells (schematic representation in Figure 56). NaChMM with N- and C-terminally fused EGFP (Figure 56A,B) were constructed for easy identification and localisation of the recombinant protein in the cell. Furthermore, the native gene encoding for NaChMM (Figure 56D) and the fusion of NaChMM with neuromodulin signal sequence (Figure 56C) were cloned under the control of a strong human cytomegalovirus (CMV) promoter, while EGFP-Zeocin was introduced under a Simian virus 40 (SV40) promoter. Such way of a construct design allows for an independent expression of voltage-gated sodium channel and selection marker (Ren *et al.*, 2001). Expression of the EGFP-Zeocin under SV40 promoter indicated successful transfection of the cells with the prepared vector, which allows the assumption that the voltage-gated sodium channel is expressed in a parallel, from the CMV promoter. In addition, a positive control for the electrophysiology experiments in the form of NaChBac sodium channel was also prepared (Figure 56E). Similarly to one of the NaChMM constructs (Figure 56D), the native gene encoding for NaChBac was cloned into modified pcDNA3.1(+) vector under CMV promoter, which allows for an independent expression of the sodium channel and the selection marker.
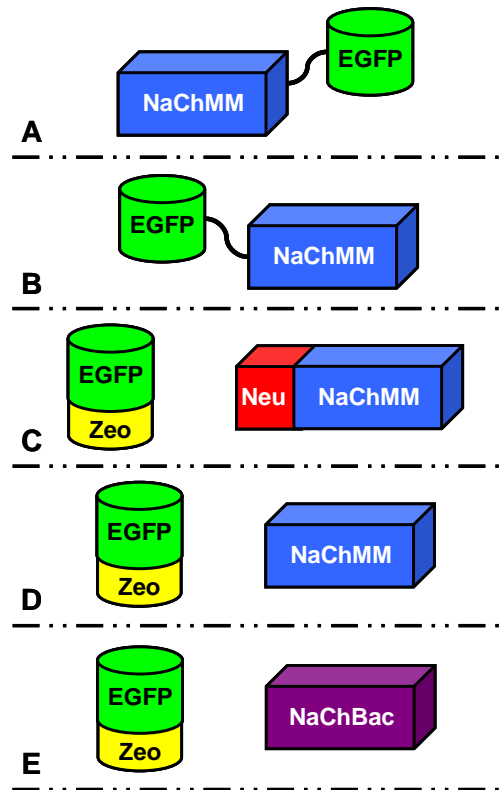
Figure 56: General representation of recombinant proteins designed for electrophysiological investigations.

NaChMM voltage-gated sodium channel from Maricaulis maris MCS10 was cloned under a CMV promoter, expressed with A) C-terminal EGFP fusion or B) N-terminal EGFP fusion; C) NaChMM cloned under CMV promoter, expressed independently from EGFP-Zeocin fusion cloned under SV40 promoter, with N-terminal neuromodulin (Wadsten et al.) signal sequence, D) native NaChMM expressed independently from EGFP-Zeocin; E) NaChBac voltage-gated sodium channel cloned from Bacillus halodurans C-125 under CMV promoter, expressed independently from EGFP-Zeocin fusion cloned under SV40 promoter.

3.6.1. Initial activity analysis of NaChMM

3.6.1.1. Activity analysis of GFP-fused NaChMM

The NaChMM protein fused to the EGFP at N-terminus and the NaChMM protein fused to the EGFP at C-terminus are encoded within the pEGFP plasmids which were then transiently transfected into the tsA201 human kidney cell line. Determination of expression yields of the recombinant proteins was performed by visual estimation of fluorescent levels by means of fluorescent microscope during a patch clamp experiment. The observation of EGFP-NaChMM and NaChMM-EGFP fluorescence indicated that high levels of those

fusion proteins accumulate in tsA201 cells. However, subsequent patch clamp experiments indicated that those fused proteins were not active. The lack of a current signal during these tests could be a result of the following: misfolding of the channel protein; incorrect insertion of the protein into cell membrane; partial protein expression or protein degradation. In order to investigate this issue further, the whole cell extract was subjected to SDS-PAGE (Figure 57).
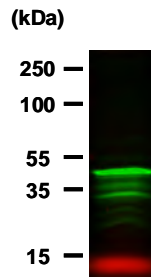
Figure 57: SDS-PAGE of recombinant fusion protein NaChMM-EGFP.
EGFP fusion protein was visualized by scanning wet SDS-PAGE with a fluorescence scanner (Typhoon 9400).

The fusion of EGFP with NaChMM enabled easy and simple visualization of expressed recombinant protein. The resulted SDS-PAGE gel was subjected to excitation with 457 nm and 532 nm filters to visualise marker bands and excite EGFP, respectively. The most prominent band is likely to present a full length protein (Gendreau *et al.*, 2004), nonetheless, with a strong tendency for degradation (Figure 57).

In order to determine membrane insertion of the protein, the cells transfected with the corresponding vectors were analysed by means of confocal microscopy. This revealed that the protein is not successfully embedded in the membrane (Figure 58). Instead, it is likely to aggregate in the endoplasmic reticulum (ER) and in Golgi apparatus. Such mis-trafficking was previously reported for mammalian $Na_v1.8$ voltage-gated sodium channel (Zhao *et al.*, 2007). In order to enhance the proper trafficking of the protein, the cells were incubated with lidocaine. However, subsequent cell voltage-treatment resulted in no response in current signal.
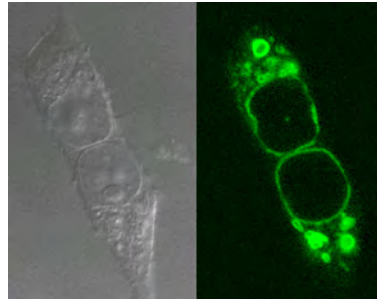
Figure 58: Laser scanning confocal microscopy (LSCM) of tsA201 cells expressing NaChMM-EGFP fusion protein.
Left – Cells without excitation; right – cells excited with 488 nm wavelength that was collected at 509 nm wavelength.

3.6.1.2. Activity assay of fusion-free NaChMM

Further analyses were conducted with pcDNA3.1(+)-based constructs in which genes encoding for the channel proteins were expressed independently from EGFP-Zeocin and in the preparation of which extensive DNA manipulation was involved. In addition, positive control NaChBac was also created in the same way. Due to the fusion-free form of the protein, the size of voltage-gated sodium channel and its cell localisation could not be investigated by SDS-PAGE or LSCM.

The tsA201 cells transfected with the vector carrying the gene encoding for NaChBac were subjected to the patch clamp experiments and, as expected, revealed a positive signal. The tsA201 cells were producing high levels of protein, making the whole-cell current investigation relatively easy. What is more, the activity of the native NaChMM and Neuromodulin-NaChMM was analysed by the same method. In the initial experiments, the levels of both proteins expressed in the tsA201 as well as the number of expressing cells were very low. To increase the level of protein produced, the amount of transfected plasmid DNA was increased to 10 μg, whilst the incubation times after the transfection and cell splitting were both increased to 18 h. This resulted in the stabilisation of the tsA201 cells and made them less sensitive to patch clamp tests.

Both, native NaChMM and Neuromodulin-NaChMM revealed inward current during patch clamp analysis, which indicated a voltage-gated activity of the produced proteins. Since the native NaChMM exhibited activity, it was chosen for further electrophysiological experiments. Furthermore, in comparison

to Neuromodulin-NaChMM and as judged by the observation of fluorescence levels of EGFP-Zeocin protein expressed from SV40 promoter, the native NaChMM additionally exhibited less toxicity to the cells.

The expression and activity measurements of the recombinant voltage-gated sodium channels produced in tsA201 cells are summarized in Table 13.

Table 13: Summary of mammalian expression.

	EGFP-NaChMM	NaChMM-EGFP	NaChMM	Neu-NaChMM	NaChBac (positive control)
Number of expressing tsA201 cells	High	High	Very low	Very low	Low
Level of expression	High	High	Low	Very low	High
Toxicity of recombinant proteins for the expressing cells	Low	Low	Very high	Very high	Low
Level of experimental difficulty	Low	Low	High	Very high	Low
Activity	Absent	Absent	Present	Present	Present
Selection of the construct for detailed activity study	N/A	N/A	Selected	N/A	N/A

3.6.2. Current measurement of the native NaChMM

Voltage-gated sodium channel from *Maricaulis maris* was cloned into a modified pcDNA3.1(+) mammalian expression vector and transfected into tsA201 cells. The channel protein was successfully expressed which further resulted in the response of large voltage-activated inward currents (up to 15 nA). Non-trasfected tsA201 cells were used as a negative control.

3.6.2.1. Current-voltage plot (I-V plot)

The high amino acid sequence identity of the NaChMM with known voltage-gated sodium channels, such as NaChBac (36 %) and NaChSP (49 %), indicates that NaChMM belongs to this protein family. However the highly conserved amino acids situated in the pore region responsible for channel selectivity are also highly conserved in the calcium channels (Figure 59). This

could raise a question of NaChMM classification as a sodium channel. Na⁺ selectivity of NaChMM voltage-gated channel was thus assayed. This was accomplished by the application of repetitive electric impulses to different voltages (Figure 60A), which caused the NaChMM to open and allowed Na⁺ ions to flow from the outside to the inside of the cell, generating an electrical current (Figure 60B).

```
        NaChBac  YFGNLQLSLLILFQVVTLESWASGVMR
        NaChMM   RFGSLGESAFALFQVMTLEGWATDVAI

    I   Cav1.2   NFDNFAFAMLIVFQCITMEGWTDVLYN
        Cav2.2   NFDNILFAILIVFQCITMEGNTDILYN

    II  Cav1.2   TFDNFPQSLLIVFQILTGEDWNSVMYD
        Cav2.2   NFDTFPAAILIVFQILTGEDWNAVMYN

    III Cav1.2   DFDNVLAAMMALFTVSTFEGWPELLYR
        Cav2.2   HYDNVLWALLTLFTVSTGEGWPMYLKH

    IV  Cav1.2   NFQTFPQAVLLLPRCATGEAWQDIMLA
        Cav2.2   NERTFLQALMLLFRSATGEAWHEIMLS
```

Figure 59: Amino acids sequence alignment of pore region of prokaryotic voltage gated sodium channels with four domains of Ca$_v$1.2 and Ca$_v$2.2 calcium channels.

The movement of positive charges across the cell membrane increases the positive charges inside the cell, the counterbalance of diffusive and electrical forces or the so-called reversal potential (equilibrium potential - E$_{eq}$) ensues, which leads to an Na⁺ arrest,. This can be established experimentally by plotting the voltage against the current (Figure 60C) and compared with the theoretical value that can be calculated (for chosen, specific ion) using the *Nernst* equation (Hille, 2001):

$$E_{eq} = \frac{RT}{zF} \ln \frac{[Ion]_{out}}{[Ion]_{in}}$$

where E$_{eq}$ – equilibrium potential [mV], R – gas constant 8.314 [Jmol^{-1}K^{-1}], T – absolute temperature [K], z – the number of elementary charges of the ion in question involved in reaction, F – Faraday constant 96485 [JV^{-1}mol^{-1}], [Ion]$_{out}$ and [Ion]$_{in}$ – extracellular and intracellular concentration of investigated ion [mM].
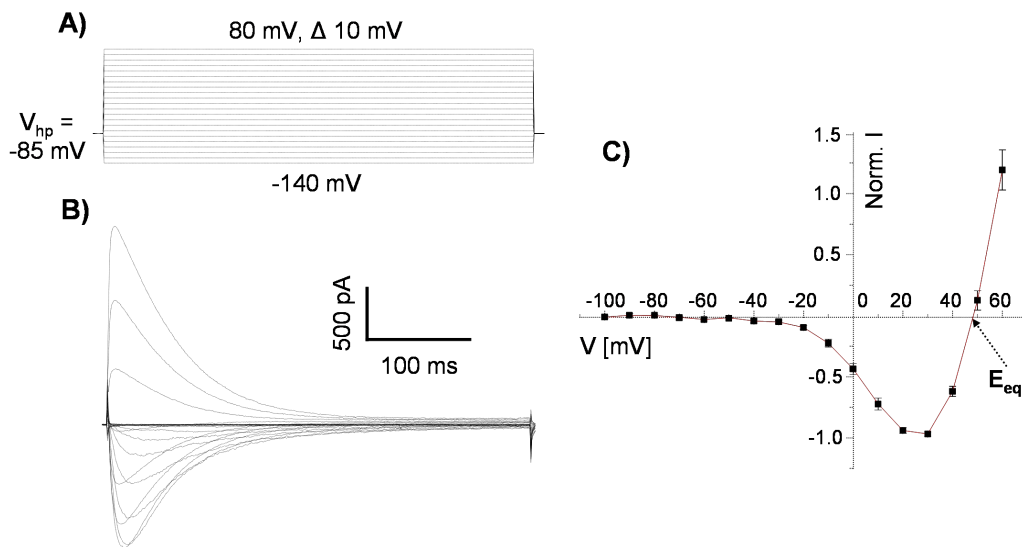
Figure 60: Current-voltage plot of NaChMM.
A) Waveform stimulus (holding potential -85; voltage impulses applied from -140 mV to 80 mV with increments of 10 mV); B) representative trace – current response C) I-V plot (n = 10), where $E_{eq} = 48.3$ mV.

►**Experimental value of reversal potential (E_{eq}) was established to be 48.3 mV.**◄

The NaChMM patch clamp experiments performed at 22 ± 2 °C with the use of buffers typical for measuring electrical current generated by transport of Na^+ ions revealed the experimental value of reversal potential (E_{eq}) of 48.3 mV (Figure 60C). Theoretical values for equilibrium of Na^+, K^+ and Mg^{2+} ions were calculated and are summarised in Table 14. The example of calculation for Na^+ is presented below. The calculations were performed with the application of the appropriate outside-cell and inside-cell concentration of chosen ions (according to the buffer used).

$$E_{eq,Na^+} = \frac{8.314\frac{J}{mol \cdot K} \times 295.15K}{+1 \times 96485\frac{J}{V \cdot mol}} \ln \frac{[160mM]}{[25mM]}$$

$$E_{eq,Na^+} = 47.2mV$$

►**Theoretical value of reversal potential (E_{eq}) was calculated as 47.2 mV.**◄

The experimentally determined value of 48.3 mV for reversal potential (E_{eq}) of Na^+ ions is in good agreement with the calculated theoretical value of 47.2 mV. Summarised in Table 14 are the experimental and calculated theoretical values of equilibrium potential which deliver a clear-cut proof that NaChMM is, indeed, a voltage-gated sodium channel.

Table 14: Comparison of experimental and theoretical values of equilibrium potential.

Experimental value	Theoretical value – *Nernst* equation		
E_{eq}	E_{eq,Na^+}	E_{eq,K^+}	$E_{eq,Mg^{2+}}$
48.3 mV	**47.2 mV**	-23.3	0.0
Experimental buffer conditions (see section 2.2.3.6.3.)	$[Na^+]_{out} = 160$ mM $[Na^+]_{in} = 25$ mM	$[K^+]_{out} = 2$ mM $[K^+]_{in} = 5$ mM	$[Mg^{2+}]_{out} = 1$ mM $[Mg^{2+}]_{in} = 5$ mM

When comparing NaChMM with the previously described prokaryotic voltage-gated sodium channels, the minimum of the I-V plot is shifted to positive potentials, which is only reported for one voltage-gated sodium channel that was cloned from *Silicibacter pomeroyi* DSS-3 (Koishi *et al.*, 2004). Moreover, the activation threshold for this channel protein appears between -30 and -25 mV and the maximum inward current falls between 20 and 30 mV (Table 15).

Table 15: Activation threshold and voltage at which the maximum inward current was recorded for different prokaryotic voltage-gated sodium channels.

	Activation threshold	Voltage – max inward current recorded	Reference
Na_vBP	-70 to -60 mV	-10 mV	(Ito *et al.*, 2004)
Na_vRosD	-60 to -50 mV	-10 mV	(Irie *et al.*, 2010)
Na_vSheP	-110 to -100 mV	-50 mV	
Na_vBacL	-100 to -90 mV	-40 mV	
Na_vSP	-35 to -25 mV	30 mV	(Koishi *et al.*, 2004)
Na_vPZ	-40 to -30 mV	10 mV	
NaChBac	-50 to -40 mV	-10 mV	(Ren *et al.*, 2001)
NaChMM	**-30 to -25 mV**	**25 mV**	**This study**
$Na_v1.7$	-45 to -35 mV	-15 mV	(Vijayaragavan *et al.*, 2004)
$Na_v1.8$	-25 to -15 mV	5 mV	

3.6.2.2. Activation of voltage gated sodium channel

The activation of the NaChMM was determined by a sequential depolarization to a variety of voltages, followed by voltage return to a holding potential of -85 mM (Figure 61A). The voltage-dependent activation was evaluated by measuring the deactivation tail currents (Figure 61B) and plotting them against voltage pre-pulses. A single Boltzmann function:

$$f(V) = V_{min} + \frac{V_{max} - V_{min}}{1 + e^{\frac{V - V_{\frac{1}{2}}}{k}}}$$

was fit to the averaged activation curve yielding a midpoint voltage V_h of 25.8 ± 0.9 mV (Figure 61C).

Figure 61: Activation of NaChMM.
A) Waveform stimulus (holding potential -85; voltage impulses applied from -100 mV to 60 mV with increments of 10 mV); B) representative trace – current response C) activation curve (n = 3), where $V_h = 25.8 \pm 0.9$ mV.

To evaluate the activation kinetics, a characteristic time constant (τ_{ON}) was derived from fitting single exponential curves to the inward current peaks recorded at different voltage test pulses (range from 0 to I_{max}). The speed of activation changes with voltage values. At negative voltages the NaChMM is opening slowly, while at positive voltages the process becomes progressively

faster (Figure62A). The deactivation kinetics (Nenov *et al.*, 1998) was established by fitting single exponential curves to the inward current peaks recorded at different voltage test pulses (range from I_{max} to 0). The speed of NaChMM deactivation changes with voltage values and is getting slower as the voltage pulses enter positive values (Figure 62B).
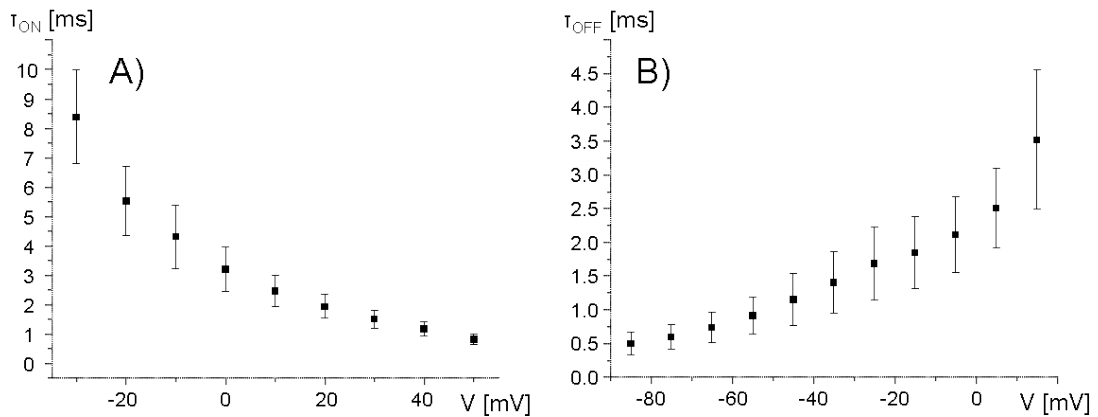
Figure 62: Activation kinetics (A) and deactivation kinetics (B).
Activation kinetics (holding potential -85; voltage test pulses applied from -30 mV to 50 mV, with increments of 10 mV, n = 4) and deactivation kinetics, (holding potential -85; voltage pre-pulse 120 mV, test pulses applied from -85 mV to 15 mV, with increments of 10 mV, n = 2).

NaChMM activation time is relatively fast (τ_{ON} = 1.5 ± 0.3 mV at 30 mV) when compared to NaChBac (τ_{ON} = 12.9 ± 0.4 ms at -10 mV). The time constant of NaChMM is as small as the one of sodium channels $Na_v1.7$ and $Na_v1.8$ from rat dorsal root ganglion (Vijayaragavan *et al.*, 2004). It may be observed that NaChMM activates at the highest membrane potential of all NaChBac homologues studied to date. However, NaChMM activation midpoint is similar to the V_h of NaChSP, which seems unsurprising, as the two prokaryotic voltage-gated sodium channels reveal the highest (49 %) amino acid identity. The summary, of the voltage dependencies of the prokaryotic and eukaryotic voltage-gated sodium channels compared to NaChMM, is presented in Table 16.

Table 16: V_h of activation and time constants of activation for selected prokaryotic and mammalian voltage-gated sodium channels.

	Activation midpoint	Time of activation (τ_{ON})	Reference
Na$_v$RosD	-25.9 ± 1.2 mV	1.6 ± 0.1 ms at 20 mV	(Irie *et al.*, 2010)
Na$_v$SheP	-80.0 ± 0.9 mV	0.9 ± 0.08 ms at -10 mV	
Na$_v$BacL	-63.7 ± 1.8 mV	4.9 ± 0.7 ms at 10 mV	
Na$_v$SP	21.0 ± 0.4 mV	3.4 ± 0.3 ms at 30 mV	(Koishi *et al.*, 2004)
Na$_v$PZ	-9.5 ± 0.8 mV	21.5 ± 1.3 at 10 mV	
NaChBac	-24 mV	12.9 ± 0.4 ms at -10 mV	(Ren *et al.*, 2001)
NaChMM	**25.8 ± 0.9 mV**	**1.5 ± 0.3 ms at 30 mV**	**This study**
Na$_v$1.7	-27.9 ± 0.8 mV	1.1 ± 0.2 ms at -10 mV	(Vijayaragavan *et al.*, 2004)
Na$_v$1.8	-1.2 ± 1.0 mV	3.6 ± 0.4 ms at 10 ms	

3.6.2.3. Inactivation of voltage gated sodium channel

The steady-state inactivation of the NaChMM was determined using a two-pulse protocol which included sequential depolarization to a variety of voltages, which was followed by a test pulse to -10 mV (Figure 63A). 35 % of NaChMM channels are inactivated (Figure 63B) at the holding potential used in this experiment (-85 mV). To observe ~ 100 % of active channels, the holding potential should be decreased to about -150 mV. The holding potential of -150 mV was not introduced because of the fragility of expressing tsA201 mammalian cells at hyperpolarising voltages. The holding potential of -85 mV used in this study did not effect the experiment's outcome. The steady-state inactivation appeared to be a voltage function where a double Boltzmann curve was fitted, resulting in 50 % channels inactivation at V_{h1} = -114.6 ± 0.6 mV and V_{h2} = -45.5 ± 0.9 mV. These results suggest that more than one gating process contributes to the inactivation of NaChMM voltage-gated sodium channel. The double mechanism of channel inactivation is often reported to be present in many eukaryotic proteins (Zhao *et al.*, 2007) but was not yet described for prokaryotic voltage-gated sodium channels.
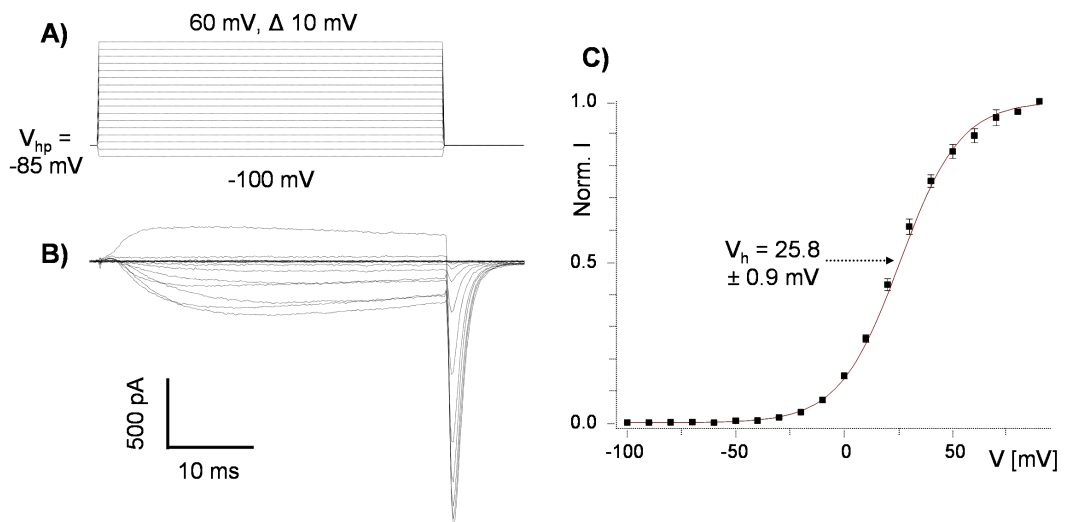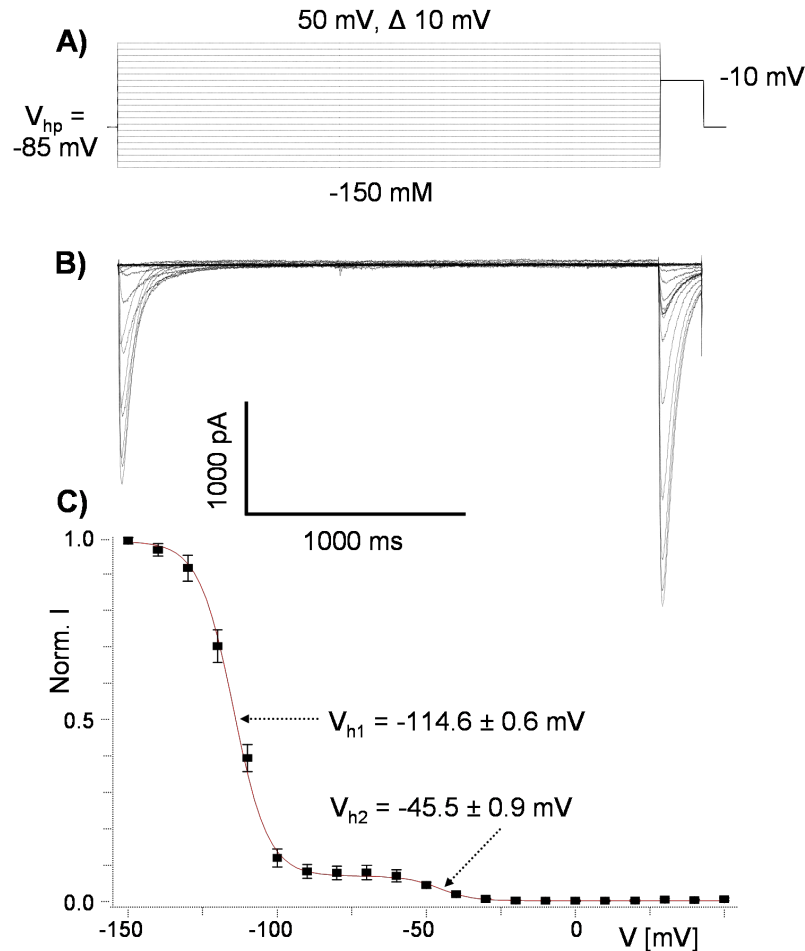
Figure 63: Steady-state inactivation of NaChMM.
A) Waveform stimulus (holding potential -85; voltage pre-pulses applied from -150 mV to 50 mV with increments of 10 mV; test pulse -10 mV); B) representative trace – current response C) Steady-state inactivation curve (n = 4), where V_{h1} = 114.6 ± 0.6 mV and V_{h2} = -45.5 ± 0.9 mV.

The evaluation of inactivation kinetics was performed by fitting a single exponential function to the decaying phase of inward current obtained during the test pulse to -10 mV. Figure 64 presents a step-change in τ_{INACT} at hyperpolarized voltages (range from -150 mV to -110 mV) and the average τ_{INACT} can be estimated as 33.4 ± 0.5 ms. However, as the membrane is entering depolarization voltage values (range from -90 mV to -50 mV), the average τ_{INACT} can be estimated as 53.6 ± 1.5 ms, which is almost twice as slow. When comparing the steady-state inactivation curve (Figure 63C) to the time course in Figure 64, the correlation is observed. The inactivation mechanism that takes place during the hyperpolarisation can be described as fast, whilst the inactivation mechanism observed during depolarization can be described as slow.
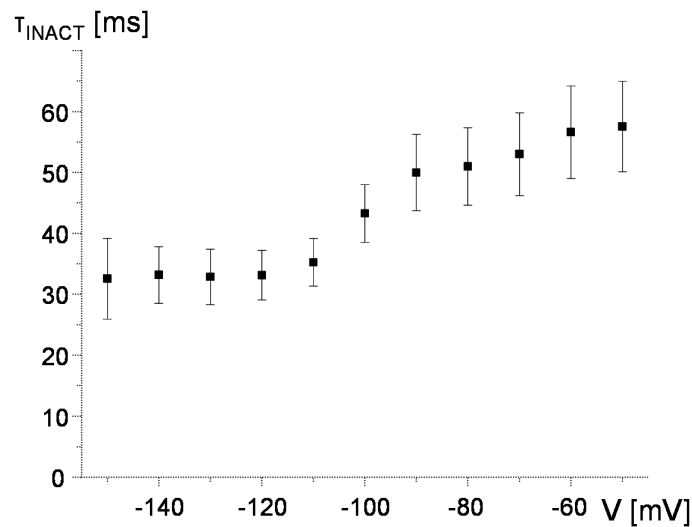
Figure 64: Inactivation kinetics (holding potential -85; voltage pre-pulses applied from -150 mV to -50 mV with increments of 10 mV, n = 4).

The fast type of inactivation **(N-type)** is typical for eukaryotic voltage-gated sodium channels due to the fact that they have the structural ability to inactivate the channel in this particular way. The part of the protein that is responsible for fast inactivation is an IMF motive (Ile-Met-Phe) in the cytoplasmic loop that links the domains III and IV. This amino acid sequence inactivates the channel by the mechanism of a hinged lid or the "ball on the chain" mechanism. The slow **(C-type)** inactivation is engaged by the conformational changes in the pore part of the channel molecule but this mechanism is yet not well understood. The prokaryotic voltage-gated channels do not posses inter-domain linkers. The N-terminus cytoplasmic hanging ends (of each monomer) could nevertheless act as the IMF motive present in eukaryotic sodium channels. This idea was abolished when no change in inactivation kinetics was observed during an investigation of tandem dimers and tetramers of NaChBac (Pavlov *et al.*, 2005). Pavlov's studies proved that a part of the selectivity pore is engaged in the inactivation process, due to which the inactivation may involve a mechanism similar to that of a C-type inactivation in potassium channels (Liu *et al.*, 1996).

The discovery of a double inactivation mechanism in NaChMM channel was surprising. What is more, both mechanisms can not be classified as N-type or C-type inactivation. Both mechanisms additionally revealed a slower kinetics

126

than Na_VSheP (9.90 ± 0.57 ms at 10 mV), Na_VRosD (9.88 ± 1.25 ms at 20 mV) and a typical fast-inactivating Na_v current (10 ms) (Hille, 2001). The NaChMM inactivation time constants were however significantly smaller than those of NaChBac (166 ± 13 ms at -10 mV) (Table 17).

Table 17: V_h of inactivation and time constants of inactivation for selected prokaryotic and mammalian voltage-gated sodium channels.

	Inactivation midpoint	Time of inactivation (τ_{OFF})	Reference
Na_vRosD	-78.7 ± 1.6 mV	9.9 ± 1.3 ms at 20 mV	(Irie *et al.*, 2010)
Na_vSheP	-116.5 ± 0.9 mV	9.9 ± 0.6 ms at -10 mV	
Na_vBacL	-83.2 ± 0.7 mV	96.1 ± 9.6 ms at 10 mV	
Na_vSP	-22.0 ± 0.8 mV	35.0 ± 1.5 ms at 30 mV	(Koishi *et al.*, 2004)
Na_vPZ	-35.0 ± 0.4 mV	102.0 ± 4.2 at 10 mV	
NaChBac	-40 mV	166 ± 13 ms at -10 mV	(Ren *et al.*, 2001)
NaChMM	**-114.6 ± 0.6 mV**	**Fast inactivation (33.4 ± 0.5 ms)**	**This study**
	-45.5 ± 0.9 mV	**Slow inactivation (53.6 ± 1.5 ms)**	
Na_v1.7	-67.7 ± 2.5 mV	Fast inactivation	(Vijayaragavan *et al.*, 2004)
Na_v1.8	-60.5 ± 2.7 mV	Fast inactivation	
Human Na_v1.8	-75.1 ± 1.4 mV	Slow inactivation	(Zhao *et al.*, 2007)
	-34.4 ± 3.3 mV	Fast inactivation	

3.6.2.4. Recovery from inactivation

The recovery from inactivation was measured at a resting potential of -85 mV which was enforced by the fragile nature of tsA201 cells expressing NaChMM. The change of the potential to more hyperpolarised values was decreasing the life span of mammalian cells. This limited the investigation and recovery of only one of the inactivation mechanisms (the slower one) was assessed. The fraction of NaChMM channels that recovered quickly is ~ 10% of the total number of channels. Another 10 % recovered slowly, which is most likely to represent a recovery from the fast inactivation that takes place at hyperpolarized voltage values. A typical set of current traces obtained using this protocol is shown in Figure 65B. The results were fitted with a double exponential curve (Figure 65C). The recovery from inactivation curve shows two components: fast and slow recovery of NaChMM.
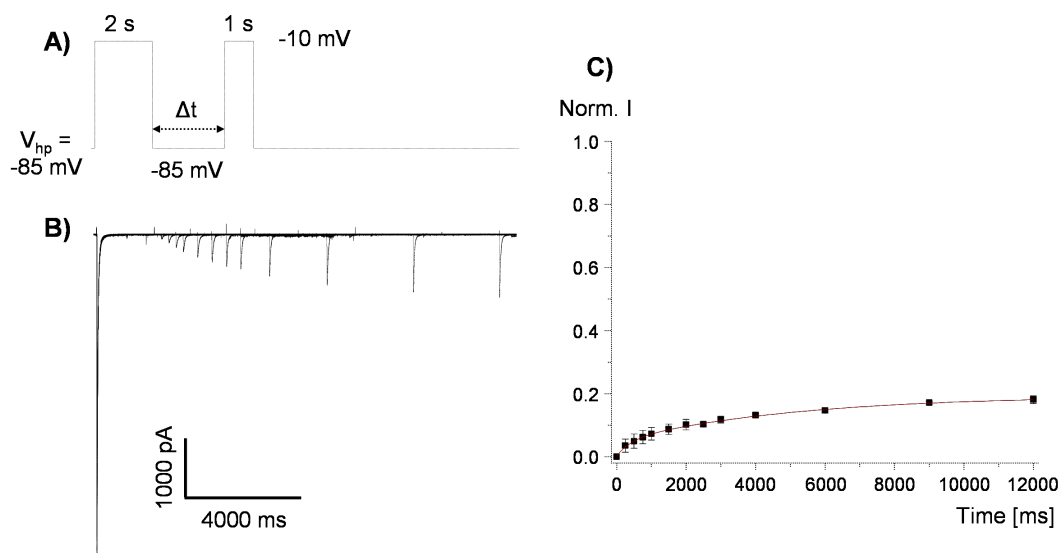
Figure 65: Recovery from inactivation of NaChMM.
A) Waveform stimulus (holding potential -85; voltage pre-pulse -10 mV for 2 s; recovery at -85 mV for various of times 250, 500, 750, 1000, 1500, 2000, 2500, 3000, 4000, 6000, 9000, 12000 ms; activation pulse -10 ms); B) representative trace – current response C) recovery curve (n = 3).

The time constant for a fast recovery was 0.4 s, whilst the time constant for a slow recovery was 5.1 s (measured at -85 mV) (Figure 65A). By contrast, the values for the prokaryotic channel recovery of NaChBac and NaChPZ are 0.66 s (at -100 mV) (Ren *et al.*, 2001) and 0.84 s (at -90) (Koishi *et al.*, 2004), respectively. The time constants for a recovery from inactivation of $Na_v1.8$ expressed in tsA201 was reported to be 2.7 ms for a fast recovery and 29.8 ms for a slow recovery (measured at -100 mV) (Zhao *et al.*, 2007) (Table 18).

Table 18: Time constants of recovery from inactivation for selected prokaryotic and mammalian voltage-gated sodium channels.

	Time of recovery from inactivation	Reference
Na_vPZ	0.84 s at -90 mV	(Koishi *et al.*, 2004)
NaChBac	0.66 s at -100 mV	(Ren *et al.*, 2001)
NaChMM	**Fast recovery 0.4 s at -85 mV**	**This study**
	Slow recovery 5.1 s at -85 mV	
Human Na_v1.8	Slow recovery 29.8 ms at -100 mV	(Zhao *et al.*, 2007)
	Fast recovery 2.7 ms at -100 mV	

To conclude, the new NaChMM voltage-gated sodium channel cloned from *M. maris* differs in its kinetics and voltage dependencies from other prokaryotic sodium channels described in the literature. This may reflect differences in the environment in which the bacteria respective to the analysed proteins live. The activation and inactivation of prokaryotic NaChMM that is cloned from a marine bacterium is faster than those reported for its homologues from *Bacillus* species (NaChBac, Na_vBP, and Na_vBacL) and, as suspected, their values correspond to the values reported for homologue sodium channels expressed in the marine bacteria (Na_vSP, Na_vSheP, and Na_vRosD).

Marine bacteria live in an environment with a higher concentration of sodium ions than soil bacteria, such as *Bacillus* species. A fast inactivation of sodium channels found in marine bacteria is likely to occur due to their environmental adaptation and evolution in order to prevent the influx of excess sodium ions into the cytoplasm (Irie *et al.*, 2010).

The double mechanism of inactivation of NaChMM sodium channel cannot be classified as a C-type or an N-type and a thorough understanding of this phenomenon will require further mutational studies.

The prokaryotic voltage-gated sodium channels are the simplest cation channels known to date. The differences in their channel characteristics are due to small changes in their primary sequences, which may provide insight into the molecular evolution of these channels and possibly reveal their basic molecular mechanisms.

4. Conclusions and Future work

In the presented study, the putative voltage-gated sodium channel from a novel marine bacterium *Maricaulis maris* (NaChMM) was selected as a target for a structural investigation. The protocol for efficient heterologous production of the protein in *E. coli* was established with the help of several optimisation approaches, such as the application of a variety of host strains, cultivation conditions and induction parameters. The optimal yields of produced recombinant protein and its insertion into the cell membrane were obtained by bacteria cultivation in terrific broth at low temperature with 1 mM IPTG induction for 4 h. The cell disruption was performed by means of the combined enzymatic (lysozyme) and ultrasound (sonication) methods, whilst the optimal extraction of voltage-gated sodium channel from the membrane was achieved with mild detergent n-dodecyl-β-D-maltopyranoside (DDM). The established robust purification protocol of NaChMM involved a standard step gradient immobilised metal affinity chromatography purification followed by the enzymatic (His)$_6$-tag removal, an additional affinity chromatography step and a size exclusion chromatography. The optimised production and accomplished purification protocol resulted in 6 mg of ~ 95 % pure NaChMM from 1 L of bacterial culture. Moreover, established purification protocol was successfully applied for truncated variants of the protein as well as for the sodium channels from *B. halodurans* (NaChBac) and *S. pomeroy*i (NaChSP). The NaChMM revealed extremely high stability, while the other targets demonstrated a clear tendency to aggregate or, in certain instances, to precipitate.

Extensive size exclusion chromatography experiments conducted in this research with various detergents revealed that NaChMM can be obtained as a homogeneous sample and indicated that the protein is purified in its native form of tetramer. However, further biochemical characterisation was performed with cross-linking and Blue-Native gel analyses, which showed the presence of monomeric, dimeric and tetrameric NaChMM populations and indicated that the protein sample is heterogeneous. Taking into account that the aforementioned methodologies are not well established for membrane protein research, the results obtained by means of those methodologies were found to be inconclusive in many cases. Further experiments, including analytical ultra-centrifugation, are

suggested to determine the oligomeric state of NaChMM. What is more, the correct folding and the expected α-helical secondary structure of NaChMM were confirmed by a circular dichroism analysis.

Extensive crystallisation trials (~ 8,000 conditions) conducted by means of a sitting drop vapour diffusion technique resulted in crystal-like structures of NaChMM protein. Further optimisation of crystallisation process, in particular, the usefulness of the so-called *in meso* crystallization method, will be explored.

The activity of NaChMM was confirmed *in vivo* by applying the whole-cell patch clamp method. In contrast to NaChBac, NaChMM demonstrated a fast activation and inactivation kinetics. Interestingly, NaChMM presented a double mechanism of inactivation, which to date was observed only in the mammalian Na_v. Due to the differences in the constitution of Na_v *vs.* NaChMM, the double mechanism of inactivation in NaChMM cannot, however, be classified as the so-called C-type or N-type mechanism. As a result, the investigation by the site-directed mutagenesis is required to further explore this novel phenomenon.

Bibliography

ABBOTT, G. W., BUTLER, M. H., BENDAHHOU, S., DALAKAS, M. C., PTACEK, L. J. & GOLDSTEIN, S. A. 2001. MiRP2 forms potassium channels in skeletal muscle with Kv3.4 and is associated with periodic paralysis. *Cell,* 104**,** 217-31.

ABRAHAM, W. R., STROMPL, C., MEYER, H., LINDHOLST, S., MOORE, E. R., CHRIST, R., VANCANNEYT, M., TINDALL, B. J., BENNASAR, A., SMIT, J. & TESAR, M. 1999. Phylogeny and polyphasic taxonomy of Caulobacter species. Proposal of Maricaulis gen. nov. with Maricaulis maris (Poindexter) comb. nov. as the type species, and emended description of the genera Brevundimonas and Caulobacter. *Int J Syst Bacteriol,* 49 Pt 3**,** 1053-73.

ALEKOV, A., RAHMAN, M. M., MITROVIC, N., LEHMANN-HORN, F. & LERCHE, H. 2000. A sodium channel mutation causing epilepsy in man exhibits subtle defects in fast inactivation and activation in vitro. *J Physiol,* 529 Pt 3**,** 533-9.

ANDRE, N., CHEROUATI, N., PRUAL, C., STEFFAN, T., ZEDER-LUTZ, G., MAGNIN, T., PATTUS, F., MICHEL, H., WAGNER, R. & REINHART, C. 2006. Enhancing functional production of G protein-coupled receptors in Pichia pastoris to levels required for structural studies via a single expression screen. *Protein Sci,* 15**,** 1115-26.

ARMSTRONG, C. M., BEZANILLA, F. & ROJAS, E. 1973. Destruction of sodium conductance inactivation in squid axons perfused with pronase. *J Gen Physiol,* 62**,** 375-91.

ARMSTRONG, C. M. & BEZANILLA, F. 1977. Inactivation of the sodium channel. II. Gating current experiments. *J Gen Physiol,* 70**,** 567-90.

ARMSTRONG, C. M. & HILLE, B. 1998. Voltage-gated ion channels and electrical excitability. *Neuron,* 20**,** 371-80.

BACK, J. W., DE JONG, L., MUIJSERS, A. O. & DE KOSTER, C. G. 2003. Chemical cross-linking and mass spectrometry for protein structural modeling. *J Mol Biol,* 331**,** 303-13.

BANNWARTH, M. & SCHULZ, G. E. 2003. The expression of outer membrane proteins for crystallization. *Biochim Biophys Acta,* 1610**,** 37-45.

BARNARD, T. J., WALLY, J. L. & BUCHANAN, S. K. 2007. Crystallization of integral membrane proteins. *Curr Protoc Protein Sci,* Chapter 17**,** Unit 17 9.

BEZANILLA, F. 2000. The voltage sensor in voltage-dependent ion channels. *Physiol Rev,* 80**,** 555-92.

BEZANILLA, F. & ARMSTRONG, C. M. 1977. Inactivation of the sodium channel. I. Sodium current experiments. *J Gen Physiol,* 70**,** 549-66.

BHATE, M. P., WYLIE, B. J., TIAN, L. & MCDERMOTT, A. E. 2010. Conformational dynamics in the selectivity filter of KcsA in response to potassium ion concentration. *J Mol Biol,* 401**,** 155-66.

BJORK, P., WETTERBERG-STRANDH, I., BAUREN, G. & WIESLANDER, L. 2006. Chironomus tentans-repressor splicing factor represses SR protein function locally on pre-mRNA exons and is displaced at correct splice sites. *Mol Biol Cell,* 17**,** 32-42.

BLANCHET, J., PILOTE, S. & CHAHINE, M. 2007. Acidic residues on the voltage-sensor domain determine the activation of the NaChBac sodium channel. *Biophys J,* 92**,** 3513-23.

BOHM, G., MUHR, R. & JAENICKE, R. 1992. Quantitative analysis of protein far UV circular dichroism spectra by neural networks. *Protein Eng,* 5**,** 191-5.

BOSHART, M., WEBER, F., JAHN, G., DORSCH-HASLER, K., FLECKENSTEIN, B. & SCHAFFNER, W. 1985. A very strong enhancer is located upstream of an immediate early gene of human cytomegalovirus. *Cell,* 41**,** 521-30.

BROSIUS, J., ERFLE, M. & STORELLA, J. 1985. Spacing of the -10 and -35 regions in the tac promoter. Effect on its in vivo activity. *J Biol Chem,* 260**,** 3539-41.

BROWNE, D. L., GANCHER, S. T., NUTT, J. G., BRUNT, E. R., SMITH, E. A., KRAMER, P. & LITT, M. 1994. Episodic ataxia/myokymia syndrome is associated with point mutations in the human potassium channel gene, KCNA1. *Nat Genet,* 8**,** 136-40.

BURNETTE, W. N. 1981. "Western blotting": electrophoretic transfer of proteins from sodium dodecyl sulfate--polyacrylamide gels to unmodified nitrocellulose and radiographic detection with antibody and radioiodinated protein A. *Anal Biochem,* 112**,** 195-203.

CAFFREY, M. 2000. A lipid's eye view of membrane protein crystallization in mesophases. *Curr Opin Struct Biol,* 10**,** 486-97.

CAFFREY, M. 2003. Membrane protein crystallization. *J Struct Biol,* 142**,** 108-32.

CAMPBELL, A., N., REECE B., J. 2002. *Biology,* California, Benjamin Cumminga.

CATTERALL, W. A. 2000. From ionic currents to molecular mechanisms: the structure and function of voltage-gated sodium channels. *Neuron,* 26**,** 13-25.

CATTERALL, W. A. 2001. Physiology. A one-domain voltage-gated sodium channel in bacteria. *Science,* 294**,** 2306-8.

CESARE, P., MORIONDO, A., VELLANI, V. & MCNAUGHTON, P. A. 1999. Ion channels gated by heat. *Proc Natl Acad Sci U S A,* 96**,** 7658-63.

CHALFIE, M., TU, Y., EUSKIRCHEN, G., WARD, W. W. & PRASHER, D. C. 1994. Green fluorescent protein as a marker for gene expression. *Science,* 263**,** 802-5.

CHEN, Y., SONG, J., SUI, S. F. & WANG, D. N. 2003. DnaK and DnaJ facilitated the folding process and reduced inclusion body formation of

magnesium transporter CorA overexpressed in Escherichia coli. *Protein Expr Purif,* 32**,** 221-31.

CHENG, H.-R. & JIANG, N. 2006. Extremely rapid extraction of DNA from bacteria and yeasts. *Biotechnology Letters,* 28**,** 55-59.

CHEREZOV, V., CLOGSTON, J., MISQUITTA, Y., ABDEL-GAWAD, W. & CAFFREY, M. 2002. Membrane protein crystallization in meso: lipid type-tailoring of the cubic phase. *Biophys J,* 83**,** 3393-407.

COLABUFO, N. A., BERARDI, F., CONTINO, M., NISO, M. & PERRONE, R. 2009. ABC pumps and their role in active drug transport. *Curr Top Med Chem,* 9**,** 119-29.

CORRY, B. 2006. Understanding ion channel selectivity and gating and their role in cellular signalling. *Mol Biosyst,* 2**,** 527-35.

DALEY, D. O., RAPP, M., GRANSETH, E., MELEN, K., DREW, D. & VON HEIJNE, G. 2005. Global topology analysis of the Escherichia coli inner membrane proteome. *Science,* 308**,** 1321-3.

DAVEY, J. 2004. G-protein-coupled receptors: new approaches to maximise the impact of GPCRS in drug discovery. *Expert Opin Ther Targets,* 8**,** 165-70.

DE FORESTA, B., HENAO, F. & CHAMPEIL, P. 1994. Cancellation of the cooperativity of Ca2+ binding to sarcoplasmic reticulum Ca(2+)-ATPase by the non-ionic detergent dodecylmaltoside. *Eur J Biochem,* 223**,** 359-69.

DEISENHOFER, J., EPP, O., MIKI, K., HUBER, R. & MICHEL, H. 1985. Structure of the Protein Subunits in the Photosynthetic Reaction Center of Rhodopseudomonas-Viridis at 3a Resolution. *Nature,* 318**,** 618-624.

DENIER, C., DUCROS, A., VAHEDI, K., JOUTEL, A., THIERRY, P., RITZ, A., CASTELNOVO, G., DEONNA, T., GERARD, P., DEVOIZE, J. L., GAYOU, A., PERROUTY, B., SOISSON, T., AUTRET, A., WARTER, J. M., VIGHETTO, A., VAN BOGAERT, P., ALAMOWITCH, S., ROULLET, E. & TOURNIER-LASSERVE, E. 1999. High prevalence of CACNA1A truncations and broader clinical spectrum in episodic ataxia type 2. *Neurology,* 52**,** 1816-21.

DI CERA, E., DE CRISTOFARO, R., ALBRIGHT, D. J. & FENTON, J. W., 2ND 1991. Linkage between proton binding and amidase activity in human alpha-thrombin: effect of ions and temperature. *Biochemistry,* 30**,** 7913-24.

DONG, H., NILSSON, L. & KURLAND, C. G. 1996. Co-variation of tRNA abundance and codon usage in Escherichia coli at different growth rates. *J Mol Biol,* 260**,** 649-63.

DOWER, W. J., MILLER, J. F. & RAGSDALE, C. W. 1988. High efficiency transformation of E. coli by high voltage electroporation. *Nucleic Acids Res,* 16**,** 6127-45.

DOYLE, D. A., MORAIS CABRAL, J., PFUETZNER, R. A., KUO, A., GULBIS, J. M., COHEN, S. L., CHAIT, B. T. & MACKINNON, R.

1998. The structure of the potassium channel: molecular basis of K+ conduction and selectivity. *Science,* 280**,** 69-77.

DREW, D., LERCH, M., KUNJI, E., SLOTBOOM, D. J. & DE GIER, J. W. 2006. Optimization of membrane protein overexpression and purification using GFP fusions. *Nat Methods,* 3**,** 303-13.

DUCRUIX, A. A. G., RICHARD 1992. *Crystallization of Nucleic Acids and Proteins: A Practical Approach.*

DULBECCO, R. & FREEMAN, G. 1959. Plaque production by the polyoma virus. *Virology,* 8**,** 396-7.

DUMON-SEIGNOVERT, L., CARIOT, G. & VUILLARD, L. 2004. The toxicity of recombinant proteins in Escherichia coli: a comparison of overexpression in BL21(DE3), C41(DE3), and C43(DE3). *Protein Expr Purif,* 37**,** 203-6.

DUTZLER, R., CAMPBELL, E. B., CADENE, M., CHAIT, B. T. & MACKINNON, R. 2002. X-ray structure of a ClC chloride channel at 3.0 A reveals the molecular basis of anion selectivity. *Nature,* 415**,** 287-94.

ECONOMOU, A. 1999. Following the leader: bacterial protein export through the Sec pathway. *Trends Microbiol,* 7**,** 315-20.

EICHACKER, V. R. A. L. A. 2006. Analysis of Membrane Protein Complexes by Blue Native PAGE. *Practical Proteomics,* 1-2.

ENGELMAN, D. M. 2005. Membranes are more mosaic than fluid. *Nature,* 438**,** 578-80.

ESCAYG, A., MACDONALD, B. T., MEISLER, M. H., BAULAC, S., HUBERFELD, G., AN-GOURFINKEL, I., BRICE, A., LEGUERN, E., MOULARD, B., CHAIGNE, D., BURESI, C. & MALAFOSSE, A. 2000. Mutations of SCN1A, encoding a neuronal sodium channel, in two families with GEFS+2. *Nat Genet,* 24**,** 343-5.

ESHAGHI, S., HEDREN, M., NASSER, M. I., HAMMARBERG, T., THORNELL, A. & NORDLUND, P. 2005. An efficient strategy for high-throughput expression screening of recombinant integral membrane proteins. *Protein Sci,* 14**,** 676-83.

FAHAM, S. & BOWIE, J. U. 2002. Bicelle crystallization: a new method for crystallizing membrane proteins yields a monomeric bacteriorhodopsin structure. *J Mol Biol,* 316**,** 1-6.

FAHLKE, C., KNITTLE, T., GURNETT, C. A., CAMPBELL, K. P. & GEORGE, A. L., JR. 1997. Subunit stoichiometry of human muscle chloride channels. *J Gen Physiol,* 109**,** 93-104.

FAHLKE, C. 2001. Ion permeation and selectivity in ClC-type chloride channels. *Am J Physiol Renal Physiol,* 280**,** F748-57.

FASMAN, D. G. 1992. Practical Handbook of Biochemistry and Molecular Biology. CRC Press, Boston.

FELIU, J. X., CUBARSI, R. & VILLAVERDE, A. 1998. Optimized release of recombinant proteins by ultrasonication of E. coli cells. *Biotechnol Bioeng,* 58**,** 536-40.

FIERS, W., CONTRERAS, R., HAEGEMANN, G., ROGIERS, R., VAN DE VOORDE, A., VAN HEUVERSWYN, H., VAN HERREWEGHE, J., VOLCKAERT, G. & YSEBAERT, M. 1978. Complete nucleotide sequence of SV40 DNA. *Nature,* 273**,** 113-20.

FONTAINE, B., KHURANA, T. S., HOFFMAN, E. P., BRUNS, G. A., HAINES, J. L., TROFATTER, J. A., HANSON, M. P., RICH, J., MCFARLANE, H., YASEK, D. M. & ET AL. 1990. Hyperkalemic periodic paralysis and the adult muscle sodium channel alpha-subunit gene. *Science,* 250**,** 1000-2.

FRANCIS, D. M. & PAGE, R. 2010. Strategies to optimize protein expression in E. coli. *Curr Protoc Protein Sci,* Chapter 5**,** Unit 5 24 1-29.

FUJIWARA, T., SUGAWARA, T., MAZAKI-MIYAZAKI, E., TAKAHASHI, Y., FUKUSHIMA, K., WATANABE, M., HARA, K., MORIKAWA, T., YAGI, K., YAMAKAWA, K. & INOUE, Y. 2003. Mutations of sodium channel alpha subunit type 1 (SCN1A) in intractable childhood epilepsies with frequent generalized tonic-clonic seizures. *Brain,* 126**,** 531-46.

GABASHVILI, I. S., SOKOLOWSKI, B. H., MORTON, C. C. & GIERSCH, A. B. 2007. Ion channel gene expression in the inner ear. *J Assoc Res Otolaryngol,* 8**,** 305-28.

GALLOWAY, C. A., SOWDEN, M. P. & SMITH, H. C. 2003. Increasing the yield of soluble recombinant protein expressed in E. coli by induction during late log phase. *Biotechniques,* 34**,** 524-6, 528, 530.

GENDREAU, S., VOSWINKEL, S., TORRES-SALAZAR, D., LANG, N., HEIDTMANN, H., DETRO-DASSEN, S., SCHMALZING, G., HIDALGO, P. & FAHLKE, C. 2004. A trimeric quaternary structure is conserved in bacterial and human glutamate transporters. *J Biol Chem,* 279**,** 39505-12.

GOLDMAN, E., ROSENBERG, A. H., ZUBAY, G. & STUDIER, F. W. 1995. Consecutive low-usage leucine codons block translation only when near the 5' end of a message in Escherichia coli. *J Mol Biol,* 245**,** 467-73.

GONZALEZ, J. M., COVERT, J. S., WHITMAN, W. B., HENRIKSEN, J. R., MAYER, F., SCHARF, B., SCHMITT, R., BUCHAN, A., FUHRMAN, J. A., KIENE, R. P. & MORAN, M. A. 2003. Silicibacter pomeroyi sp. nov. and Roseovarius nubinhibens sp. nov., dimethylsulfoniopropionate-demethylating bacteria from marine environments. *Int J Syst Evol Microbiol,* 53**,** 1261-9.

GURNETT, C. A. & CAMPBELL, K. P. 1996. Transmembrane auxiliary subunits of voltage-dependent ion channels. *J Biol Chem,* 271**,** 27975-8.

GUSTAFSSON, C., GOVINDARAJAN, S. & MINSHULL, J. 2004. Codon bias and heterologous protein expression. *Trends Biotechnol,* 22**,** 346-53.

HABEEB, A. J. & HIRAMOTO, R. 1968. Reaction of proteins with glutaraldehyde. *Arch Biochem Biophys,* 126**,** 16-26.

HAMILL, O. P., MARTY, A., NEHER, E., SAKMANN, B. & SIGWORTH, F. J. 1981. Improved patch-clamp techniques for high-resolution current

recording from cells and cell-free membrane patches. *Pflugers Arch,* 391**,** 85-100.

HANAKAM, F., ECKERSKORN, C., LOTTSPEICH, F., MULLER-TAUBENBERGER, A., SCHAFER, W. & GERISH, G. 1995. The pH-sensitive actin-binding protein hisactophilin of Dictyostelium exists in two isoforms which both are myristoylated and distributed between plasma membrane and cytoplasm. *J Biol Chem,* 270**,** 596-602.

HANNA, M. G., STEWART, J., SCHAPIRA, A. H., WOOD, N. W., MORGAN-HUGHES, J. A. & MURRAY, N. M. 1998. Salbutamol treatment in a patient with hyperkalaemic periodic paralysis due to a mutation in the skeletal muscle sodium channel gene (SCN4A). *J Neurol Neurosurg Psychiatry,* 65**,** 248-50.

HEIM, R., CUBITT, A. B. & TSIEN, R. Y. 1995. Improved green fluorescence. *Nature,* 373**,** 663-4.

HEUBERGER, E. H., VEENHOFF, L. M., DUURKENS, R. H., FRIESEN, R. H. & POOLMAN, B. 2002. Oligomeric state of membrane transport proteins analyzed with blue native electrophoresis and analytical ultracentrifugation. *J Mol Biol,* 317**,** 591-600.

HILLE, B. 2001. Ion Channels of Excitable Membranes. *Ion Channels of Excitable Membranes.* Third ed.: Sinauer Associates, Inc.

HODGKIN, A. L. & HUXLEY, A. F. 1952a. Currents carried by sodium and potassium ions through the membrane of the giant axon of Loligo. *J Physiol,* 116**,** 449-72.

HODGKIN, A. L. & HUXLEY, A. F. 1952b. A quantitative description of membrane current and its application to conduction and excitation in nerve. *J Physiol,* 117**,** 500-44.

HOSHI, T., ZAGOTTA, W. N. & ALDRICH, R. W. 1990. Biophysical and molecular mechanisms of Shaker potassium channel inactivation. *Science,* 250**,** 533-8.

HUANG, Y., LEMIEUX, M. J., SONG, J., AUER, M. & WANG, D. N. 2003. Structure and mechanism of the glycerol-3-phosphate transporter from Escherichia coli. *Science,* 301**,** 616-20.

HUNTE, C., MICHEL,H. 2003. Membrane protein crystallization. *Membrane Protein Purification and Crystallization: A Practical Guide.* 2nd ed. California: Academic Press.

IIZUKA, K., KAWAGUCHI, H. & KITABATAKE, A. 1993. Effects of thiol protease inhibitors on fodrin degradation during hypoxia in cultured myocytes. *J Mol Cell Cardiol,* 25**,** 1101-9.

IKEMURA, T. 1981. Correlation between the abundance of Escherichia coli transfer RNAs and the occurrence of the respective codons in its protein genes. *J Mol Biol,* 146**,** 1-21.

IRIE, K., KITAGAWA, K., NAGURA, H., IMAI, T., SHIMOMURA, T. & FUJIYOSHI, Y. 2010. Comparative study of the gating motif and C-type

inactivation in prokaryotic voltage-gated sodium channels. *J Biol Chem,* 285**,** 3685-94.

ISOM, L. L., DE JONGH, K. S., PATTON, D. E., REBER, B. F., OFFORD, J., CHARBONNEAU, H., WALSH, K., GOLDIN, A. L. & CATTERALL, W. A. 1992. Primary structure and functional expression of the beta 1 subunit of the rat brain sodium channel. *Science,* 256**,** 839-42.

ISOM, L. L., DE JONGH, K. S. & CATTERALL, W. A. 1994. Auxiliary subunits of voltage-gated ion channels. *Neuron,* 12**,** 1183-94.

ITO, M., XU, H., GUFFANTI, A. A., WEI, Y., ZVI, L., CLAPHAM, D. E. & KRULWICH, T. A. 2004. The voltage-gated Na+ channel NaVBP has a role in motility, chemotaxis, and pH homeostasis of an alkaliphilic Bacillus. *Proc Natl Acad Sci U S A,* 101**,** 10566-71.

IWATA, S. 2003. *Methods and Results in Crystallization of Membrane Proteins.*

IYER, R., IVERSON, T. M., ACCARDI, A. & MILLER, C. 2002. A biological role for prokaryotic ClC chloride channels. *Nature,* 419**,** 715-8.

JAN, L. Y. & JAN, Y. N. 1997. Cloned potassium channels from eukaryotes and prokaryotes. *Annu Rev Neurosci,* 20**,** 91-123.

JANAS, R. M., MARKS, D. L. & LARUSSO, N. F. 1994. Purification and partial characterization of a heat-resistant, cytosolic neuropeptidase from rat liver. *Biochem Biophys Res Commun,* 198**,** 574-81.

JAY, S. D., SHARP, A. H., KAHL, S. D., VEDVICK, T. S., HARPOLD, M. M. & CAMPBELL, K. P. 1991. Structural characterization of the dihydropyridine-sensitive calcium channel alpha 2-subunit and the associated delta peptides. *J Biol Chem,* 266**,** 3287-93.

JENTSCH, T. J., GUNTHER, W., PUSCH, M. & SCHWAPPACH, B. 1995. Properties of voltage-gated chloride channels of the ClC gene family. *J Physiol,* 482**,** 19S-25S.

JENTSCH, T. J., STEIN, V., WEINREICH, F. & ZDEBIK, A. A. 2002. Molecular structure and physiological function of chloride channels. *Physiol Rev,* 82**,** 503-68.

JURKAT-ROTT, K., LEHMANN-HORN, F., ELBAZ, A., HEINE, R., GREGG, R. G., HOGAN, K., POWERS, P. A., LAPIE, P., VALE-SANTOS, J. E., WEISSENBACH, J. & ET AL. 1994. A calcium channel mutation causing hypokalemic periodic pahralysis. *Hum Mol Genet,* 3**,** 1415-9.

KAMKIN, A., KIRISCHUK, S. & KISELEVA, I. 2010. Single mechano-gated channels activated by mechanical deformation of acutely isolated cardiac fibroblasts from rats. *Acta Physiol (Oxf),* 199**,** 277-92.

KANE, J. F. 1995. Effects of rare codon clusters on high-level expression of heterologous proteins in Escherichia coli. *Curr Opin Biotechnol,* 6**,** 494-500.

KAPOOR, M. 2007. How to cross-link proteins. *Protocols on Molecular Station.*

KEKOW, J., PAP, T. & ZIELINSKI, S. 2000. Multifunctional role of proteases in rheumatic diseases. *Adv Exp Med Biol,* 477**,** 467-76.

KENDREW, J. C., DICKERSON, R. E., STRANDBERG, B. E., HART, R. G., DAVIES, D. R., PHILLIPS, D. C. & SHORE, V. C. 1960. Structure of myoglobin: A three-dimensional Fourier synthesis at 2 A. resolution. *Nature,* 185**,** 422-7.

KERAMIDAS, A., MOORHOUSE, A. J., SCHOFIELD, P. R. & BARRY, P. H. 2004. Ligand-gated ion channels: mechanisms underlying ion selectivity. *Prog Biophys Mol Biol,* 86**,** 161-204.

KIEFER, H. 2003. In vitro folding of alpha-helical membrane proteins. *Biochim Biophys Acta,* 1610**,** 57-62.

KOISHI, R., XU, H., REN, D., NAVARRO, B., SPILLER, B. W., SHI, Q. & CLAPHAM, D. E. 2004. A superfamily of voltage-gated sodium channels in bacteria. *J Biol Chem,* 279**,** 9532-8.

KOREPANOVA, A., GAO, F. P., HUA, Y., QIN, H., NAKAMOTO, R. K. & CROSS, T. A. 2005. Cloning and expression of multiple integral membrane proteins from Mycobacterium tuberculosis in Escherichia coli. *Protein Sci,* 14**,** 148-58.

KORNREICH, B. G. 2007. The patch clamp technique: principles and technical considerations. *J Vet Cardiol,* 9**,** 25-37.

KRAUS, R. L., SINNEGGER, M. J., GLOSSMANN, H., HERING, S. & STRIESSNIG, J. 1998. Familial hemiplegic migraine mutations change alpha1A Ca2+ channel kinetics. *J Biol Chem,* 273**,** 5586-90.

KUHLBRANDT, W. & WILLIAMS, K. A. 1999. Analysis of macromolecular structure and dynamics by electron cryo-microscopy. *Curr Opin Chem Biol,* 3**,** 537-43.

KULLMANN, D. M. & HANNA, M. G. 2002. Neurological disorders caused by inherited ion-channel mutations. *Lancet Neurol,* 1**,** 157-66.

KUNJI, E. R., CHAN, K. W., SLOTBOOM, D. J., FLOYD, S., O'CONNOR, R. & MONNE, M. 2005. Eukaryotic membrane protein overproduction in Lactococcus lactis. *Curr Opin Biotechnol,* 16**,** 546-51.

KURLAND, C. & GALLANT, J. 1996. Errors of heterologous protein expression. *Curr Opin Biotechnol,* 7**,** 489-93.

LACINOVA, L. 2005. Voltage-dependent calcium channels. *Gen Physiol Biophys,* 24 Suppl 1**,** 1-78.

LAEMMLI, U. K. 1970. Cleavage of structural proteins during the assembly of the head of bacteriophage T4. *Nature,* 227**,** 680-5.

LANDAU, E. M. & ROSENBUSCH, J. P. 1996. Lipidic cubic phases: a novel concept for the crystallization of membrane proteins. *Proc Natl Acad Sci U S A,* 93**,** 14532-5.

LE MAIRE, M., KWEE, S., ANDERSEN, J. P. & MOLLER, J. V. 1983. Mode of interaction of polyoxyethyleneglycol detergents with membrane proteins. *Eur J Biochem,* 129**,** 525-32.

LEE, H. C. & BERNSTEIN, H. D. 2001. The targeting pathway of Escherichia coli presecretory and integral membrane proteins is specified by the

hydrophobicity of the targeting signal. *Proc Natl Acad Sci U S A,* 98**,** 3471-6.

LEHMANN-HORN, F. & JURKAT-ROTT, K. 1999. Voltage-gated ion channels and hereditary disease. *Physiol Rev,* 79**,** 1317-72.

LIU, Y., JURMAN, M. E. & YELLEN, G. 1996. Dynamic rearrangement of the outer mouth of a K+ channel during gating. *Neuron,* 16**,** 859-67.

LUDEWIG, U., PUSCH, M. & JENTSCH, T. J. 1996. Two physically distinct pores in the dimeric ClC-0 chloride channel. *Nature,* 383**,** 340-3.

MACKINNON, R. 1991. Determination of the subunit stoichiometry of a voltage-activated potassium channel. *Nature,* 350**,** 232-5.

MADUKE, M., PHEASANT, D. J. & MILLER, C. 1999. High-level expression, functional reconstitution, and quaternary structure of a prokaryotic ClC-type chloride channel. *J Gen Physiol,* 114**,** 713-22.

MARBAN, E., YAMAGISHI, T. & TOMASELLI, G. F. 1998. Structure and function of voltage-gated sodium channels. *J Physiol,* 508 (Pt 3)**,** 647-57.

MCPHERSON, A. 2004. Introduction to protein crystallization. *Methods,* 34**,** 254-65.

MEISLER, M. H. & KEARNEY, J. A. 2005. Sodium channel mutations in epilepsy and other neurological disorders. *J Clin Invest,* 115**,** 2010-7.

MIDDLETON, R. E., PHEASANT, D. J. & MILLER, C. 1994. Purification, reconstitution, and subunit composition of a voltage-gated chloride channel from Torpedo electroplax. *Biochemistry,* 33**,** 13189-98.

MIDDLETON, R. E., PHEASANT, D. J. & MILLER, C. 1996. Homodimeric architecture of a ClC-type chloride ion channel. *Nature,* 383**,** 337-40.

MIROUX, B. & WALKER, J. E. 1996. Over-production of proteins in Escherichia coli: mutant hosts that allow synthesis of some membrane proteins and globular proteins at high levels. *J Mol Biol,* 260**,** 289-98.

MULLIGAN, M. E., BROSIUS, J. & MCCLURE, W. R. 1985. Characterization in vitro of the effect of spacer length on the activity of Escherichia coli RNA polymerase at the TAC promoter. *J Biol Chem,* 260**,** 3529-38.

MUSATOV, A., ORTEGA-LOPEZ, J. & ROBINSON, N. C. 2000. Detergent-solubilized bovine cytochrome c oxidase: dimerization depends on the amphiphilic environment. *Biochemistry,* 39**,** 12996-3004.

NEHER, E. & SAKMANN, B. 1976. Single-channel currents recorded from membrane of denervated frog muscle fibres. *Nature,* 260**,** 799-802.

NENOV, A. P., CHEN, C. & BOBBIN, R. P. 1998. Outward rectifying potassium currents are the dominant voltage activated currents present in Deiters' cells. *Hear Res,* 123**,** 168-82.

NIELSEN, P., DAGMAR FRITZE AND FERGUS G. PRIEST 1995. Phenetic diversity of alkaliphilic Bacillus strains: proposal for nine new species. *Microbiology,* 141**,** 1745-1761.

NOLLERT, P., QIU, H., CAFFREY, M., ROSENBUSCH, J. P. & LANDAU, E. M. 2001. Molecular mechanism for the crystallization of bacteriorhodopsin in lipidic cubic phases. *FEBS Lett,* 504**,** 179-86.

NOLLERT, P. 2005. Membrane protein crystallization in amphiphile phases: practical and theoretical considerations. *Prog Biophys Mol Biol,* 88**,** 339-57.

NURANI, G., RADFORD, M., CHARALAMBOUS, K., O'REILLY, A. O., CRONIN, N. B., HAQUE, S. & WALLACE, B. A. 2008. Tetrameric bacterial sodium channels: characterization of structure, stability, and drug binding. *Biochemistry,* 47**,** 8114-21.

OPHOFF, R. A., TERWINDT, G. M., VERGOUWE, M. N., VAN EIJK, R., OEFNER, P. J., HOFFMAN, S. M., LAMERDIN, J. E., MOHRENWEISER, H. W., BULMAN, D. E., FERRARI, M., HAAN, J., LINDHOUT, D., VAN OMMEN, G. J., HOFKER, M. H., FERRARI, M. D. & FRANTS, R. R. 1996b. Familial hemiplegic migraine and episodic ataxia type-2 are caused by mutations in the Ca2+ channel gene CACNL1A4. *Cell,* 87**,** 543-52.

OSTERMEIER, C. & MICHEL, H. 1997. Crystallization of membrane proteins. *Curr Opin Struct Biol,* 7**,** 697-701.

OVERATH, P., STEVERDING, D., CHAUDHRI, M., STIERHOF, Y. D. & ZIEGELBAUER, K. 1994. Structure and function of GPI-anchored surface proteins of Trypanosoma brucei. *Braz J Med Biol Res,* 27**,** 343-7.

PATTON, D. E., WEST, J. W., CATTERALL, W. A. & GOLDIN, A. L. 1993. A peptide segment critical for sodium channel inactivation functions as an inactivation gate in a potassium channel. *Neuron,* 11**,** 967-74.

PATZELT, H., KRAMER, G., RAUCH, T., SCHONFELD, H. J., BUKAU, B. & DEUERLING, E. 2002. Three-state equilibrium of Escherichia coli trigger factor. *Biol Chem,* 383**,** 1611-9.

PAVLOV, E., BLADEN, C., WINKFEIN, R., DIAO, C., DHALIWAL, P. & FRENCH, R. J. 2005. The pore, not cytoplasmic domains, underlies inactivation in a prokaryotic sodium channel. *Biophys J,* 89**,** 232-42.

PAYNE, J. W. 1973. Polymerization of proteins with glutaraldehyde. Soluble molecular-weight markers. *Biochem J,* 135**,** 867-73.

PLASTER, N. M., TAWIL, R., TRISTANI-FIROUZI, M., CANUN, S., BENDAHHOU, S., TSUNODA, A., DONALDSON, M. R., IANNACCONE, S. T., BRUNT, E., BAROHN, R., CLARK, J., DEYMEER, F., GEORGE, A. L., JR., FISH, F. A., HAHN, A., NITU, A., OZDEMIR, C., SERDAROGLU, P., SUBRAMONY, S. H., WOLFE, G., FU, Y. H. & PTACEK, L. J. 2001. Mutations in Kir2.1 cause the developmental and episodic electrical phenotypes of Andersen's syndrome. *Cell,* 105**,** 511-9.

PRASHER, D. C., ECKENRODE, V. K., WARD, W. W., PRENDERGAST, F. G. & CORMIER, M. J. 1992. Primary structure of the Aequorea victoria green-fluorescent protein. *Gene,* 111**,** 229-33.

RAINE, A., ULLERS, R., PAVLOV, M., LUIRINK, J., WIKBERG, J. E. & EHRENBERG, M. 2003. Targeting and insertion of heterologous membrane proteins in E. coli. *Biochimie,* 85**,** 659-68.

REN, D., NAVARRO, B., XU, H., YUE, L., SHI, Q. & CLAPHAM, D. E. 2001. A prokaryotic voltage-gated sodium channel. *Science,* 294**,** 2372-5.

RICHARDS, F. M. & KNOWLES, J. R. 1968. Glutaraldehyde as a protein cross-linkage reagent. *J Mol Biol,* 37**,** 231-3.

ROOSILD, T. P., GREENWALD, J., VEGA, M., CASTRONOVO, S., RIEK, R. & CHOE, S. 2005. NMR structure of Mistic, a membrane-integrating protein for membrane protein expression. *Science,* 307**,** 1317-21.

SAMBROOK, J. A. R. D. W. 2001. *Molecular cloning: A laboratory manual.*

SAMUEL, B. U., MOHANDAS, N., HARRISON, T., MCMANUS, H., ROSSE, W., REID, M. & HALDAR, K. 2001. The role of cholesterol and glycosylphosphatidylinositol-anchored proteins of erythrocyte rafts in regulating raft protein content and malarial infection. *J Biol Chem,* 276**,** 29319-29.

SATO, C., UENO, Y., ASAI, K., TAKAHASHI, K., SATO, M., ENGEL, A. & FUJIYOSHI, Y. 2001. The voltage-sensitive sodium channel is a bell-shaped molecule with several cavities. *Nature,* 409**,** 1047-51.

SCHEEL, J., ZIEGELBAUER, K., KUPKE, T., HUMBEL, B. M., NOEGEL, A. A., GERISCH, G. & SCHLEICHER, M. 1989. Hisactophilin, a histidine-rich actin-binding protein from Dictyostelium discoideum. *J Biol Chem,* 264**,** 2832-9.

SCHEIN, C. H. 1989. Production of Soluble Recombinant Proteins in Bacteria. *Nature Biotechnology,* 7**,** 1141-1149.

SCHMIDT-ROSE, T. & JENTSCH, T. J. 1997. Transmembrane topology of a CLC chloride channel. *Proc Natl Acad Sci U S A,* 94**,** 7633-8.

SINGER, D., BIEL, M., LOTAN, I., FLOCKERZI, V., HOFMANN, F. & DASCAL, N. 1991. The roles of the subunits in the function of the calcium channel. *Science,* 253**,** 1553-7.

SORENSEN, H. P. & MORTENSEN, K. K. 2005. Advanced genetic strategies for recombinant protein expression in Escherichia coli. *J Biotechnol,* 115**,** 113-28.

STUDIER, F. W. 2005. Protein production by auto-induction in high density shaking cultures. *Protein Expr Purif,* 41**,** 207-34.

STUHMER, W., CONTI, F., SUZUKI, H., WANG, X. D., NODA, M., YAHAGI, N., KUBO, H. & NUMA, S. 1989. Structural parts involved in activation and inactivation of the sodium channel. *Nature,* 339**,** 597-603.

SUGAWARA, T., TSURUBUCHI, Y., AGARWALA, K. L., ITO, M., FUKUMA, G., MAZAKI-MIYAZAKI, E., NAGAFUJI, H., NODA, M., IMOTO, K., WADA, K., MITSUDOME, A., KANEKO, S., MONTAL, M., NAGATA, K., HIROSE, S. & YAMAKAWA, K. 2001. A missense mutation of the Na+ channel alpha II subunit gene Na(v)1.2 in a patient

with febrile and afebrile seizures causes channel dysfunction. *Proc Natl Acad Sci U S A,* 98**,** 6384-9.

SWAMY, M., SIEGERS, G. M., MINGUET, S., WOLLSCHEID, B. & SCHAMEL, W. W. 2006. Blue native polyacrylamide gel electrophoresis (BN-PAGE) for the identification and analysis of multiprotein complexes. *Sci STKE,* 2006**,** pl4.

TAWIL, R., MCDERMOTT, M. P., BROWN, R., JR., SHAPIRO, B. C., PTACEK, L. J., MCMANIS, P. G., DALAKAS, M. C., SPECTOR, S. A., MENDELL, J. R., HAHN, A. F. & GRIGGS, R. C. 2000. Randomized trials of dichlorphenamide in the periodic paralyses. Working Group on Periodic Paralysis. *Ann Neurol,* 47**,** 46-53.

TERSTAPPEN, G. C. & REGGIANI, A. 2001. In silico research in drug discovery. *Trends Pharmacol Sci,* 22**,** 23-6.

TUCKER, J. & GRISSHAMMER, R. 1996. Purification of a rat neurotensin receptor expressed in Escherichia coli. *Biochem J,* 317 (Pt 3)**,** 891-9.

TUSNADY, G. E., DOSZTANYI, Z. & SIMON, I. 2004. Transmembrane proteins in the Protein Data Bank: identification and classification. *Bioinformatics,* 20**,** 2964-72.

TUSNADY, G. E., DOSZTANYI, Z. & SIMON, I. 2005. PDB_TM: selection and membrane localization of transmembrane proteins in the protein data bank. *Nucleic Acids Res,* 33**,** D275-8.

VAN GEEST, M. & LOLKEMA, J. S. 2000. Membrane topology and insertion of membrane proteins: search for topogenic signals. *Microbiol Mol Biol Rev,* 64**,** 13-33.

VASINA, J. A. & BANEYX, F. 1996. Recombinant protein expression at low temperatures under the transcriptional control of the major Escherichia coli cold shock promoter cspA. *Appl Environ Microbiol,* 62**,** 1444-7.

VIJAYARAGAVAN, K., BOUTJDIR, M. & CHAHINE, M. 2004. Modulation of Nav1.7 and Nav1.8 peripheral nerve sodium channels by protein kinase A and protein kinase C. *J Neurophysiol,* 91**,** 1556-69.

VON HEIJNE, G. 1999. Recent advances in the understanding of membrane protein assembly and structure. *Q Rev Biophys,* 32**,** 285-307.

WADSTEN, P., WOHRI, A. B., SNIJDER, A., KATONA, G., GARDINER, A. T., COGDELL, R. J., NEUTZE, R. & ENGSTROM, S. 2006. Lipidic sponge phase crystallization of membrane proteins. *J Mol Biol,* 364**,** 44-53.

WAGNER, S., BADER, M. L., DREW, D. & DE GIER, J. W. 2006. Rationalizing membrane protein overexpression. *Trends Biotechnol,* 24**,** 364-71.

WALLACE, R. H., WANG, D. W., SINGH, R., SCHEFFER, I. E., GEORGE, A. L., JR., PHILLIPS, H. A., SAAR, K., REIS, A., JOHNSON, E. W., SUTHERLAND, G. R., BERKOVIC, S. F. & MULLEY, J. C. 1998. Febrile seizures and generalized epilepsy associated with a mutation in the Na+-channel beta1 subunit gene SCN1B. *Nat Genet,* 19**,** 366-70.

WALLACE, B. A., LEES, J. G., ORRY, A. J., LOBLEY, A. & JANES, R. W. 2003. Analyses of circular dichroism spectra of membrane proteins. *Protein Sci,* 12**,** 875-84.

WALLIN, E. & VON HEIJNE, G. 1998. Genome-wide analysis of integral membrane proteins from eubacterial, archaean, and eukaryotic organisms. *Protein Sci,* 7**,** 1029-38.

WEETALL, H. H. 1974. Immobilized enzymes: analytical applications. *Anal Chem,* 46**,** 602A-4A p.

WEISS, H. M. & GRISSHAMMER, R. 2002. Purification and characterization of the human adenosine A(2a) receptor functionally expressed in Escherichia coli. *Eur J Biochem,* 269**,** 82-92.

WEISS, H. M., HAASE, W. & REILANDER, H. 1998. Expression of an integral membrane protein, the 5HT5A receptor. *Methods Mol Biol,* 103**,** 227-39.

WEST, J. W., PATTON, D. E., SCHEUER, T., WANG, Y., GOLDIN, A. L. & CATTERALL, W. A. 1992. A cluster of hydrophobic amino acid residues required for fast Na(+)-channel inactivation. *Proc Natl Acad Sci U S A,* 89**,** 10910-4.

WHITE, S. H. 2004. The progress of membrane protein structure determination. *Protein Sci,* 13**,** 1948-9.

WIENER, M. C. 2004. A pedestrian guide to membrane protein crystallization. *Methods,* 34**,** 364-72.

WILLS, N. K. & FONG, P. 2001. ClC chloride channels in epithelia: recent progress and remaining puzzles. *News Physiol Sci,* 16**,** 161-6.

WUTHRICH, K. 2003. NMR studies of structure and function of biological macromolecules (Nobel lecture). *Angew Chem Int Ed Engl,* 42**,** 3340-63.

YANG, Z. R., THOMSON, R., MCNEIL, P. & ESNOUF, R. M. 2005. RONN: the bio-basis function neural network technique applied to the detection of natively disordered regions in proteins. *Bioinformatics,* 21**,** 3369-76.

YAROV-YAROVOY, V., BAKER, D. & CATTERALL, W. A. 2006. Voltage sensor conformations in the open and closed states in ROSETTA structural models of K(+) channels. *Proc Natl Acad Sci U S A,* 103**,** 7292-7.

YOSHIKAWA, S., TSUKHIHARA, T. & SHINZAWA-ITOH, K. 1996. [Crystal structure of fully oxidized cytochrome c-oxidase from the bovine heart at 2.8 A resolution]. *Biokhimiia,* 61**,** 1931-40.

YUE, L., NAVARRO, B., REN, D., RAMOS, A. & CLAPHAM, D. E. 2002. The cation selectivity filter of the bacterial sodium channel, NaChBac. *J Gen Physiol,* 120**,** 845-53.

ZHANG, H., KURISU, G., SMITH, J. L. & CRAMER, W. A. 2003. A defined protein-detergent-lipid complex for crystallization of integral membrane proteins: The cytochrome b6f complex of oxygenic photosynthesis. *Proc Natl Acad Sci U S A,* 100**,** 5160-3.

ZHAO, Y., SCHEUER, T. & CATTERALL, W. A. 2004a. Reversed voltage-dependent gating of a bacterial sodium channel with proline substitutions

in the S6 transmembrane segment. *Proc Natl Acad Sci U S A,* 101**,** 17873-8.

ZHAO, Y., YAROV-YAROVOY, V., SCHEUER, T. & CATTERALL, W. A. 2004b. A gating hinge in Na+ channels; a molecular switch for electrical signaling. *Neuron,* 41**,** 859-65.

ZHAO, J., ZIANE, R., CHATELIER, A., O'LEARY M, E. & CHAHINE, M. 2007. Lidocaine promotes the trafficking and functional expression of Na(v)1.8 sodium channels in mammalian cells. *J Neurophysiol,* 98**,** 467-77.

ZHUCHENKO, O., BAILEY, J., BONNEN, P., ASHIZAWA, T., STOCKTON, D. W., AMOS, C., DOBYNS, W. B., SUBRAMONY, S. H., ZOGHBI, H. Y. & LEE, C. C. 1997. Autosomal dominant cerebellar ataxia (SCA6) associated with small polyglutamine expansions in the alpha 1A-voltage-dependent calcium channel. *Nat Genet,* 15**,** 62-9.

ZUBERI, S. M., EUNSON, L. H., SPAUSCHUS, A., DE SILVA, R., TOLMIE, J., WOOD, N. W., MCWILLIAM, R. C., STEPHENSON, J. B., KULLMANN, D. M. & HANNA, M. G. 1999. A novel mutation in the human voltage-gated potassium channel gene (Kv1.1) associates with episodic ataxia type 1 and sometimes with partial epilepsy. *Brain,* 122 (Pt 5)**,** 817-25.

Appendix I: Crystallisation screens

The ModifMemGold crystallisation screen is a modified MemGold screen (Molecular Dimensions Limited). The changes introduced to the MemGold screen are listed in Table 19.

Table 19: Modifications introduced to MemGold commercial crystallisation screen.

Original agent	New replacing agent
Bicine	Tricine
Sodium cacodylate	Sodium citrate
Magnesium nitrate	Magnesium acetate
Potassium nitrate	Potassium chloride
Lithium citrate	Sodium citrate
Cadmium chloride	Barium chloride
Bis-tris-propane	Bis-tris
PEG 200	PEG 300
PEG 350 MME	
Tri-ethylene glycol	
PEG 550 MME	PEG 400
Jeffamine-M600	PEG 1000
PEG 5000 MME	PEG 4000
Pentaerythritol propoxylate (5/4 PO/OH)	

The reagents included in PEG Screen are listed in Table 20.

Table 20: List of conditions in PEG Screen.

No	Condition
1	50 mM sodium acetate pH = 4, 10% PEG 400
2	50 mM sodium acetate pH = 5, 10% PEG 400
3	50 mM Bis-tris pH = 6, 10% PEG 400
4	50 mM Bis-tris pH = 7, 10% PEG 400
5	50 mM HEPES pH = 7.5, 10% PEG 400
6	50 mM Tris pH = 8, 10% PEG 400
7	50 mM sodium acetate pH = 4, 15% PEG 400
8	50 mM sodium acetate pH = 5, 15% PEG 400
9	50 mM Bis-tris pH = 6, 15% PEG 400
10	50 mM Bis-tris pH = 7, 15% PEG 400

11	50 mM HEPES pH = 7.5, 15% PEG 400
12	50 mM Tris pH = 8, 15% PEG 400
13	50 mM sodium acetate pH = 4, 20% PEG 400
15	50 mM sodium acetate pH = 5, 20% PEG 400
15	50 mM Bis-tris pH = 6, 20% PEG 400
16	50 mM Bis-tris pH = 7, 20% PEG 400
17	50 mM HEPES pH = 7.5, 20% PEG 400
18	50 mM Tris pH = 8, 20% PEG 400
19	50 mM sodium acetate pH = 4, 25% PEG 400
20	50 mM sodium acetate pH = 5, 25% PEG 400
21	50 mM Bis-tris pH = 6, 25% PEG 400
22	50 mM Bis-tris pH = 7, 25% PEG 400
23	50 mM HEPES pH = 7.5, 25% PEG 400
24	50 mM Tris pH = 8, 25% PEG 400
25	50 mM sodium acetate pH = 4, 10% PEG 1000
26	50 mM sodium acetate pH = 5, 10% PEG 1000
27	50 mM Bis-tris pH = 6, 10% PEG 1000
28	50 mM Bis-tris pH = 7, 10% PEG 1000
29	50 mM HEPES pH = 7.5, 10% PEG 1000
30	50 mM Tris pH = 8, 10% PEG 1000
31	50 mM sodium acetate pH = 4, 15% PEG 1000
32	50 mM sodium acetate pH = 5, 15% PEG 1000
33	50 mM Bis-tris pH = 6, 15% PEG 1000
34	50 mM Bis-tris pH = 7, 15% PEG 1000
35	50 mM HEPES pH = 7.5, 15% PEG 1000
36	50 mM Tris pH = 8, 15% PEG 1000
37	50 mM sodium acetate pH = 4, 20% PEG 1000
38	50 mM sodium acetate pH = 5, 20% PEG 1000
39	50 mM Bis-tris pH = 6, 20% PEG 1000
40	50 mM Bis-tris pH = 7, 20% PEG 1000
41	50 mM HEPES pH = 7.5, 20% PEG 1000
42	50 mM Tris pH = 8, 20% PEG 1000
43	50 mM sodium acetate pH = 4, 25% PEG 1000
44	50 mM sodium acetate pH = 5, 25% PEG 1000
45	50 mM Bis-tris pH = 6, 25% PEG 1000
46	50 mM Bis-tris pH = 7, 25% PEG 1000
47	50 mM HEPES pH = 7.5, 25% PEG 1000
48	50 mM Tris pH = 8, 25% PEG 1000
49	50 mM sodium acetate pH = 4, 10% PEG 1500

50	50 mM sodium acetate pH = 5, 10% PEG 1500
51	50 mM Bis-tris pH = 6, 10% PEG 1500
52	50 mM Bis-tris pH = 7, 10% PEG 1500
53	50 mM HEPES pH = 7.5, 10% PEG 1500
54	50 mM Tris pH = 8, 10% PEG 1500
55	50 mM sodium acetate pH = 4, 15% PEG 1500
56	50 mM sodium acetate pH = 5, 15% PEG 1500
57	50 mM Bis-tris pH = 6, 15% PEG 1500
58	50 mM Bis-tris pH = 7, 15% PEG 1500
59	50 mM HEPES pH = 7.5, 15% PEG 1500
60	50 mM Tris pH = 8, 15% PEG 1500
61	50 mM sodium acetate pH = 4, 20% PEG 1500
62	50 mM sodium acetate pH = 5, 20% PEG 1500
63	50 mM Bis-tris pH = 6, 20% PEG 1500
64	50 mM Bis-tris pH = 7, 20% PEG 1500
65	50 mM HEPES pH = 7.5, 20% PEG 1500
66	50 mM Tris pH = 8, 20% PEG 1500
67	50 mM sodium acetate pH = 4, 25% PEG 1500
68	50 mM sodium acetate pH = 5, 25% PEG 1500
69	50 mM Bis-tris pH = 6, 25% PEG 1500
70	50 mM Bis-tris pH = 7, 25% PEG 1500
71	50 mM HEPES pH = 7.5, 25% PEG 1500
72	50 mM Tris pH = 8, 25% PEG 1500
73	50 mM sodium acetate pH = 4, 10% PEG 4000
74	50 mM sodium acetate pH = 5, 10% PEG 4000
75	50 mM Bis-tris pH = 6, 10% PEG 4000
76	50 mM Bis-tris pH = 7, 10% PEG 4000
77	50 mM HEPES pH = 7.5, 10% PEG 4000
78	50 mM Tris pH = 8, 10% PEG 4000
79	50 mM sodium acetate pH = 4, 15% PEG 4000
80	50 mM sodium acetate pH = 5, 15% PEG 4000
81	50 mM Bis-tris pH = 6, 15% PEG 4000
82	50 mM Bis-tris pH = 7, 15% PEG 4000
83	50 mM HEPES pH = 7.5, 15% PEG 4000
84	50 mM Tris pH = 8, 15% PEG 4000
85	50 mM sodium acetate pH = 4, 20% PEG 4000
86	50 mM sodium acetate pH = 5, 20% PEG 4000
87	50 mM Bis-tris pH = 6, 20% PEG 4000
88	50 mM Bis-tris pH = 7, 20% PEG 4000

89	50 mM HEPES pH = 7.5, 20% PEG 4000
90	50 mM Tris pH = 8, 20% PEG 4000
91	50 mM sodium acetate pH = 4, 25% PEG 4000
92	50 mM sodium acetate pH = 5, 25% PEG 4000
93	50 mM Bis-tris pH = 6, 25% PEG 4000
94	50 mM Bis-tris pH = 7, 25% PEG 4000
95	50 mM HEPES pH = 7.5, 25% PEG 4000
96	50 mM Tris pH = 8, 25% PEG 4000